LATE PROTEROZOIC BEDROCK GEOLOGY AND ITS INFLUENCE ON NEOGENE LITTORAL MARINE DIAMONDIFEROUS TRAPSITES, MA1 – SPERRGEBIET, NAMIBIA

Jana Jacob

Thesis Presented for the Degree of
MASTER OF SCIENCE
in the Department of Geological Sciences
UNIVERSITY OF CAPE TOWN
January 2001

DECLARATION

I hereby declare that all the work presented in this thesis is my own, except where otherwise stated.

Jana Jacob

Abstract

Namibia's south western coast, the Sperrgebiet, hosts one of the world's largest diamond placer deposits. Diamond distribution in this placer deposit is directly related to the presence of a diamond-carrying gravel, the degree of reworking of the gravel and the quantity and quality of the diamond trapsites. The diamond-carrying gravel is present in the form of palaeo-beaches. Six Plio-Pleistocene beaches have been identified lying onshore between the Orange River mouth and Chameis Bay. The Plio-Pleistocene beaches are underlain by Late Proterozoic footwall. The Late-Proterozoic footwall has undergone extensive marine erosion and development of marine platforms during different sea-level stillstands. Diamond trapsites in the form of potholes and gullies are incised into palaeo platforms formed during the sea-level stillstands.

The marine erosion palaeo-platforms have been cut into the predominantly siliciclastic rocks of the Gariep Belt. The Late Proterozoic Gariep Belt is divided into an eastern para-autochthonous passive continental margin zone, the Port Nolloth Zone, and a western allochthonous Marmora Terrane. Previous work suggested that the Marmora Terrane had been thrust on top of the Port Nolloth Zone in a south-easterly direction and that the Marmora Terrane could be subdivided into three tectonostratigraphic units: the Schakalsberge Complex, the Oranjemund Complex and the Chameis Complex. In addition, previous work indicated that the Oranjemund Complex had been stacked tectonically between the Chameis Complex in the northwest and the Schakalsberge Complex in the southeast. However, this study questions the subdivision of the Marmora Terrane into three separate tectonic complexes. The rocks in the study area forms part of the newly defined Oranjemund Group, Oranjemund Sub-terrane.

Field mapping demonstrates that in spite of differences in the lithology, correlation of the major lithostratigraphic units between these three complexes is possible, and their respective successions may have been deposited contiguously. New geochemical data indicate that the rare earth element distribution of the metasedimentary rocks of the Oranjemund Sub-terrane have a similar pattern to that of the meta-basites of the Grootderm Formation, Schakalsberge Complex. Furthermore, the metasedimentary rocks of the Oranjemund Sub-terrane carry a trace element signature of within plate basalts (Zr/Y *versus* Y plot). It is therefore highly likely that these sediments have been derived from metabasites of the adjacent Chameis Complex and the Grootderm Formation metabasites of the Schakalsberge Complex, hence, the three complexes are not different terranes, but should be seen as three sub-terranes of the Marmora Terrane. The Oranjemund Sub-terrane crops out in a narrow coastal belt 120km along the coast from the Orange River mouth in the south to Chameis Bay in the north. This area falls within a

longstanding diamond mining licence area, with restricted access, hence very little is known presently about the details of the rocks in the Oranjemund Sub-terrane.

The metasedimentary rocks of the Oranjemund Sub-terrane underwent south eastward compression (D_1) followed by major E-W compression (D_2), characterised by one major N-S striking syncline and finally by late stage D_3 buckling. This study has also shown that the Oranjemund Formation should be upgraded to the Oranjemund Group. Although no primary contact is exposed, a normal stratigraphic superposition of the Oranjemund Group above the Grootderm Formation is indicated by the fold geometry along the boundary between the two units. The nature of the Oranjemund Sub-terrane is therefore lithostratigraphically determined by the Schakalsberge Sub-terrane and possibly by the Chameis Sub-terrane.

The bedrock lithology and structure influence diamond trapsite formation. Three dominant types of diamond trapsites (gullies) have been identified in the study area: "Swash parallel gullies", "Strike gullies" and "Joint gullies". A gradation of the type of gully (trapsite) formed can be seen from the Orange River mouth northward along the 120 km long coastline to Chameis Bay. This gradation is associated with the amount of abrasive agents (boulders) available and is influenced by the large scale structural features in the bedrock. In the south of the study area near the Orange River mouth, the quantity of abrasive agents (boulders) was most abundant and it decreases progressively northwards towards Chameis Bay. Near the Orange River mouth to 60 km north of the Orange River mouth (Kerbehuk area), where abrasive agents were abundant and s_2 dips 45 degrees west, "Swash gullies" override lithological or structural controls in the bedrock. "Strike gullies" dominate in the Kerbehuk area where s_2 dips between 80-85 degrees west. The harder lithological units stand proud in this area where differential weathering took place. 90km north of the Orange River mouth (Affenrücken area) s_2 dips 45-60 degrees to the east. "Joint gullies" are dominant here due to the exploitation of structural features in the bedrock and the sharp decrease of abrasive agents. Diamond concentration is directly linked to the quality of trapsites. The quality of diamond trapsites is controlled by the depth of incision into the bedrock. New data in the form of corrected ortho-photos (30cm elevation accuracy) obtained from an "Airborne Laser Survey" (ALS) made it possible to accurately contour the outcrop over the whole study area. Palaeo-platforms were identified using the contoured outcrop. Deepest incision into the bedrock was found to be on the seaward end of the palaeo-platforms and thus the highest quality of trapsites appears to be associated with transitions between palaeo-platforms. This finding should also be applicable to palaeo-platforms directly offshore between the Orange River mouth and Chameis Bay.

ACKNOWLEDGEMENTS

- The Namdeb Mineral Resource Department in particular Mr R. Burrell (Chief Geologist) for the very generous funding of the project.
- Hartwig Frimmel and Brian Bluck for guidance and for greatly improving the work through their reviews, suggestions and advice.
- John Ward for his never-ending encouragement, energy and support. Thank you for being there in the very dark moments.
- Roger Jacob for always only being a phone call away.
- Jurgen Jacob for the 3 dimensional Vulcan model of the surveyed gully. Many thanks for your patience and help and taking me on honeymoon before the final version of the thesis was handed in.
- The Namdeb Mineral Resource Department's Drawing Office staff (Annette Schoeman, Johan Langenhoven, Johan van Zyl, Johan Walters and Wimpie Schechter) for their tremendous help with the printing and layout of the final thesis.
- Andre Fourie and Dave Devine for surveying sampling positions.
- Koos O'Kennedy for spending two days in a gully to do a 3 dimensional survey of the gully.
- John Pether, Ian McMillan, Marais Loubser, Renato Spaggiari, Alastair Bauman and Ralph Scholtz for stimulating discussions.
- Alex MacKay for a constant source of ideas and stimulating thoughts and for assisting Clayton Summers in developing a contoured model of the bedrock over the whole study area.
- Karen MacKay for meticulous linguistic editing.
- Joseph Botes for showing me the road to geology and Mignonette, Annel and Mom for encouraging me to stay on this road.
- Dane Gerneke for his dedicated help in obtaining cathodoluminescence and backscatter images at the University of Cape Town.
- Andreas Späth for performing the ICP-MS analyses.

CONTENTS

CHAPTER 1 – INTRODUCTION

The diamond-bearing beaches and shore platforms of southern Namibia host the world's largest diamond placers (Hallam, 1964). Although diamond-bearing beach deposits along coastal southern Africa exist between the Olifants River (Republic of South Africa) in the south to the Angolan border in the north (Figure 1.1), they never reach the high diamond concentrations of the beaches of southern Namibia.

The west coast of Africa was generated during the early Cretaceous opening of the South Atlantic (Dingle *et al.*, 1987). Since that time, coastal and shelf deposits have been forming and a wide continental shelf has built up (Dingle *et al.*, 1987). Along with other passive margins that have developed throughout the world, this Atlantic-African margin has been greatly influenced by sea-level changes. Coastal deposits from the Olifants River northwards have, to a greater or lesser degree, developed along this margin. In most places deposits of earlier still-stands are currently being eroded (Hallam, 1964). The Namibian beaches are an exception to this. The Plio-Holocene gravel beaches (Hallam, 1964) are partly covered by beach and aeolian sands and have therefore largely been preserved.

The diamond-bearing beaches and platforms studied form part of an extensive swathe of beach deposits and associated platforms that form the inner part of the continental shelf. The world-wide sea level changes throughout the Late-Cenozoic which have had such a dominant influence on passive margin shelf sedimentation, have had a great influence on this Namibian shelf. The placer deposits exploited above sea level therefore extend beyond the coast and beneath the current sea level and have for the past 60 years been the subject of much exploration. The Namibian coast, along with that of South Africa is micro-tidal with high wave energy (De Decker, 1986).

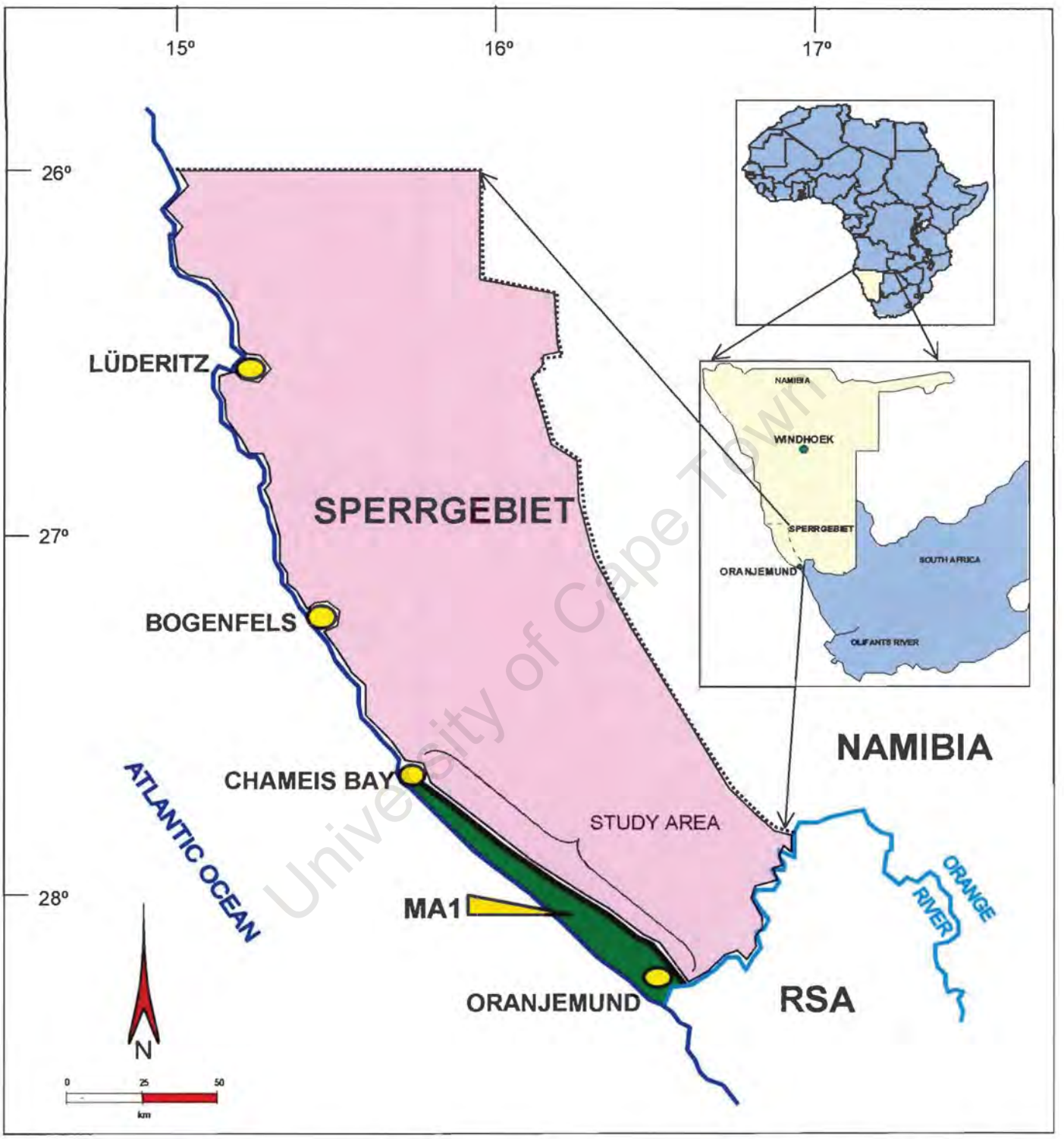

Figure 1.1 Locality map of the Sperrgebiet, Southern Namibia showing the study area, the marine diamondiferous deposit (in green) in Mining Area No. 1 (MA1).

The southern Namibian beaches are located in Diamond Area No. 1, which is administered by Namdeb, a diamond consortium partly owned by the Namibian government and partly owned by De Beers. The area is more commonly referred to as the Sperrgebiet (Figure 1.1) which is under restricted access. The coastal strip studied stretches from the Orange River mouth 120 km northwards to Chameis Bay and is referred to as Mining Area No. 1 (MA1) (Figure 1.2). Chlorite schist and meta-arenite belonging to the Late Proterozoic Gariep Belt underlie the beaches here. These rocks vary not only in lithology but also in structure along the coastline, and this variation has greatly influenced beaches, platforms and the quality of the diamond placer. Although the influence of bedrock on coastal development will be expanded upon in this thesis, its influence can be seen most clearly in the south, where the Orange River has made its coastal entry into soft bedrock and where marine platforms are poorly developed.

In Cretaceous times the western region of Africa has been subject to uplift and this, amongst other things, has caused the Orange River to incise into the largely Neoproterozoic rocks (Dingle and Hendey, 1984).

Diamond discovery near Port Nolloth in 1925 was followed by 1927 discovery of the Alexander Bay diamond deposits. In 1928 CDM discovered diamonds north of the Orange River mouth, followed by a comprehensive sampling programme. The sampling programme resulted in the delineation of an ore body made up of six raised beaches (Hallam, 1964). The ore body developed over a distance of 120 km along the coast from the Orange River mouth to Chameis Bay (Figure 1.2) and is located in Mining Area No. 1. (MA1). The raised gravel beaches are characterised by an exotic suite of resistant pebbles, including agate, jasper, ironstone and quartzite. Diamonds are trapped in these raised beaches with the highest concentration of diamonds found in the beach toes and beach crests (Spaggiari *et al.*, 1997).

In MA1 six onshore (raised) diamondiferous beaches (Hallam, 1964) rest on a series of six marine platforms (Kalbskopf, 1978) (Figure 1.3 and Figure 1.4) cut into Late Proterozoic chlorite schist and meta-arenite of the Gariep Belt.

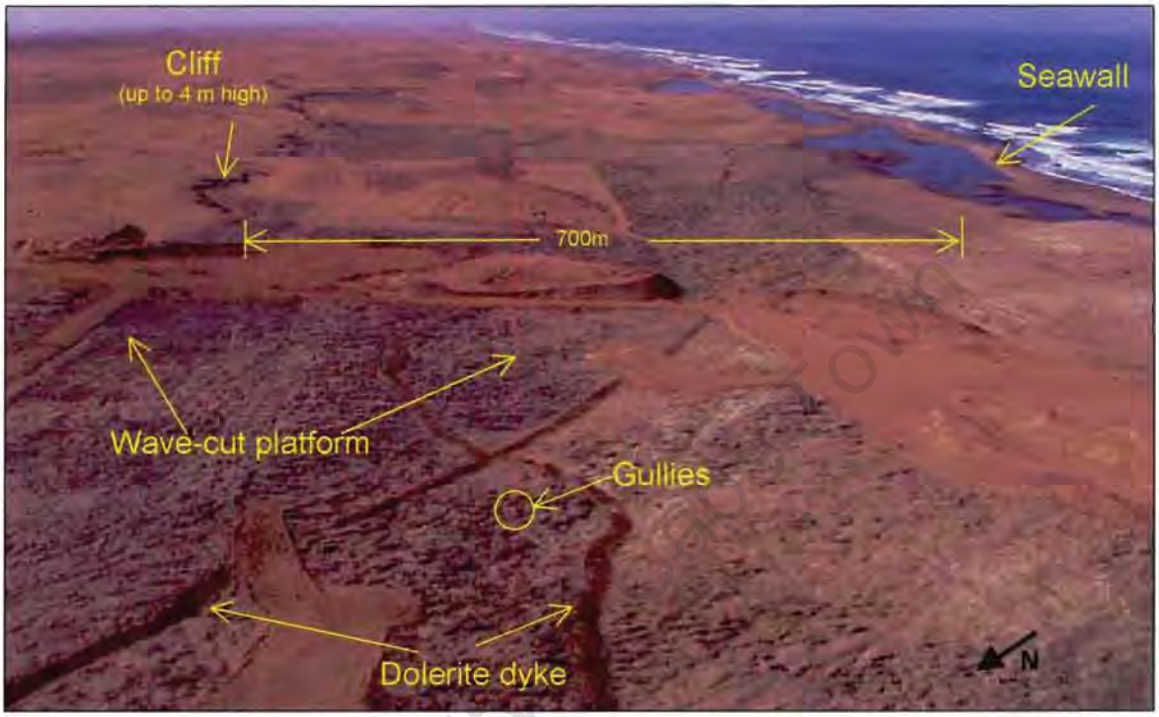

Figure 1.3 Oblique aerial photograph of the Late Proterozoic bedrock, with cross-cutting dolerite intrusions and well developed gullies on a marine platform (55 km north of the Orange River mouth).

The Gariep Belt has been divided into an eastern para-autochthonous passive continental margin zone, the Port Nolloth Zone (PNZ) and the allochthonous Marmora Terrane (MT) in the west. The latter has been subdivided further into three tectonostratigraphic units: the Schakalsberge Complex, the Oranjemund Complex and the Chameis Complex (Hartnady and Von Veh, 1990) (Figure 1.5). As will be shown in this work, the differences between these complexes are not sufficient to describe them as separate terranes or complexes. They were most likely deposited contiguously and will therefore be referred to as sub-terranes (Frimmel, 2001a).

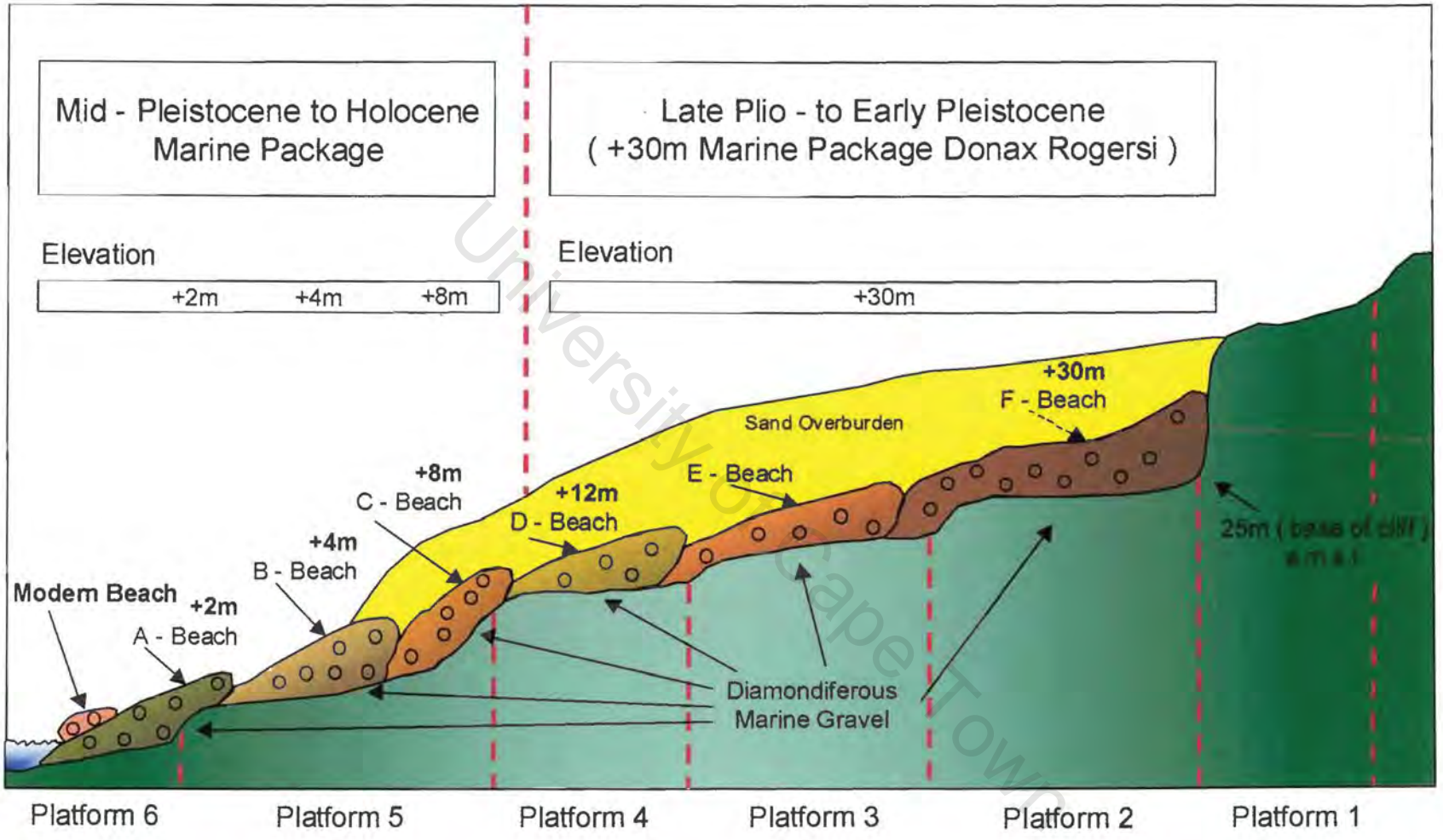

Figure 1.4 An exaggerated cross section through the raised beach deposits of Mining Area No. 1 (MA1), showing the approximate elevation of beaches and platforms (after Hallam, 1964 and Kalbskopf, 1978).

Above mean sea-level (a.m.s.l.)

The Oranjemund Sub-terrane comprises the Oranjemund Formation (Kröner, 1974) which consists of predominantly metamorphosed siliciclastic rocks. The bedrock in the study area is made up of this Oranjemund Formation. This study will show that the rank of the Oranjemund Formation should be upgraded to Group. Published geological maps of the bedrock in the region date back to Kaiser (1926). Not only has the understanding of the Gariep Belt greatly improved since then (Frimmel, 1995 and 2001a&b, Hartnady and Von Veh, 1990), but a lot more outcrop has been exposed by mining activities in the area. For this reason, a re-assesment of the geology of the Oranjemund Group appears appropriate.

The detrital components of clastic sediments of the Oranjemund Group are described by element ratios that should be representative of the source material. At present the palaeo-stratigraphic position of the Oranjemund Group is uncertain. The source and structural evolution of the sediments of the Oranjemund Group could help to determine the palaeo-stratigraphic position. Geochemical data have proven to be useful in constraining the depositional environment and source of siliciclastic rocks (e.g. Floyd *et al.*, 1991 and Kalsbeek *et al.*, 1998). It is speculated that marine erosion pattern development is related to small-scale (local) structures, lithological differences and/or compositional differences in the bedrock. As no detailed study of the Oranjemund Group has been carried out to date, this study aims at providing a detailed documentation of the lithology, structural geology and geochemistry of the Oranjemund Group.

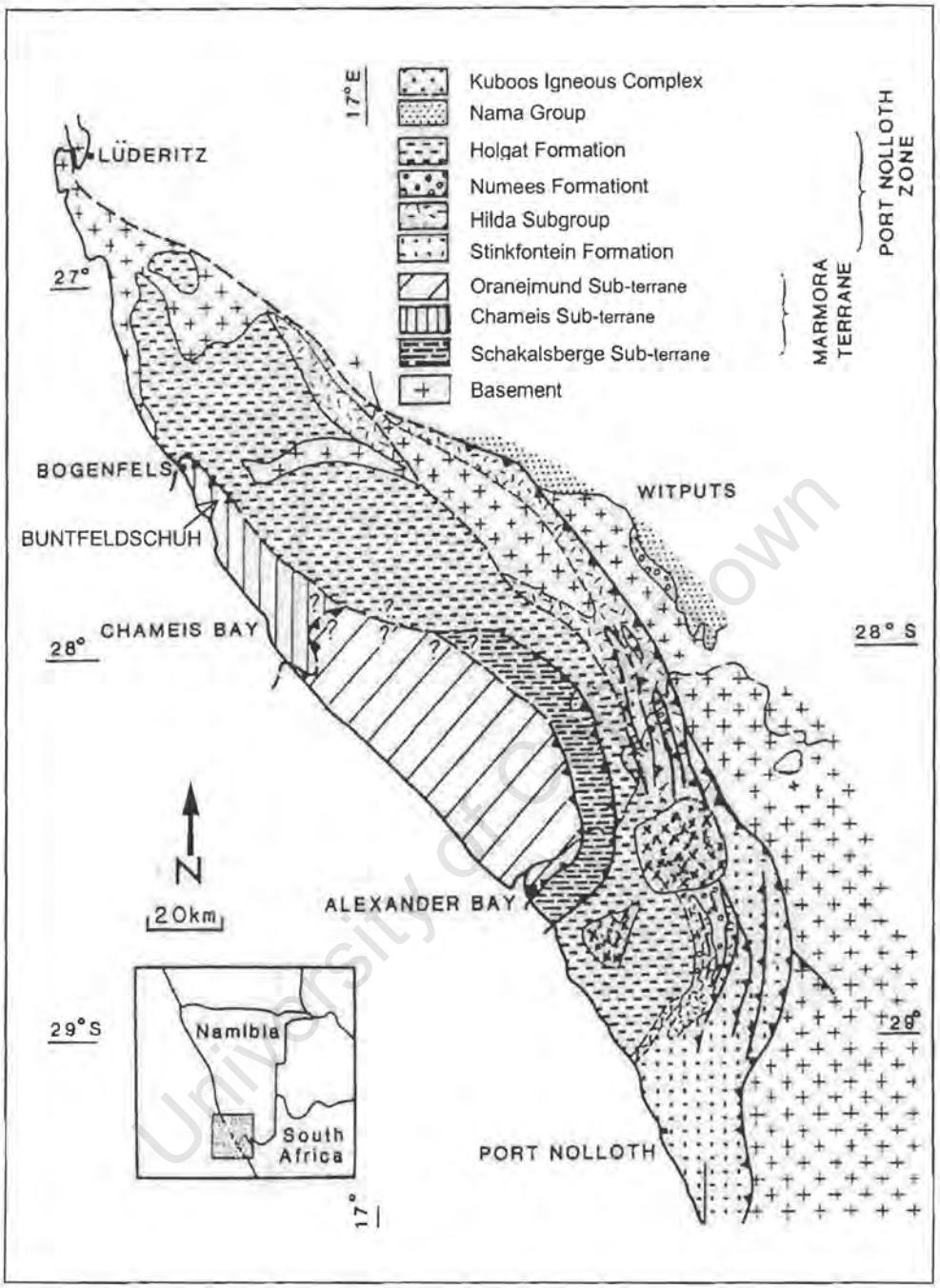

Figure 1.5 Tectonostratigraphic subdivision of the Gariep Belt (after Hartnady and Von Veh, 1990).

Wave-cut platforms (that have been cut into the rocks of Oranjemund Group) of Pliocene-Holocene age (Hallam, 1964; Kalbskopf, 1978) are, with some exception, the most landward preserved of a series of platforms cut by the oscillating sea level from the Eocene to Holocene. At some distance (100 km) in the offshore as well as closer to the coast at depths of 70 m and 130m (Rogers, 1977) marine platforms are present. A poorly preserved marine wave-cut platform also occurs beneath Eocene sediments in the Buntfeldschuh region (Figure 1.5) and they are related to an Eocene high stand of about 170m (Stöcken, 1978).

The platforms studied here are therefore probably re-cut into what was almost certainly a major surface truncation of Eocene age. In the area studied, there is, however, no certain remnant of this truncation surface. The ages of the diamondiferous beaches are summarised in Figure 1.4. There are no known ages for the platforms underlying these beaches. An assumption therefore has to be made that the cutting ages for these platforms are more or less the same as the age of the overlying gravel.

Incision into platforms that causes potholes and gullies to form is not uncommon (Wright, 1964). Diamonds can be trapped in these, and the development of gullies and potholes on platforms plays a fundamental role in diamond concentration in the study area. Despite their economic significance, the spatial relationships and distribution of diamond trapsites are to date not fully understood.

An impressive sea cliff (up to 4 m high – Figure 1.3) backs Kalbskopf's (1978) six major marine platforms (Figure 1.4) in places. The older bedrock platforms (platforms 1-4) have been preserved owing to a cover of diamondiferous conglomerate in the study area that has, in turn, undergone additional erosion. The four older platforms are characterised by smooth wave-cut platforms and slope-controlled gullies that have originated through the

abrasive effect of boulders agitated in wave surges. On the two younger platforms structural features in the bedrock determine the orientation of gullies because of the lack of boulders as abrasive agents in the system. The older platforms host higher diamond concentration than the younger marine platforms but in both cases diamond concentrations remains a function of the amount of reworking of diamondiferous gravel (Kalbskopf, 1978).

Although the area has been mined for more than 60 years, the spatial relationships of the marine erosion patterns have not been documented and the genesis of these erosion patterns on the bedrock is not fully understood. New technology "Airborne Laser Survey" (ALS) (methodological details in appendix) has made it possible, for the first time, to obtain accurate (within 30 cm) elevations for the outcrop over the whole study area which has made accurate correction of ortho-photos possible. By determining the spatial relationship and genesis of the marine erosion patterns it will become possible to predict the nature of marine erosion patterns in the inner shelf area adjoining the study area.

A better understanding of the marine erosion patterns will assist in developing a method to identify areas with a very high likelihood for diamond concentration to the direct nearshore (where Holocene shelf and deltaic sediments (Rogers, 1977a) are absent) between the Orange River mouth and Chameis Bay. A detailed documentation of the main structural features and lithological and geochemical variations in the Oranjemund Group will not only aid in interpreting the marine erosion patterns. It will also aid in determining the source for the sediments of the Oranjemund Group and in determining the palaeo-geographical position of the Oranjemund Group.

The principal aims of this study are, therefore, to determine the lithology, structural geology and geochemistry of the Oranjemund Group and to establish the nature and control of marine erosion patterns on the bedrock surface of the vigorous southwestern coast of the Sperrgebiet in Namibia.

CHAPTER 2 – REGIONAL GEOLOGY

2.1 Precambrian to Palaeozoic

The composite mega-continent Gondwana consisted of six or more pre-1.0 Ga cratons welded together by Pan-African/Brasiliano orogenic belts. These orogenic belts resulted from the closures of Neoproterozoic basins and were internally disrupted as a result of collision indentation and lateral extrusion (Hoffman, 1999). The Congo and Kalahari Cratons were loosely joined by the Zambezi Belt about 820 Ma (Hanson *et al.*, 1994). The western and central portion of the join re-opened and did not finally close until 600-550 Ma forming the Damara and Katangan Belts (Wilson *et al.*, 1997). Closure of the southern Adamastor Ocean (Hartnady *et al.*, 1985) can be taken as the time when the Kalahari passive margin entered the subduction zone dipping beneath the active South American margin.

In Southern Africa the composite Kalahari Craton is partly surrounded by the Pan African Zambezi Belt, Damara Belt and Gariep Belt (Figure 2.1). The Gariep Belt occurs as a south-trending arcuate tectonic belt and is underlain by the 1.0 Ga Namaqua-Natal Metamorphic Belt. The Gariep Belt extends up to 70 km inland where exposures can be viewed (Figure 2.2) in the Richtersveld region between 80 km south of the Orange River and the Orange River. Towards the south the Gariep Belt strikes out to sea and re-emerges over a short distance in an erosional window at 31° S along the South African west coast and then continues into the Saldania Belt (Figure 2.1).

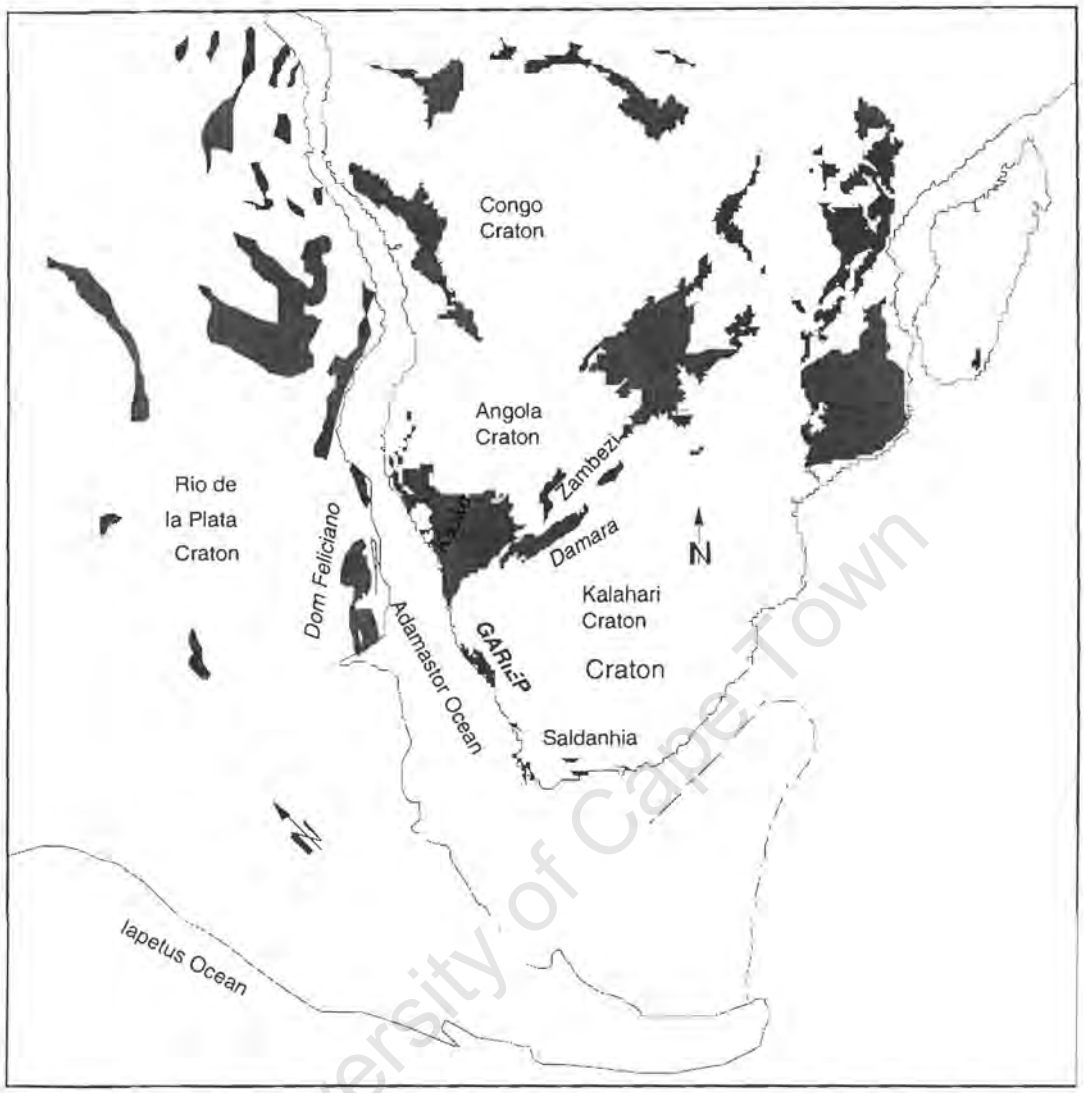

Figure 2.1 The position of the Gariep Belt within a network of Neoproterozoic/ early Palaeozoic orogenic belts (after Frimmel, 2000a).

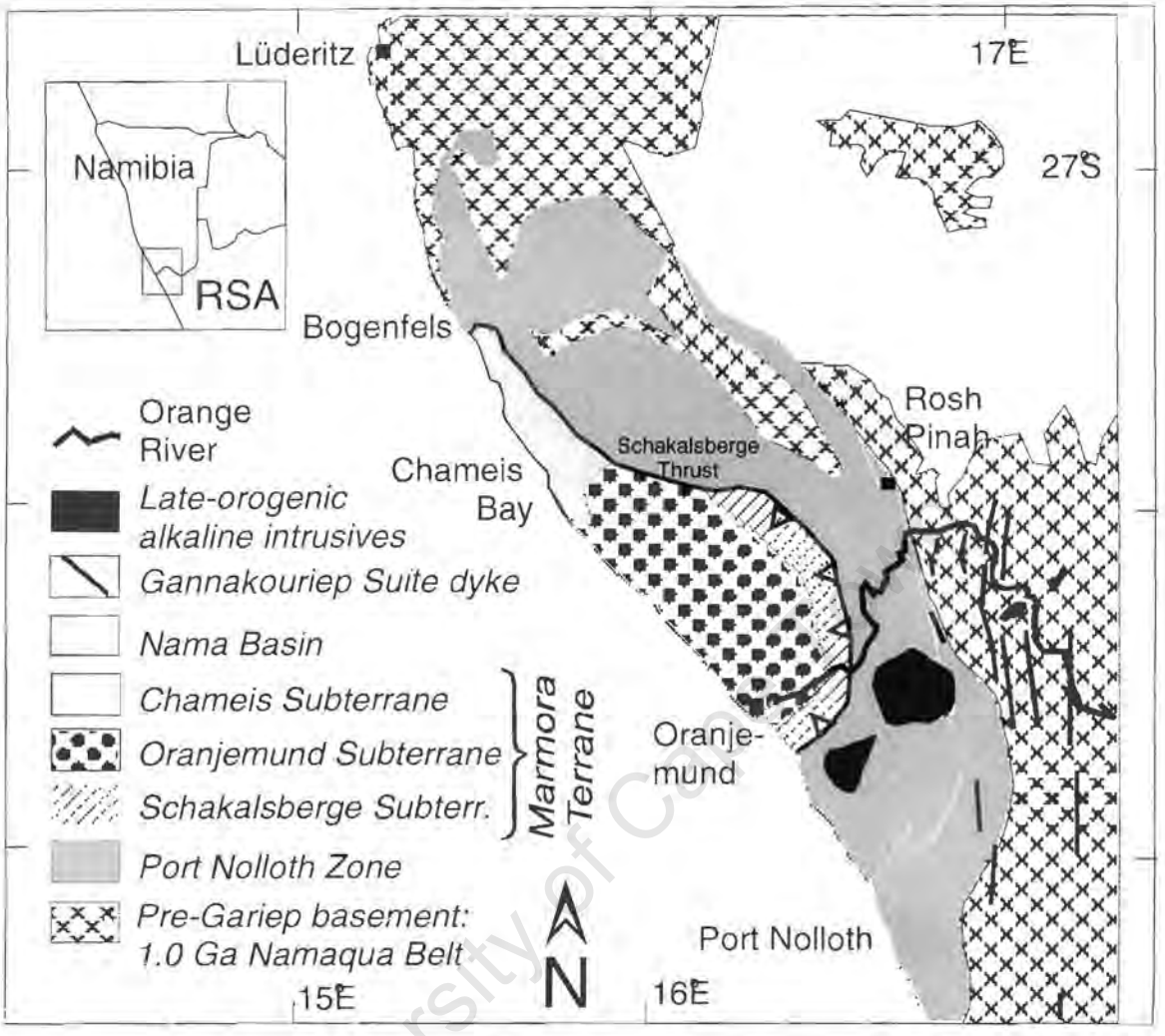

Figure 2.2 Tectonic subdivision of the Gariep Belt (Frimmel, 2000a).

The 540-550 Ma Gariep Belt consists of low-grade metamorphic volcano-sedimentary successions, which include two diamictite units that are overlain by carbonates. The predominantly siliciclastic sediments of the Nama Group were deposited in an active foreland basin known as the Nama Basin (Germs and Gresse, 1991). The Schakalsberge and Chameis Sub-terranes consist largely of metamorphosed mafic volcanic and intrusive rocks capped by dolomite and minor siliciclastic metasedimentary rocks. In contrast, the Oranjemund Sub-terrane lacks any significant igneous component and is made up of predominantly siliciclastic rocks of low metamorphic grade referred to here as the Oranjemund Group. Geochemical and petrological studies on the Schakalsberge

and Chameis Sub-terranes (Frimmel et al., 1996a) indicate an oceanic setting for these units, characterised by oceanic seamounts or an aseismic ridge. In the Chameis Sub-terrane relics of mid-oceanic ridge material were also found.

2.1.1 The Port Nolloth Zone

The Port Nolloth Zone (PNZ) (Figure 2.2) consists of a thick heterogeneous sequence of sedimentary rocks, including quartz arenite, shallow marine siliciclastic rocks and carbonate sedimentary rocks, with minor volcanic intercalations (Port Nolloth Group). At its base, the Stinkfontein Subgroup comprises a siliciclastic continental rift graben sequence, accompanied by bimodal, predominantly felsic volcanism. This is overlain by a locally developed proximal glaciogenic diamictite (Kaigas Formation) followed by carbonate shelf sediments, which contain intercalated near-shore volcanic deposits (Hilda Subgroup). A massive diamictite horizon (Numees Formation) formed during a second glacial period. The Numees Formation is capped by carbonates and siliciclastic metasedimentary rocks of the Holgat Formation (Figure 2.3) (Frimmel, 2000a).

2.1.2 The Marmora Terrane

The Marmora Terrane (MT) comprises three tectonostratigraphic units: the Schakalsberge Sub-terrane, the Oranjemund Sub-terrane and the Chameis Sub-terrane (Hartnady and von Veh, 1990; Frimmel, 2000a). The MT was thrust over the PNZ in a southeasterly direction (Davies and Coward, 1982; Hartnady and Von Veh, 1990) giving rise to a major tectonic discontinuity, the Schakalsberge Thrust (Figure 2.2). The frontal part of the belt in the south-east is dominated by compressional structures and the eastern part by transpressional structures due to oblique collision (Davies and Coward, 1982; Von Veh, 1993).

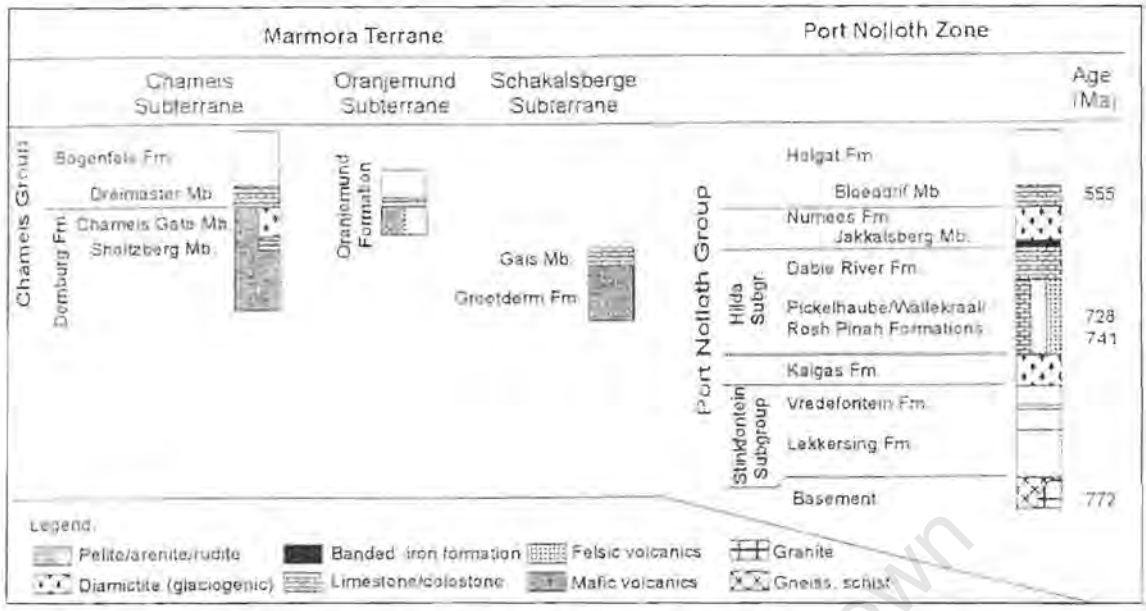

Figure 2.3 Stratigraphic subdivision of the Gariep Supergroup, with proposed correlations between the Marmora Terrane and the Port Nolloth Zone (after Frimmel, 2000a).

The Schakalsberge Sub-terrane is tectonically emplaced on top of the rocks of the Holgat Formation (PNZ) along the Schakalsberge Thrust. The predominant rock type of the Schakalsberge Sub-terrane is metabasite of the Grootderm Formation which is capped by reef dolomite of the Gais Member (Figure 2.3). The Grootderm Formation consists of aphyric, porphyritic and amygdaloidal metabasalt of alkaline composition, which was intruded by serpentinized picrite and alkali metagabbro near its base (Frimmel *et al.*, 1996a). Pillow structures and abundant hyaloclastites are testimony to a relatively shallow subaqueous eruption. The metavolcanic rocks have geochemical signatures typical of oceanic within-plate basalts indicating a seamount or aseismic rise, rather than an intra-continental or near-continental margin setting. The depositional environment may be compared with that of a guyot with a local shallow-water environment allowing reef growth during the waning stages of volcanism (Frimmel *et al.*, 1996a).

The Oranjemund Sub-terrane consists of metasedimentary rocks and chlorite schist of the Oranjemund Group. This area has been subject to intense folding with the development of isoclinal folds and axial-planar foliation (De Villiers and Söhnge, 1959). This makes it very difficult to estimate the stratigraphic thickness of the Oranjemund strata on the basis of the average orientation of graded beds.

The Chameis Sub-terrane is exposed in a narrow coastal strip between Bogenfels and Chameis Bay (Figure 2.2). The primary lithological contacts are obscured by isoclinal folding and thrusting thus inhibiting a lithostratigraphic subdivision (Frimmel, 2001a). The lowermost unit of the broad volcano-sedimentary sequence consists of thinly laminated greenschist, representing former tuff beds and intercalated metapelite, mafic hyaloclastite, metamorphosed alkali basaltic lava flows, and serpentinized picrite, all of which form the bulk of the so-called Dernburg Formation (Frimmel *et al.*, 2000c) (Figure 2.3). The presence of exotic dropstones in the mafic sequence is ascribed to ice rafting at the time of volcanism (Frimmel and Jiang, 2001). Similarly to the Grootderm Formation, the association of metabasalt, hyaloclastite and stromatolitic dolomite in the Dernburg Formation is interpreted as reflecting a former guyot on which algal reef growth took place (Frimmel, 2000a). The dolomite in this case is underlain by a thin layer of chert.

2.1.3 Structural evolution

The arcuate shape of the Gariep Belt is related to D1 collisional tectonism (Gresse, 1994). The most penetrative schistosity S_1 developed during D1. s_1 is sub-parallel to S_0 and almost horizontal in the west of the PNZ but steepens towards the margin of the belt (closer to the basement in the east) (Gresse, 1994). Local isoclinal folding of basic schists and metasedimentary rocks produced a new axial planar schistosity. These isoclinal folds are probably synchronous with the emplacement of the Marmora Terrane and are not found in the underlying rocks of the PNZ (Davies and Coward 1982). The PNZ contains a

number of dominant stress vectors. In the northern and north-eastern parts of the PNZ, F_1 folds are northeast-vergent (Davies and Coward, 1982), but they swing to east and southeast-vergent in the eastern and south-eastern parts (Von Veh, 1993). The east-west collision of a western semi-circular, oceanic crustal block (MT) with a concave continental margin (PNZ) in the east could explain the radial distribution of dominant stress vectors (Frimmel, 2000a).

The contact between the Oranjemund Sub-terrane and the Schakalsberge Sub-terrane is a south-east verging thrust fault with top-to-southeast transport direction. The Oranjemund Sub-terrane has been thrust on top of the Schakalsberge Terrane along this fault. The nature of the tectonic contact between the Chameis Sub-terrane and the Oranjemund Sub-terrane is unclear, but Hartnady and Von Veh (1990) suggested that the Chameis Sub-terrane has been thrust on top of the Oranjemund Sub-terrane.

The main phases of deformation can thus be described as follows. Firstly, an east-west compression (D_1) that evolved into secondly, sinistral transpression and plane wrenching (D_2) with top to the southeast transport. Subsequent deformation (D_3) mainly recorded in the PNZ, is related to southeast-trending sinistral transtension (Frimmel, 2000a).

2.1.4 Comparison between MT and PNZ

Tectonic dismemberment complicates the stratigraphic correlation between the MT and the PNZ, although geochemical data ($\delta^{13}C$, $^{87}Sr/^{86}Sr$; Fölling *et al.*, 1998) and certain lithological characteristics permit some comparisons to be made. A correlation between the diamictite beds in the Gariep Belt and those in the Damara Belt remains problematic. Ar-Ar ages in excess of 600 Ma obtained on relics of the oldest of three amphibole generations in metagabbro from the Chameis Sub-terrane (Frimmel and Frank, 1998), indicate that the mafic magmatism in the MT must have commenced prior to the glacial period of

deposition of the Numees Formation (Frimmel, 2000a). An age for the Numees Formation diamictite is assumed to be correlated with the global 580 Ma Varangian glaciation (Figure 2.4).

The mafic volcanism in the Chameis and Schakalsberge Sub-terranes is believed to have commenced prior to the deposition of the Numees Formation glacial deposits, i.e. during Hilda Subgroup times (Frimmel, 2000a). The change from a continental-rift to a carbonate-platform environment in the PNZ would therefore coincide with the formation of oceanic crust in the MT (Frimmel, 2000a).

The PNZ experienced one regional metamorphic overprint that can be ascribed to crustal thickening due to thrusting and the loading of the MT on top of the PNZ. The mafic rocks of the MT experienced a multiphase metamorphic overprint not recognised in the surrounding sedimentary rocks (Frimmel and Hartnady, 1992). The peak of metamorphism (lower greenschist) in the surrounding siliciclastic rocks was of lower grade than in the PNZ (uppermost greenschist facies) (Frimmel, 1995).

The minimum age for the Oranjemund Group within the constraints of the Gariep Belt is the start of metamorphism at 545±2Ma (Reid *et al.*, 1991; Frimmel and Frank, 1998). The maximum age for the Oranjemund Group is the age obtained from the Lekkersing granite at the base of the Port Nolloth Group of 771±6Ma (Frimmel *et al.*, 2000d). The timing of rift-related magmatism (741 Ma) in the Gariep Belt is within error of that in the northern Damara Belt 756±2 and 746±2 Ma (Hoffman *et al.*, 1996). Ocean closure and formation of an accretionary prism and a continental magmatic arc associated with eastward dipping subduction of the Rio de la Plata Craton (Figure 2.1) are recorded in the Vila Nova and Tijucas Belts in southern Brazil which took place at about the same time that rifting took place in the Gariep Belt (Chemale, 1998, da Silva *et al.*, 1997).

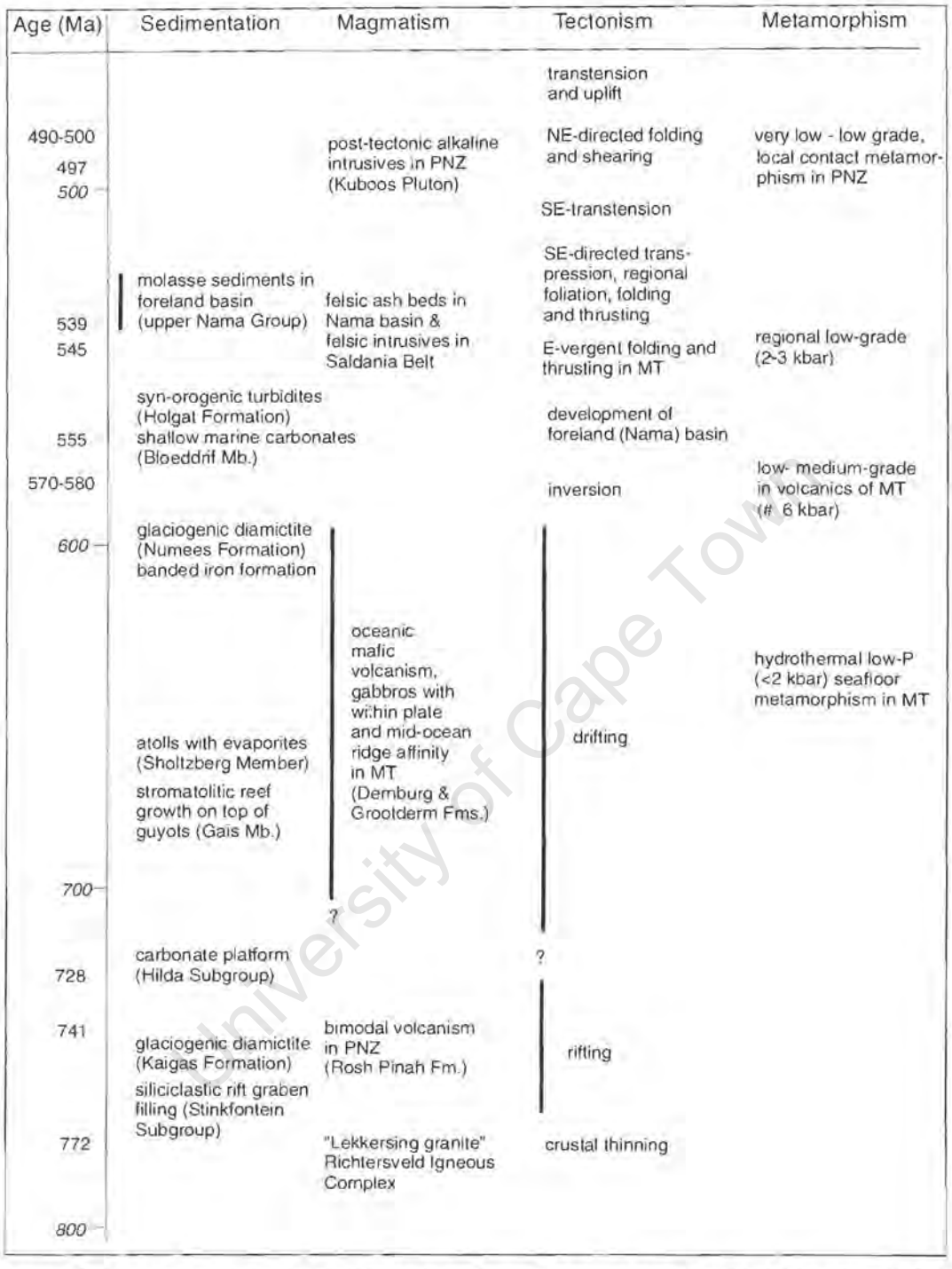

Figure 2.4 Summarised chronological evolution of the Gariep Belt (Frimmel, 2000a)

2.2 Mesozoic to Holocene

The splitting up of Gondwana led to the deposition of Cretaceous to modern sediments upon the rifted Late-Proterozoic bedrock (usually within a few

kilometres of the present coastline) (Rogers, 1977a) along the south western coast of Africa. The Orange River is the main supply of sediment to the Atlantic Ocean in southern Africa (Jacob *et al.*, 1999) and has been active for at least 100 m. y. (Dingle and Hendey, 1984; Ward and Bluck, 1997). Epeirogenic uplift of the subcontinent around the Cretaceous-Ternary boundary led to the incision of a mature, meandering Orange River (Ward and Bluck, 1997).

The delta of the Orange River has changed from a fluvial dominated delta in the Cretaceous, to a wave-dominated delta in the Cenozoic. By Eocene times a northward longshore drift and prevailing southerly wind regime were strengthened by arid to hyper-arid conditions along the Namibian coast during the Neogene (Siesser, 1978). A shelf by-pass system gave rise to thick mud belts offshore central Namibian coast, and desert sand seas onhore (Rogers, 1977). The nature of sediment outfall has changed, largely in response to continental uplift, from fine-grained (clays, silts and sands) in the Late-Cretaceous to progressively more coarse grained clastics through to the Neogene into the Quarternary (Partridge and Maud, 1987; Ward and Bluck, 1997). Clast assemblages of siliceous resistant pebbles including agate, jasper, banded iron-stone and chalcedony were sourced from some rocks of the interior sub-continent since the incision of the Orange River in the Palaeogene. The clast assemblage also contains diamonds and is present in Eocene marine deposits within the Sperrgebiet between Buntfeldschuh and Bogenfels (Stocken, 1978; Ward and Bluck, 1997) (Figure 2.5 and 2.6). Miocene fluvial diamondiferous deposits onshcre at Arrisdrift (Figure 2.5) are dated at 17-19 Ma on an extensive fossil assemblage recovered at Arrisdrift (Pickford, 1987). The +30 m marine package (diamondiferous) found between the Orange River mouth and Chameis Bay is associated with the Meso-Orange River gravels and is in places overlain by the younger (Mid-Pleistocene to Holocene) marine diamondiferous beaches (Figure 1.4) (Hallam, 1964).

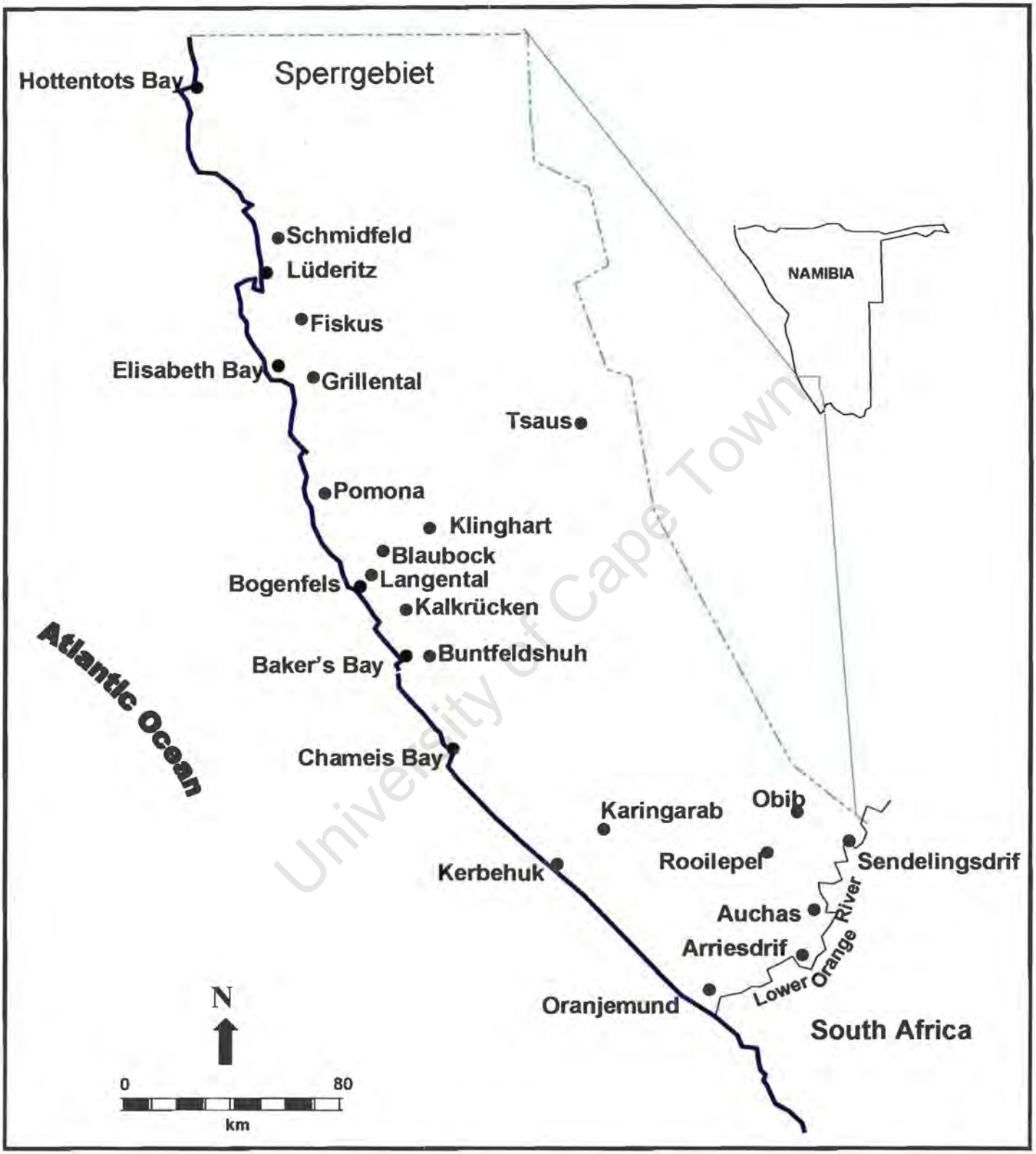

Figure 2.5 Locality map for the Sperrgebiet of Namibia (Ward, 2000)

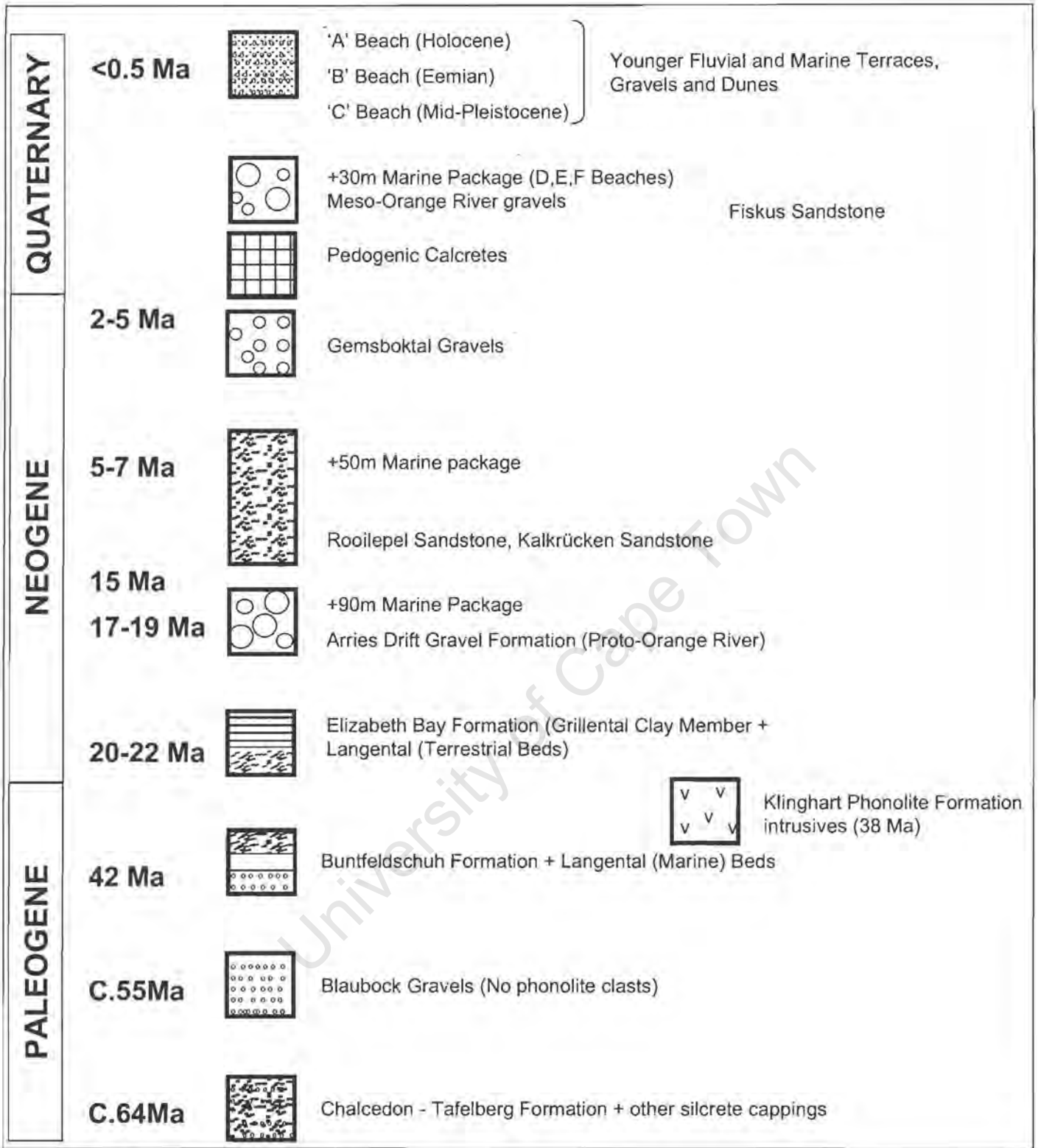

Figure 2.6 Stratigraphic framework for Cenozoic deposits of the Sperrgebiet of southern Namibia (Ward, 2000).

CHAPTER 3 – LITHOLOGY

The Oranjemund Group comprises about 65 volume percent meta-arenite, 30 percent chlorite schist, 3 percent dolomite, 2 percent metacalc-arenite and less than 1 percent chert and banded-ironstone. The meta-arenite and chlorite schist are interlayered, but there are zones where meta-arenite is dominant (Figure 3.1). A small outcrop of dolomite (100m long and up to 3m wide) occurs 30 km north of the Orange River mouth. Chlorite schist occurs in the north near Chameis Bay and in the south near the Orange River mouth. In the north at the contact with the Chameis Sub-terrane, the chlorite schist is, in places, overlain by a very thin (less than 10 cm) chert layer overlain by a metre thick brown carbonate layer (Figure 3.2), which in turn is overlain by siliciclastic rocks. Most of the outcrops display zones of intensive weathering. Methods used include petrography, point-counting (Appendix 8) and (Scanning electron microscope – Cathodoluminescence) SEM-CL. Semi-quantitative spectra produced by the SEM can be used in combination with an image to identify and interpret mineral growth history. The sample conditions for the (Scanning electron microscope) SEM (at the Electron Microscope Unit, UCT) were as follows for all spectra. A beam current of 1100.0 pA, 15.0 kV and a working distance of 25.0 mm were used.

3.1 Chlorite schist

The very fine grained, in places well laminated chlorite schist is green to grey green in fresh outcrop and when weathered it turns grey-brown (Figure 3.3). It is found predominantly in the south of the study area (Figure 3.1). Modal analyses revealed the following mean volumetric proportions: 29.8 % quartz, 57.0 % chlorite, 0.6 % biotite, 4.6 % albite, 1.0 % muscovite, 0.2 % carbonate and 6.8 % opaque minerals. Accessory minerals include zircon, apatite, (Figure 3.4) monazite, hematite, pyrite, titanite and tourmaline. Coarse and fine-grained chlorite occur. Biotite has retrogressed to chlorite in places. The feldspars are albite that appears partly sericitised.

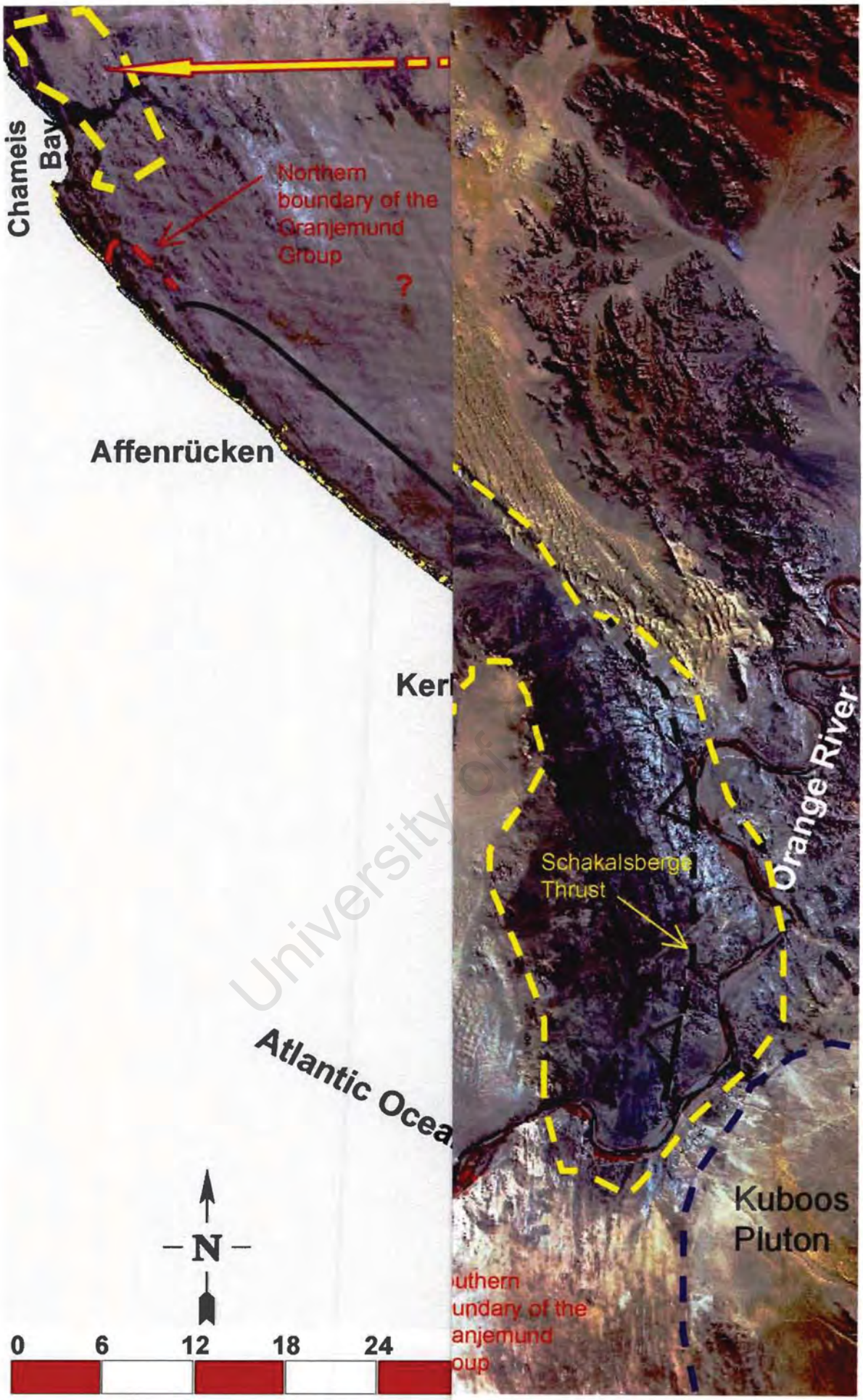

Figure 3.1 Satelilite im green).

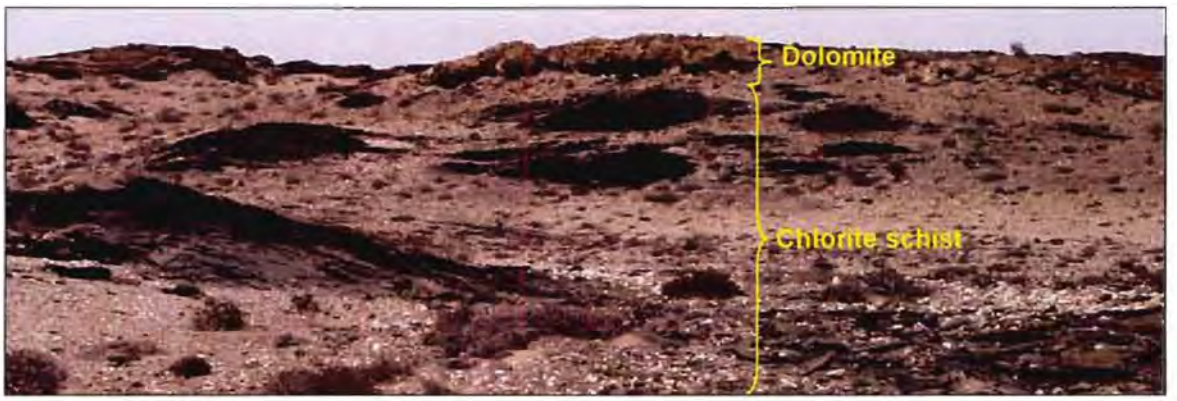

Figure 3.2 Contact between the chlorite schist and the brown dolomite about 6 km south of Chameis Bay.

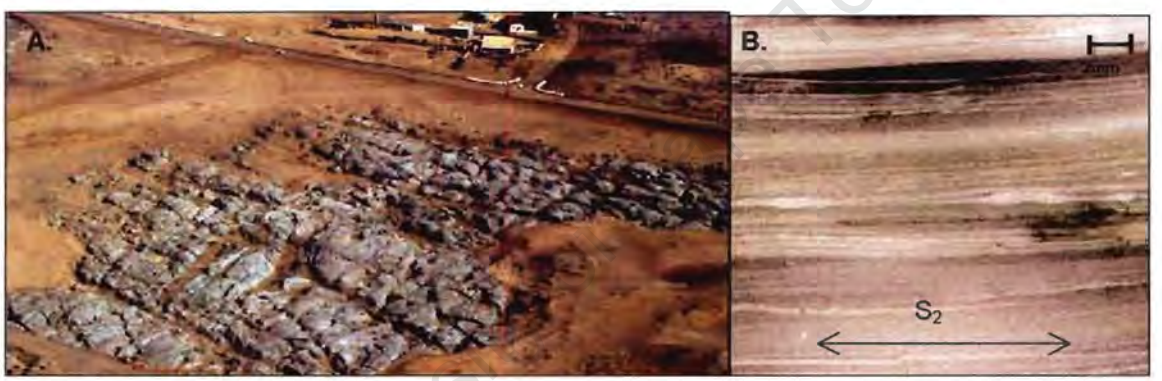

Figure 3.3 A. Aerial photograph of a green to grey-green chlorite schist outcrop (8 km north of the Orange River mouth). **B.** A photomicrograph of thin section (sample JM058) showing alignment of chlorite and micaceous minerals.

Porphyroblasts of albite (up to 2 mm) occur and in places these porphyroblasts show metamorphic growth zonation (Figure 3.5). Some of the feldspars show an in internal fabric of inclusions representing s_1 (Figure 3.6). The matrix comprises very fine grained chlorite, biotite, muscovite, and albite. Quartz occurs as detrital grains and in recrystallized form.

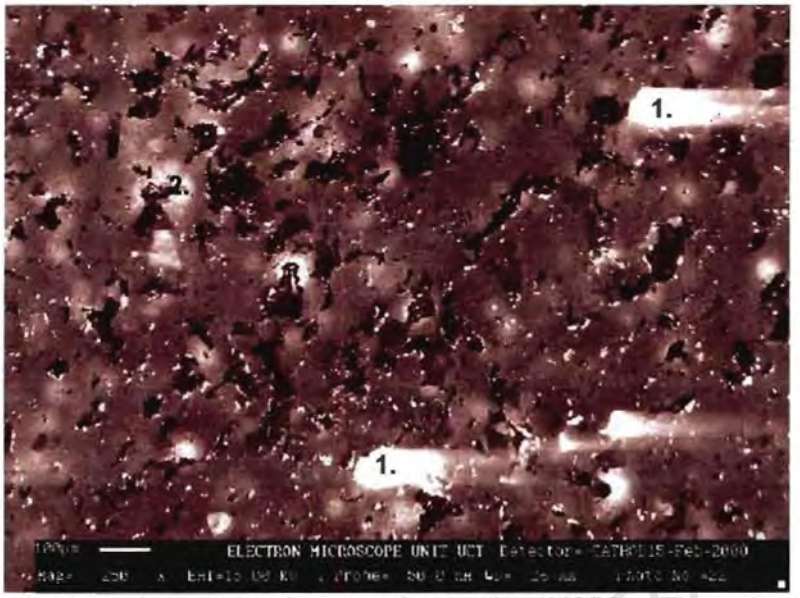

Figure 3.4 Cathodoluminescence image of sample JM058. The minerals with high luminescence here are: 1. apatite and 2. titanite.

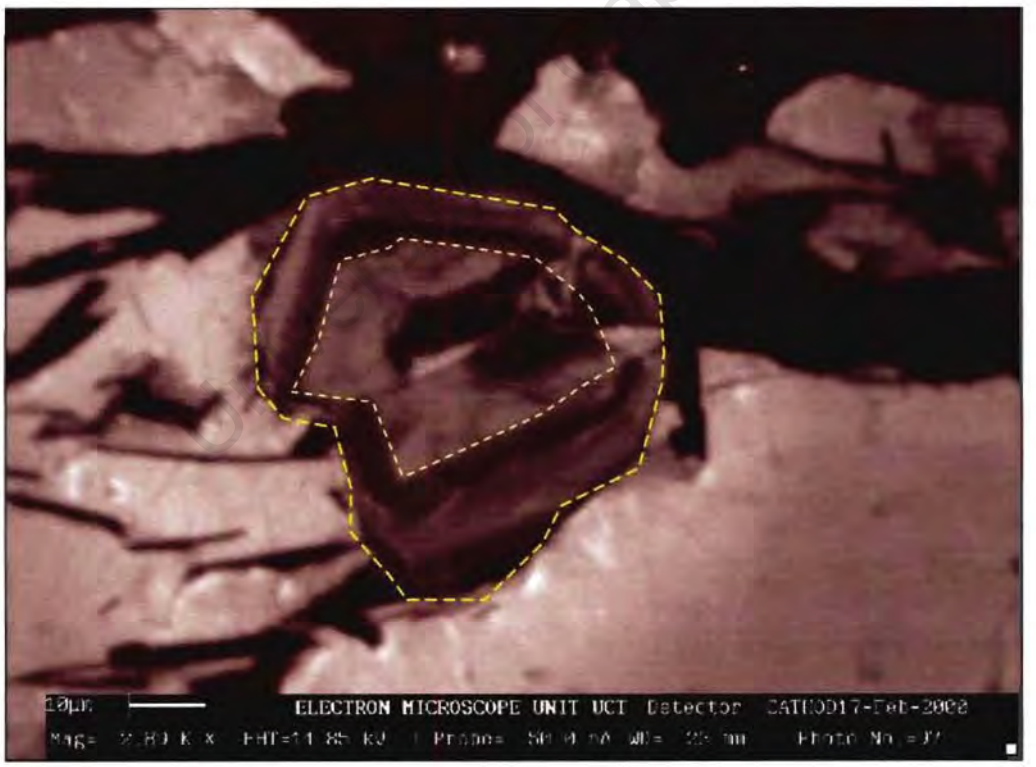

Figure 3.5 Metamorphic growth zonation in a feldspar grain detected using SEM-CL, note the metamorphic concentric growth zones in the grain (sample JM040).

The bedding s_0 has been transposed to bedding-parallel s_2 foliation with the alignment of chlorite and micaceous minerals (Figure 3.7). No lava flow structures were observed in the chlorite schist. Micro-veins (identified with SEM-CL images and transmitted light petrography) are filled with quartz and carbonate minerals. Epidote and pyrite occur in the chlorite schist about 6 km south of Chameis Bay but were not found in the chlorite schist in the south of the study area.

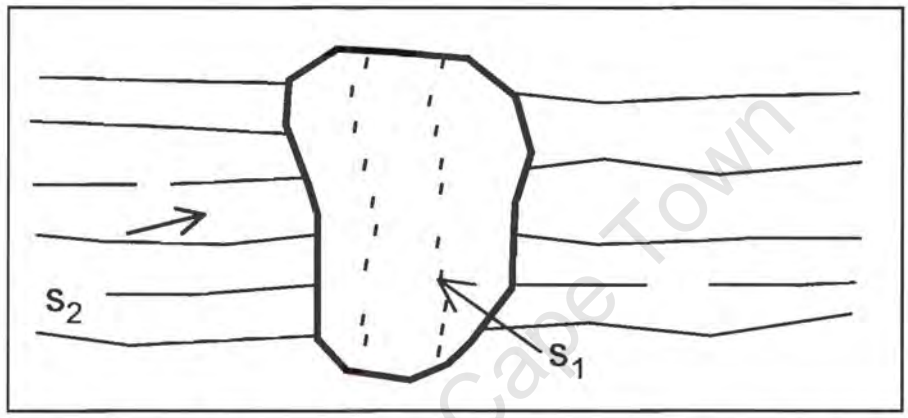

Figure 3.6 Porphyroblast of albite containing inclusions displaying remnants of s_1 in the internal fabric. Meta-arenite 18 km north of the Orange River mouth.

Figure 3.7 Syn-tectonic growth of phyllosilicates (in yellow) with regard to a dominating bedding parallel s_2 foliation. Meta-arenite 22 km north of the Orange River mouth.

3.2 Meta-arenite

Meta-arenite is the dominant rock type in the study area and occurs in the central and northern part (Figure 3.1). In the south there is a graded contact between the chlorite schist and the meta-arenite (Figure 3.8). It occurs in both massive and laminated form (Figure 3.10). The thickness of the laminae varies from less than 1 cm to 10cm. Meta-arenite is interlayered with chlorite schist and the thickness of these layers can vary from 30 cm to 3 m. In places the meta-arenite is highly weathered and in other places gradation within the laminae can be seen. Kröner (1974) interpreted these graded meta-arenites as cyclic turbidites. Fresh outcrop is brown-grey and weathered outcrop ranges from orange-brown, yellow to white. Modal analyses reveal the following volumetric proportions for the meta-arenite: 42.4 % quartz, 35.0 % chlorite, 3.8 % biotite,14.6 % albite, 0.4 % muscovite and 3.8 % organic matter. Accessory minerals include zircon, apatite, monazite, hematite, titanite and tourmaline (Figure 3.9).

The feldspar is albite that appears partly sericitised in places. The same metamorphic zonation of albite as in the chlorite schist is present in the meta-arenite. Metamorphic differentiation produced the alignment of chlorite and micaceous minerals parallel to axial planes in places (Figure 3.11)

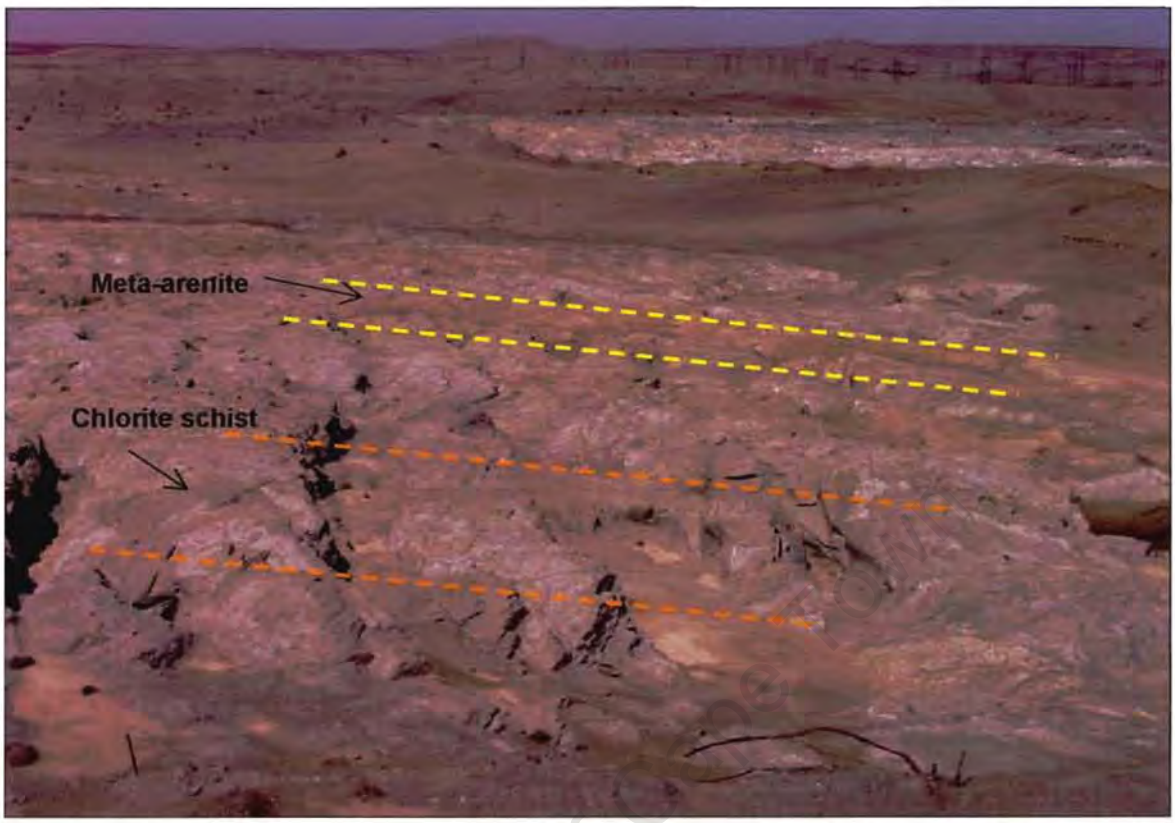

Figure 3.8 A photograph of the graded contact between the chlorite schist and the meta-arenite, 8 km north of the Orange River mouth.

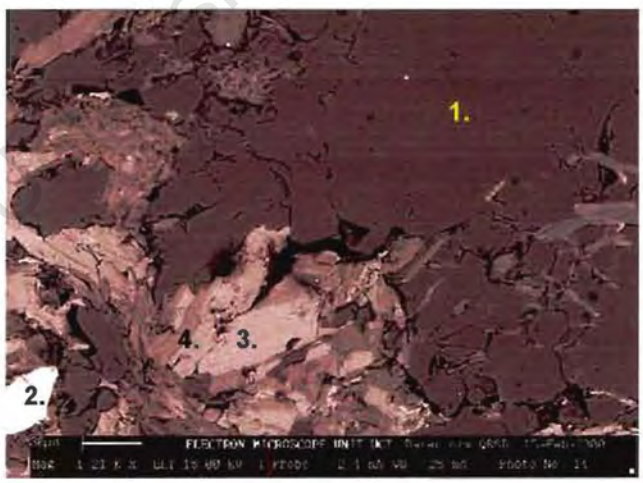

Figure 3.9 Back scatter SEM image. Minerals identified: 1. quartz; 2. zircon, 3. biotite; 4. chlorite (meta-arenite, 20 km north of the Orange River mouth).

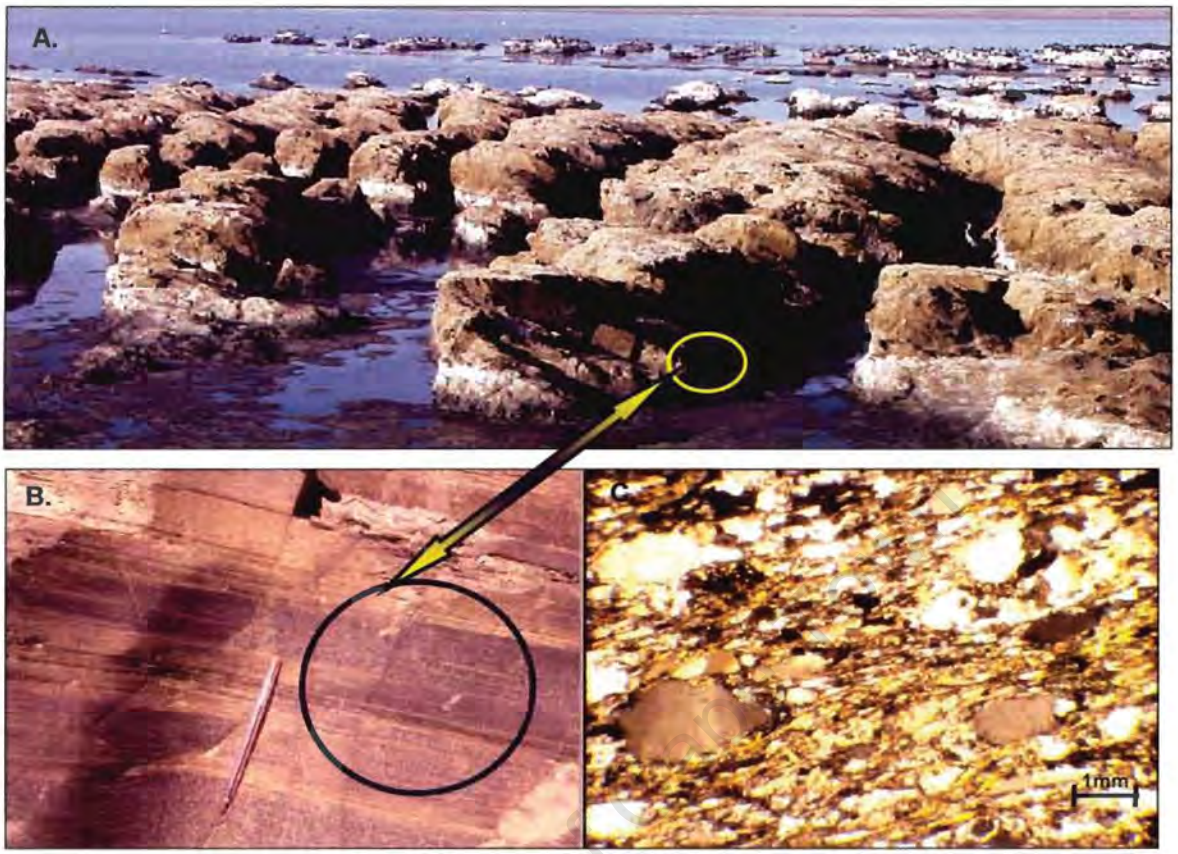

Figure 3.10 A. Meta-arenite (20 km north of the Orange River mouth) in outcrop highly weathered in places. **B**. Graded laminae of meta-arenite. **C**. Photomicrograph of meta-arenite (JM020) with orientated chlorite and mica minerals and detrital quartz, crossed polars.

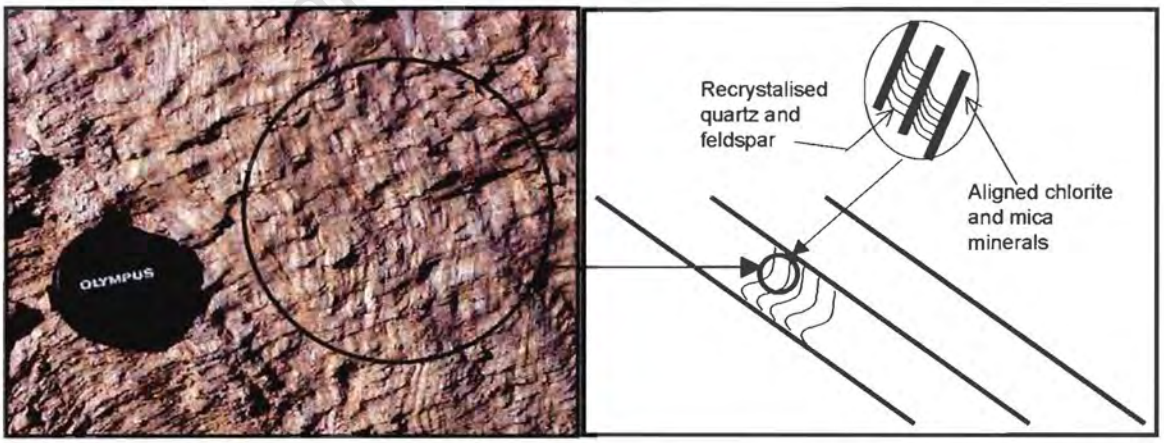

Figure 3.11 A meta-arenite 80 km north of the Orange River mouth .In places evenly spaced, continuous, homogeneous layers (cm scale) occur. This is interpreted as metamorphic differentiation aligned parallel to axial planes.

3.3 Dolomite and Meta-calcarenite

A single dolomite outcrop about 100m long and up to 3m wide (Figure 3.12) striking N-S, parallel to the meta-arenite was found about 30 km north of the Orange River mouth. The white-pink dolomite is very fine grained and comprises dolomite. Calcite and quartz veins cut across the dolomite that is highly fractured in places. The orientation of these veins appears random.

A meta-calcarenite adjacent to the dolomite is purple and shows syntectonic recrystallization and ribbon structures of quartz and comprises more than 50 % carbonate (dolomite), 30 % albite, 10 % quartz, 5 % phlogopite, 4 % hematite and <1 % talc.

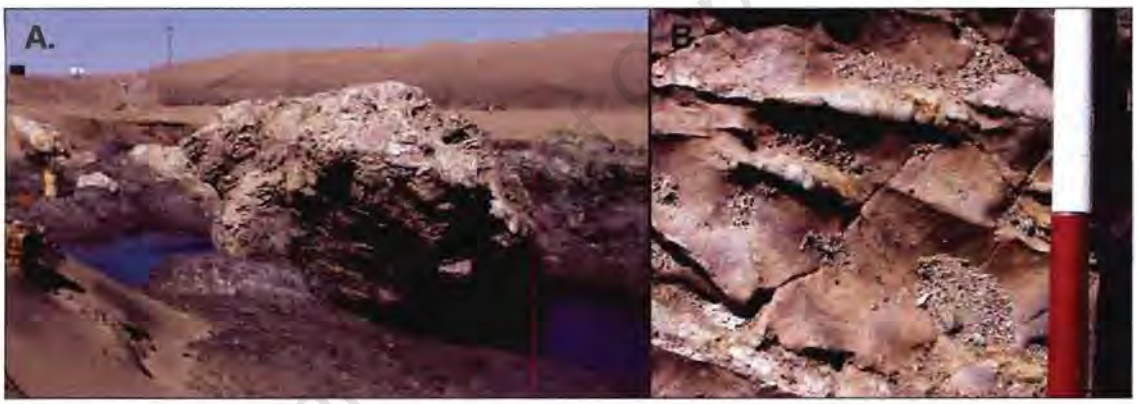

Figure 3.12 A. A single white-pink dolomite outcrop about 30km north of the Orange River mouth. **B.** Quartz and calcite veins (with random orientation) cross cut the highly brecciated dolomite in places.

CHAPTER 4 – STRUCTURAL GEOLOGY

The deformation of the Marmora Terrane is dominated by compressional structures. In order to build up a picture of the deformational history of the Oranjemund Sub-terrane, local structures were documented. Correlation between these local structures was obtained by analysing styles and patterns of orientation of structures.

Previous workers (e.g. Kröner, 1974, and De Villiers and Söhnge, 1959, 1963), found that the original bedding planes (s_0) of the sedimentary rocks in the Oranjemund Formation have been transposed into bedding parallel foliation (s_2), with the alignment of micaceous minerals.

4.1 Foliation

On a micro-structural scale inclusions in albite (Figure 3.6) display remnants of s_1 and micaceous minerals have been aligned to form bedding parallel s_2 foliation (Figure 4.1). The orientation of s_2 on macro structural scale over the whole study is represented in Figure 4.2.

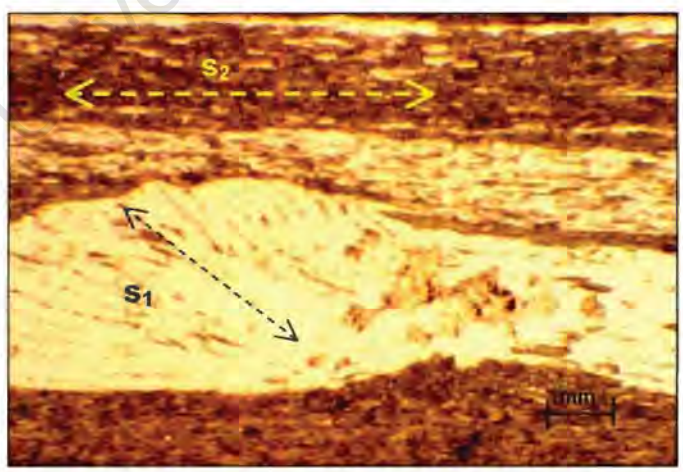

Figure 4.1 Photomicrograph of a thin section (crossed polars) of chlorite schist (JM050) showing s_1 and chlorite aligned along bedding parallel s_2 (8 km NW of the Orange River mouth).

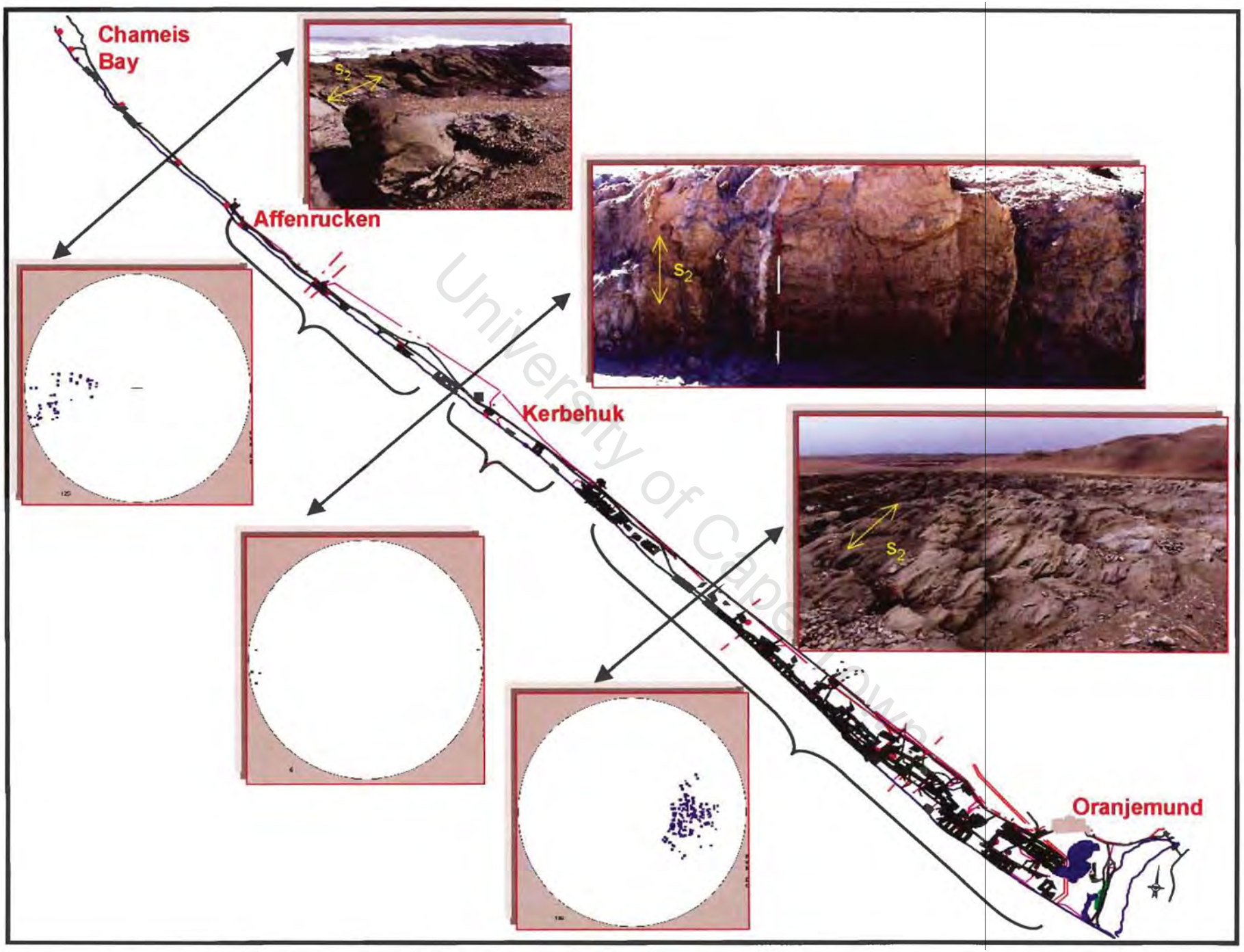

Figure 4.2 Map of MA1 with equal area stereoplots of the poles for s_2 for different areas.

s_2 strikes roughly N-S over the whole study area. A coast parallel traverse (Figure 4.3) across the area revealed three major s_2 orientations: 1. From the Orange River mouth to Kerbehuk, 45 degrees to the west. 2. From Kerbehuk to roughly 15km north of Kerbehuk, 80-85 degrees to the west. 3. From roughly 15km north of Kerbehuk to Affenrücken, 45-60 degrees to the east.

Figure 4.3 Plan view of the strike and dip of s_2 along the study area. The value of each dip and strike direction in this figure has been calculated by using the average of 10 readings 10 metres apart.

4.2 Folding

Large-scale tight parasitic folds are visible in the outcrop along the 120 km coastal strip. The hinges of these parasitic folds strike N-S mimicking the host fold orientation. Tight folds can be observed from micro to macro-scale (Figures 4.4 to 4.6). In some cases (Figure 4.6) it is impossible to measure the plunge of hinges due to the flat surface of the highly weathered outcrop. This flat surface has been created by marine erosion (wavecut platform). Near the contact with the Chameis Sub-terrane, 6 km south of Chameis Bay, NE-SW trending hinges occur. N-S trending hinges as in the rest of the Oranjemund Sub-terrane and in the Chameis Sub-terrane are very prominent especially along the contact between the chlorite schist and the dolomite (Figures 4.7 and 4.8). Open folds (F_3) with NW-SE trending hinges (Figure 4.9), representing late stage buckling, occur near the contact with the Schakalsberge Sub-terrane, just north of the Orange River mouth.

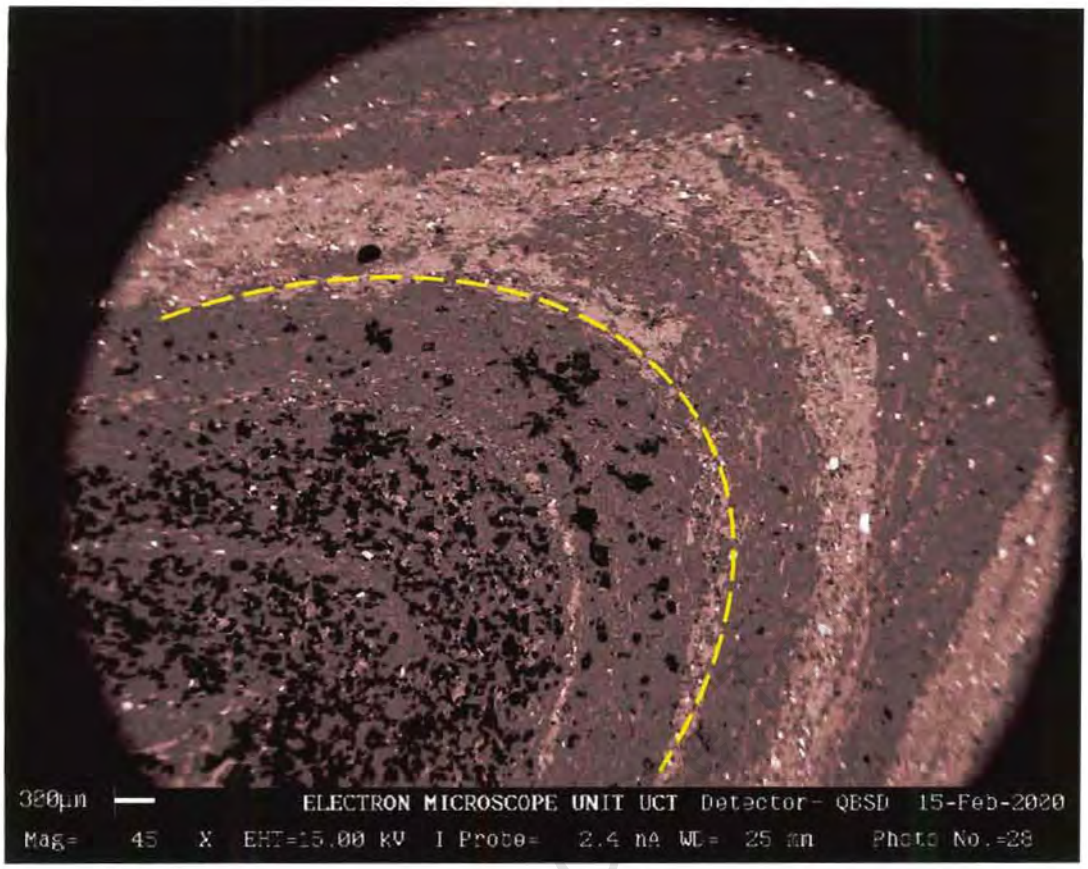

Figure 4.4 SEM Backscatter image showing tight folding on micro-scale (in yellow), sample JM053.

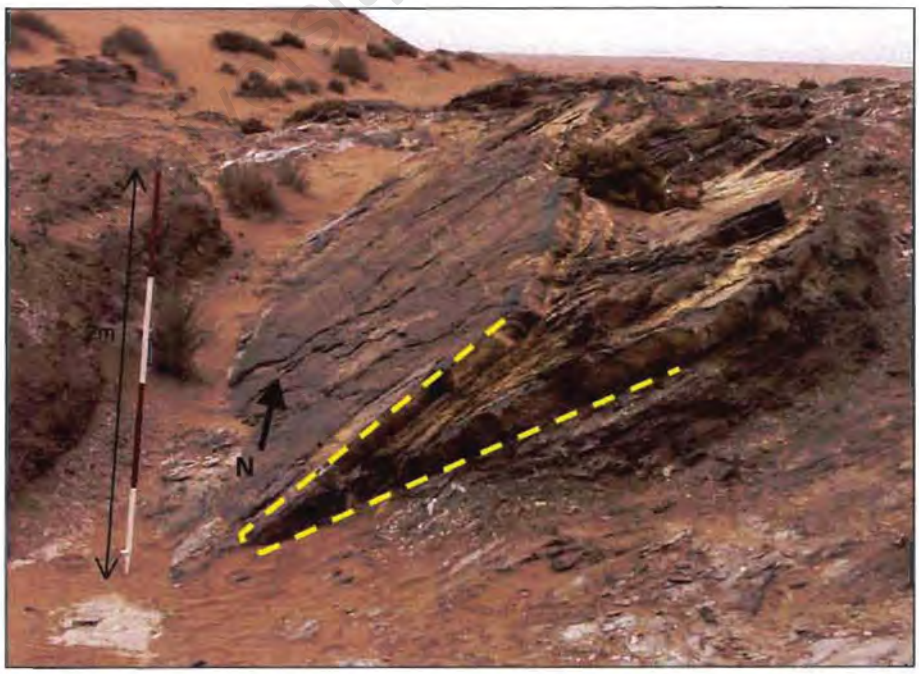

Figure 4.5 Tight folding (metre scale), about 8 km north of the Orange River mouth.

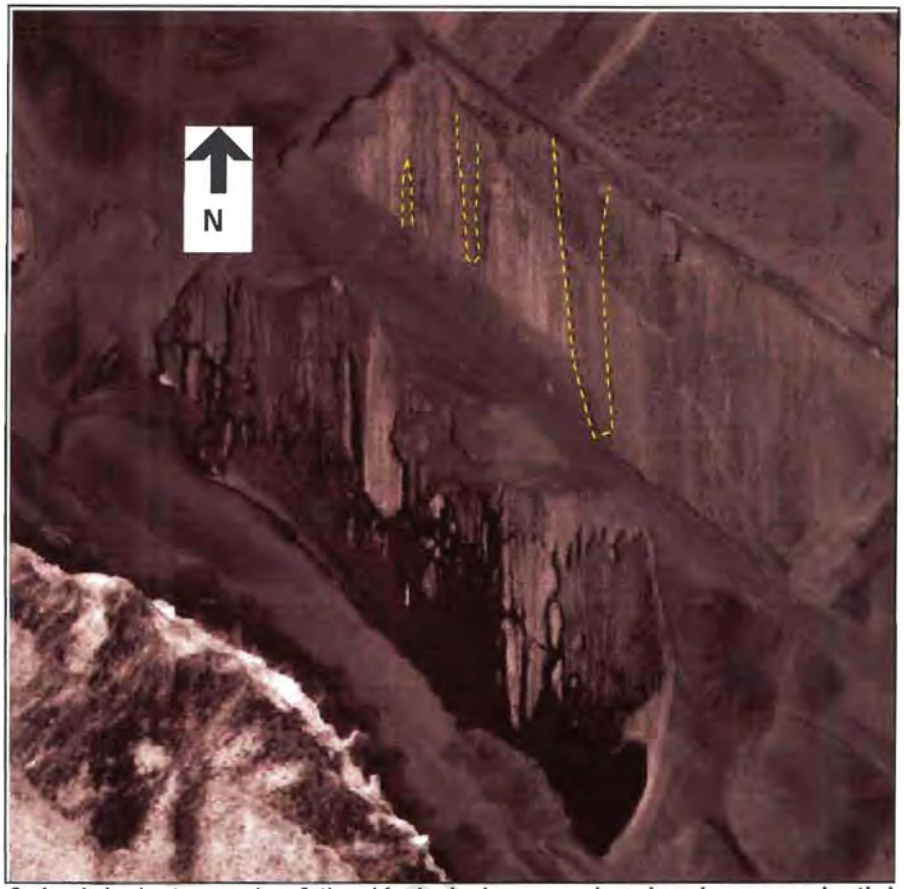

Figure 4.6 Aerial photograph of the Kerbehuk area showing large-scale tight folds, with fold axes striking N-S.

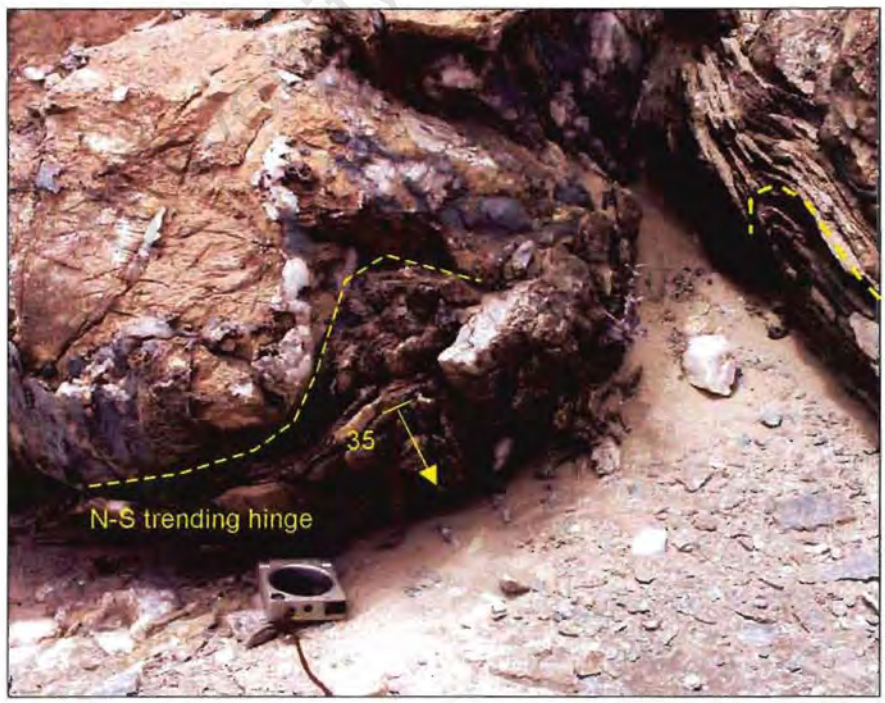

Figure 4.7 N-S trending hinges on the contact between chlorite schist and dolomite 6 km south of Chameis Bay.

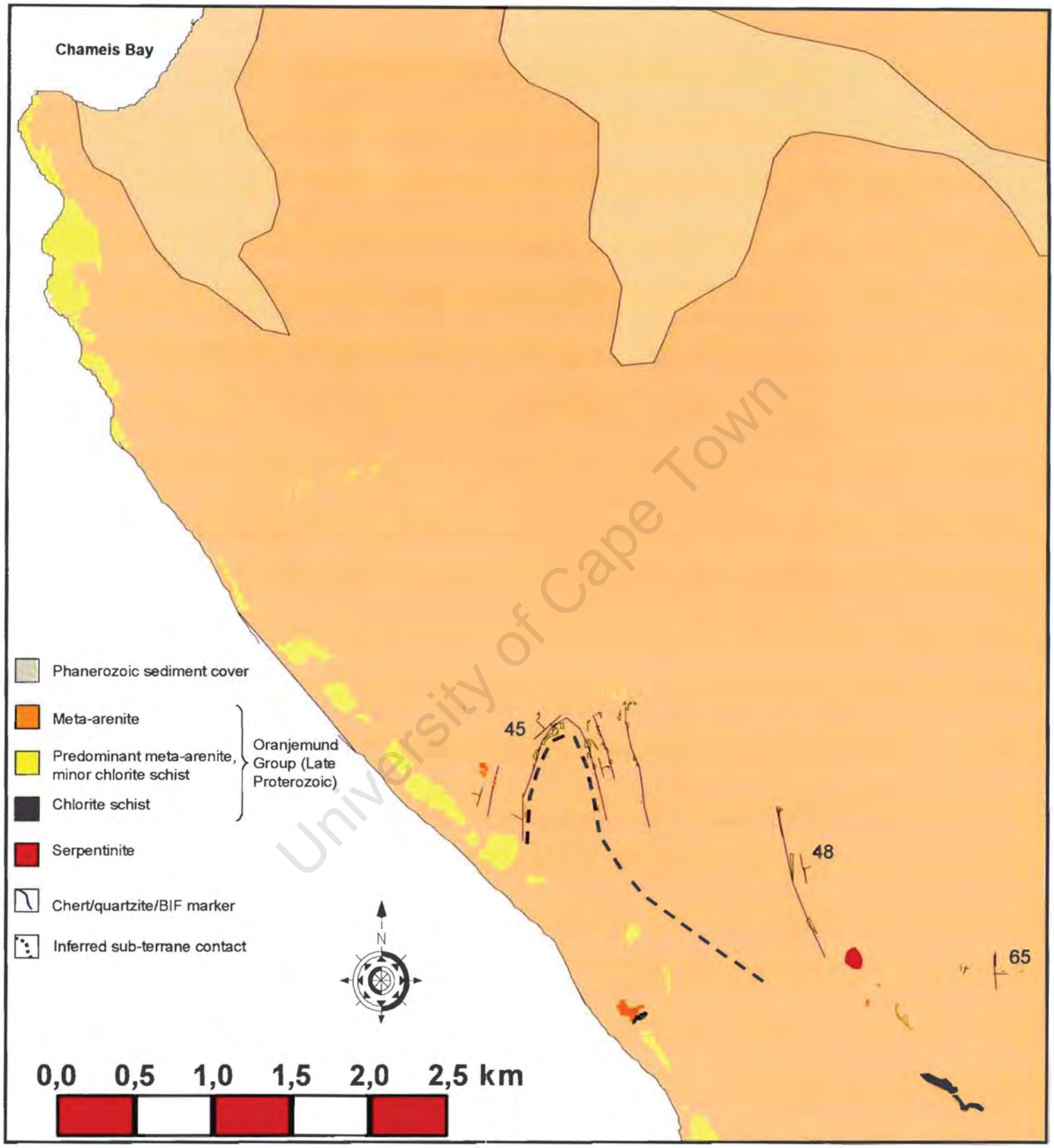

Figure 4.8 Detailed map of the inferred contact between the Chameis and Oranjemund Sub-terranes.

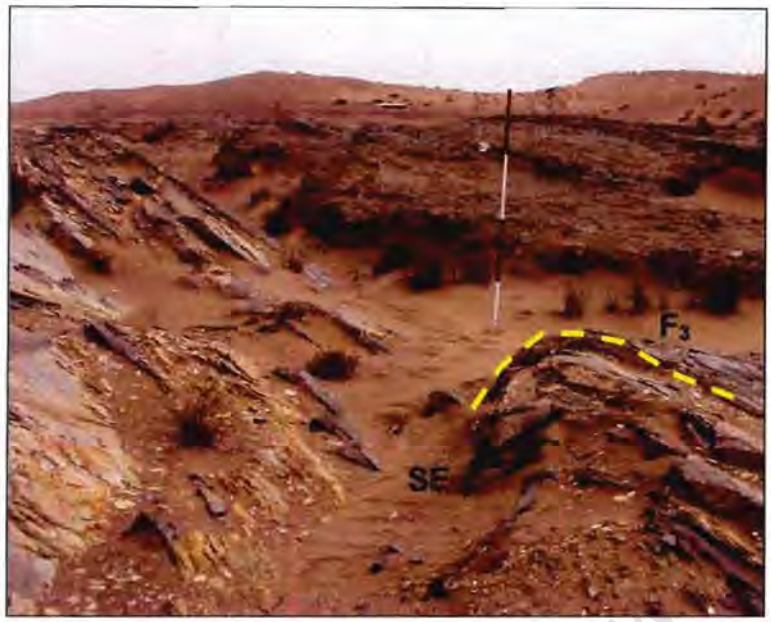

Figure 4.9 F_3 open fold with hinge trending NW-SE, 8 km north of the Orange River mouth.

In folded mixed sedimentary rocks the positions of hinges and direction in which they close (of some large folds) can be predicted from small exposures on the limbs which clearly show cleavage/bedding relations or parasitic Z and S folds (Ramsay, 1967). Different sedimentary rocks react differently to deformation depending on their rock competencies (Figure 4.10). The schistose unit forms tight folds with N-S striking hinges. The more competent arenitic unit does not show any folding and only shows a well-developed N-S striking s_2.

Greater axial thickening can be seen in chlorite schists than in arenites in folded mixed sedimentary rocks (Figure 4.11). The meta-arenites develop spaced cleavage and the chlorite schists slaty cleavage. A stereoplot of the hinges of parasitic folds (Figure 4.12) show a scattered plot of NNW-SSE trending hinges. S-type folds show sinistral vergence and Z-type parasitic folds show dextral vergence (Figure 4.13).

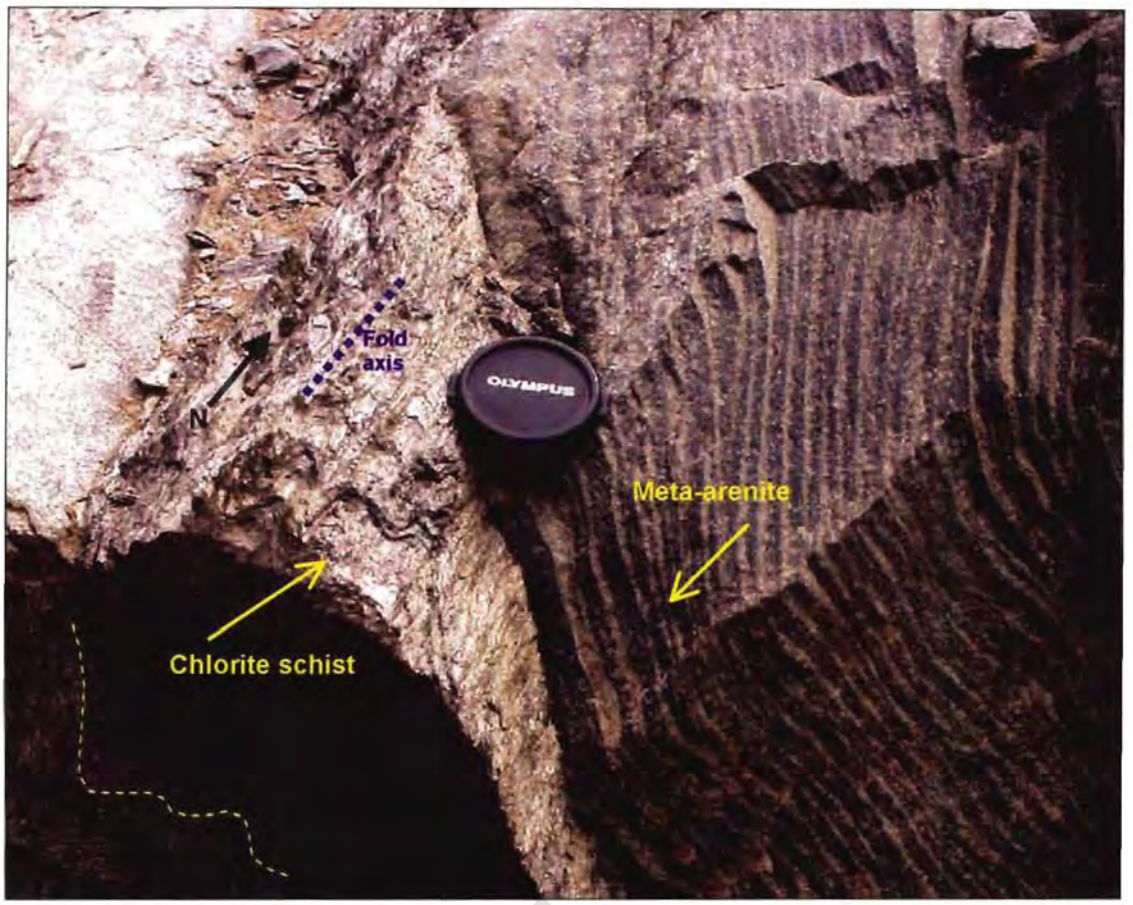

Figure 4.10 Different responses of a meta-arenitic unit and a chlorite schist unit to deformation (85 km north of the Orange River mouth). The fold axis is trending N-S.

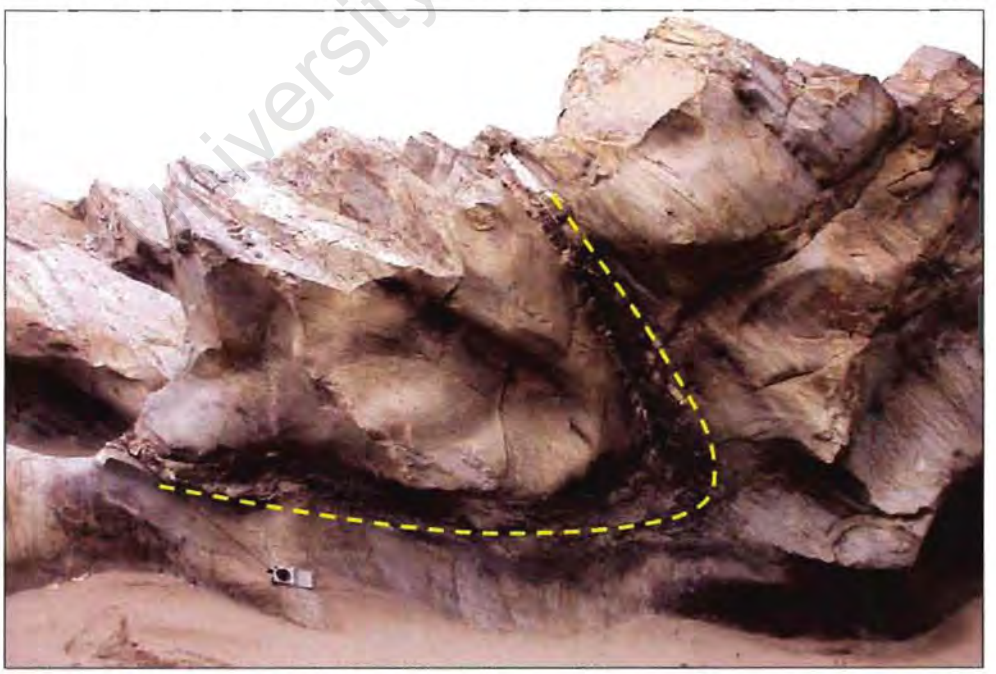

Figure 4.11 A class 2 (similar) Ramsay fold (25 km north of the Orange River mouth), formed in mixed sediment folding. The schistose unit shows greater axial thickening.

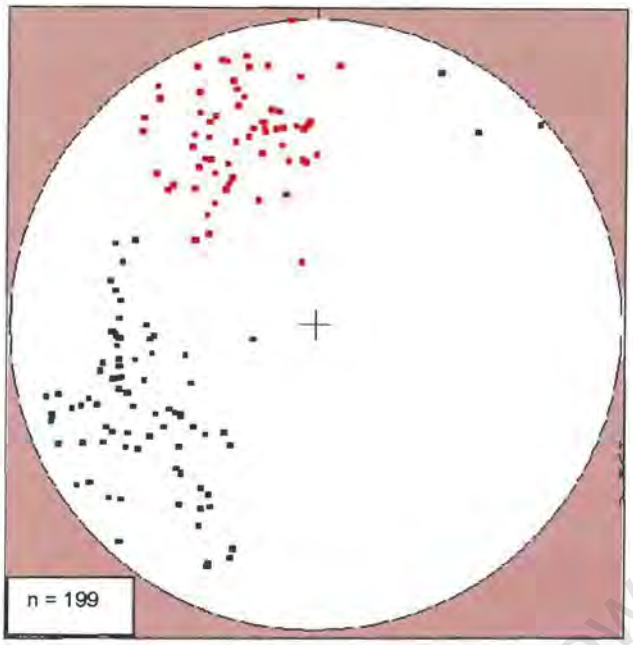

Figure 4.12 Equal area stereoplot of the fold axes. Black dots (F_1) show W to SSW plunging axes and red dots (F_2) show NNW plunging axes.

4.3 Main host fold

The orientation of the main fold axis (84/178) (Figure 4.13) can be calculated by taking the s_2 co-planar bedding readings and plotting their poles on an equal area stereoplot.

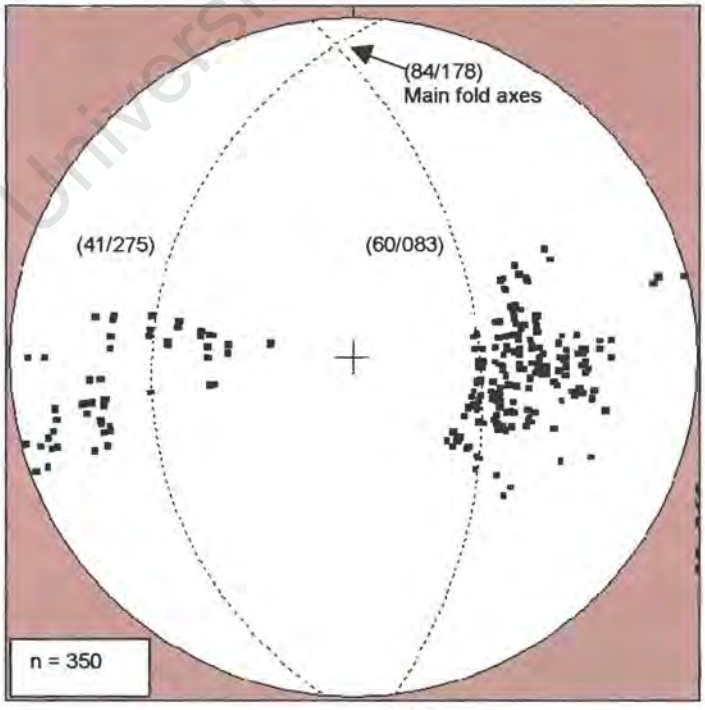

Figure 4.13 Equal area stereoplot of the poles to the co-planar s_2 with the position of the main fold axis, striking N-S dipping slightly towards the north.

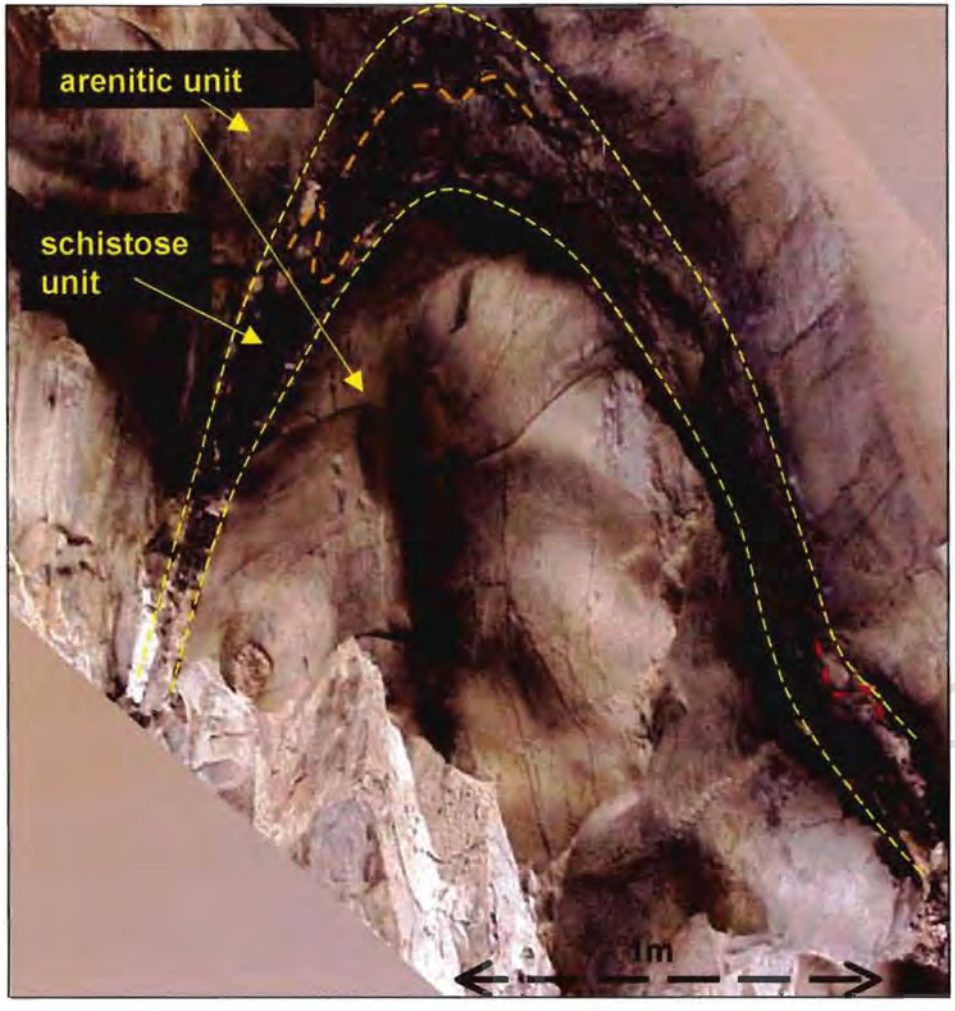

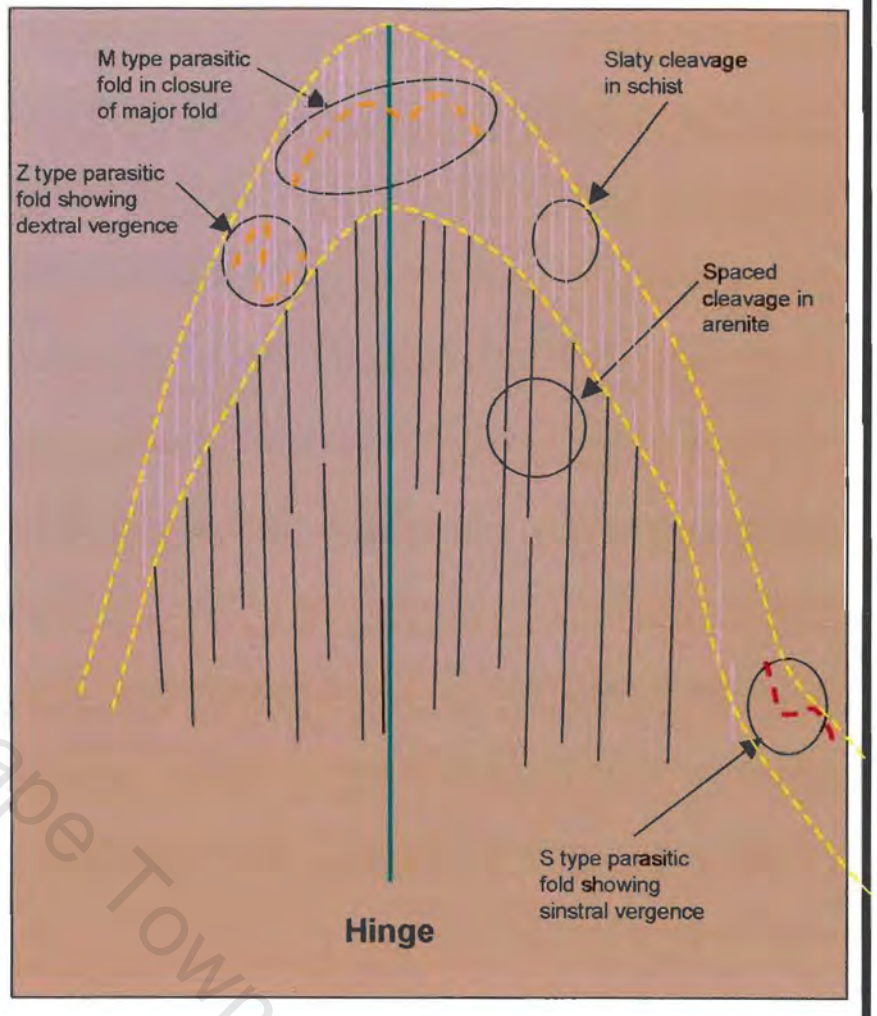

Figure 4.14 A Class 2 (similar) Ramsay fold (25 km north of the Orange River mouth). Photograph rotated from Figure 4.8 to show the relationship of parasitic Z, M and S folds, from left to right and cleavage as found in the study area. The cleavage is axial co-planar in this case .

4.4 Linear structures

Non-penetrative quartz rods (Figure 4.15) on s_2 foliation surfaces in the arenitic units have a NE-SW trend (Figure 4.16). Non-penetrative and penetrative lineations are defined by preferred platy mineral orientations and intersection of 2 foliations (Figure 4.17).

Figure 4.15 Quartz rods found on s_2 foliation surfaces in meta-arenitic units (40 km north of the Orange River mouth).

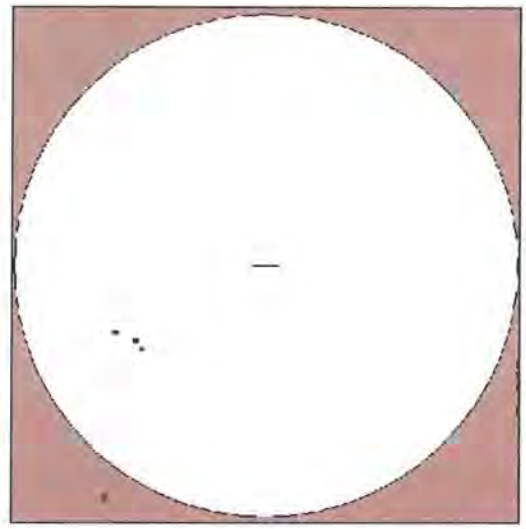

Figure 4.16 Equal area stereoplot of quartz rods orientation in Figure 4.15

Near the contact with the Schakalsberge Sub-terrane L_1 penetrative lineations formed by the intersection of 2 foliations, have a mean trend and plunge of 300/28. Near the contact with the Chameis Sub-terrane L_1 lineations have a mean plunge and trend of 32/167. L_2 lineations formed by allignement of micaceous minerals and chlorite have a mean plunge and trend of 40/278.

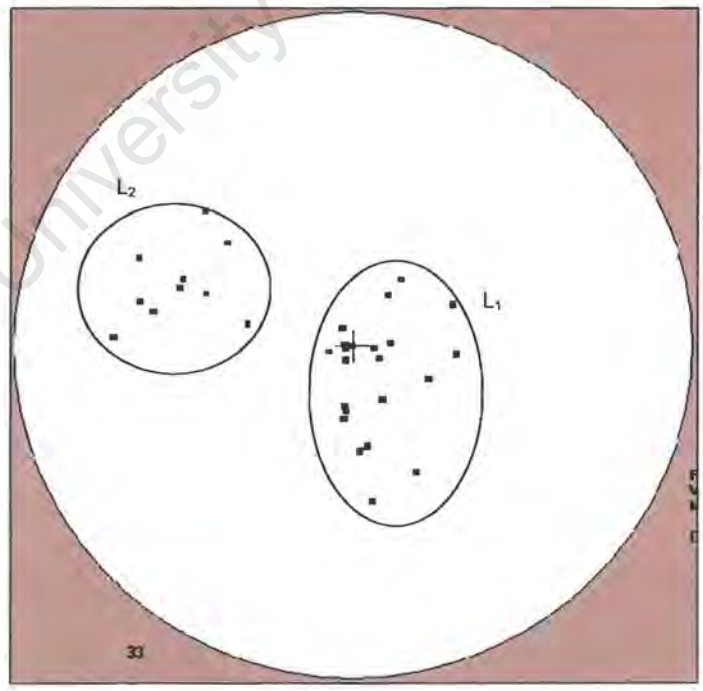

Figure 4.17 Equal area stereoplot of lineations L_1 and L_2.

4.5 Joints

The main joint directions in the study area are 110 degrees and 140 degrees (Figure 4.18). Locally sets with direction 60-70 degrees and 120-135 are dominant. Both filled and unfilled joints occur and the spacing of the joint sets varies from decimetre to metre scale. E-W striking fractures filled with quartz, up to 50 cm wide, occur sporadically. The last fracture phase was very brittle and poorly filled fractures could be related to a very late event, younger than Late Proterozoic. The distribution of joints is clearly visible in places due to the exploitation of joints by Neogene marine erosion processes. The spacing and density distribution of joints in the study area can best be observed in the arenitic units (Figure 4.19).

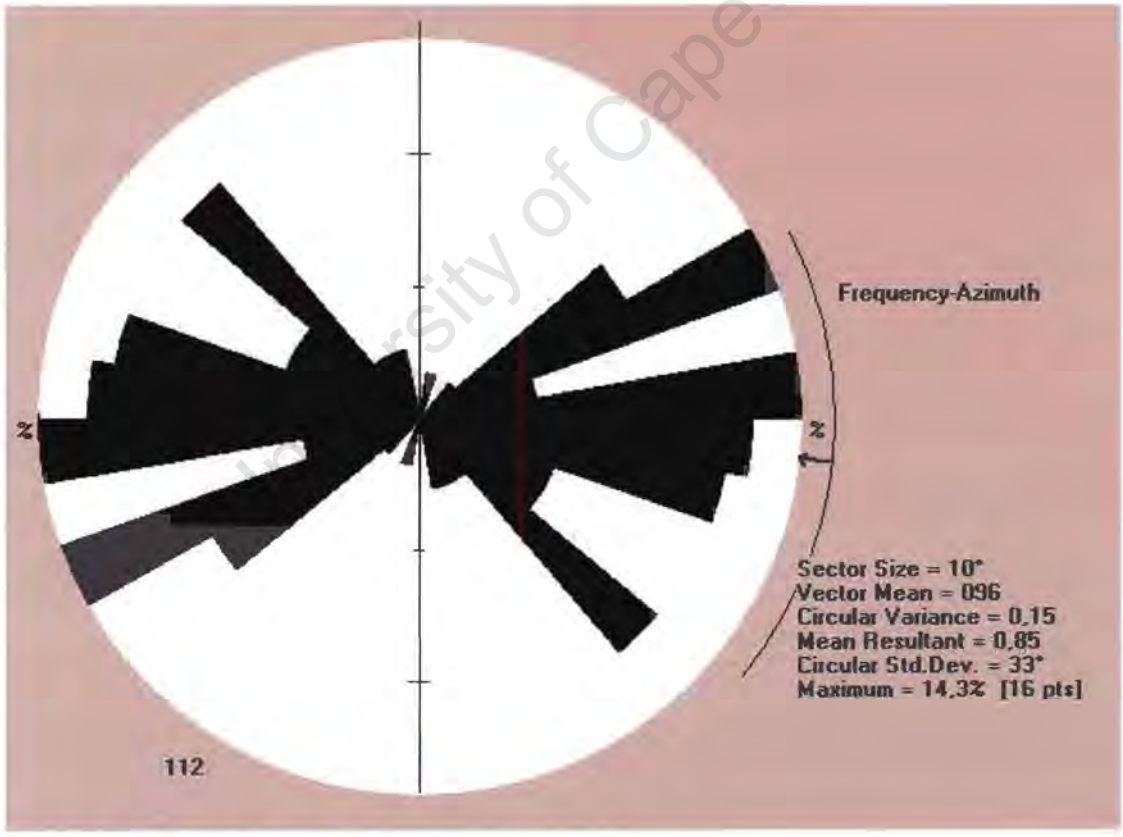

Figure 4.18 Rose diagram of joint directions

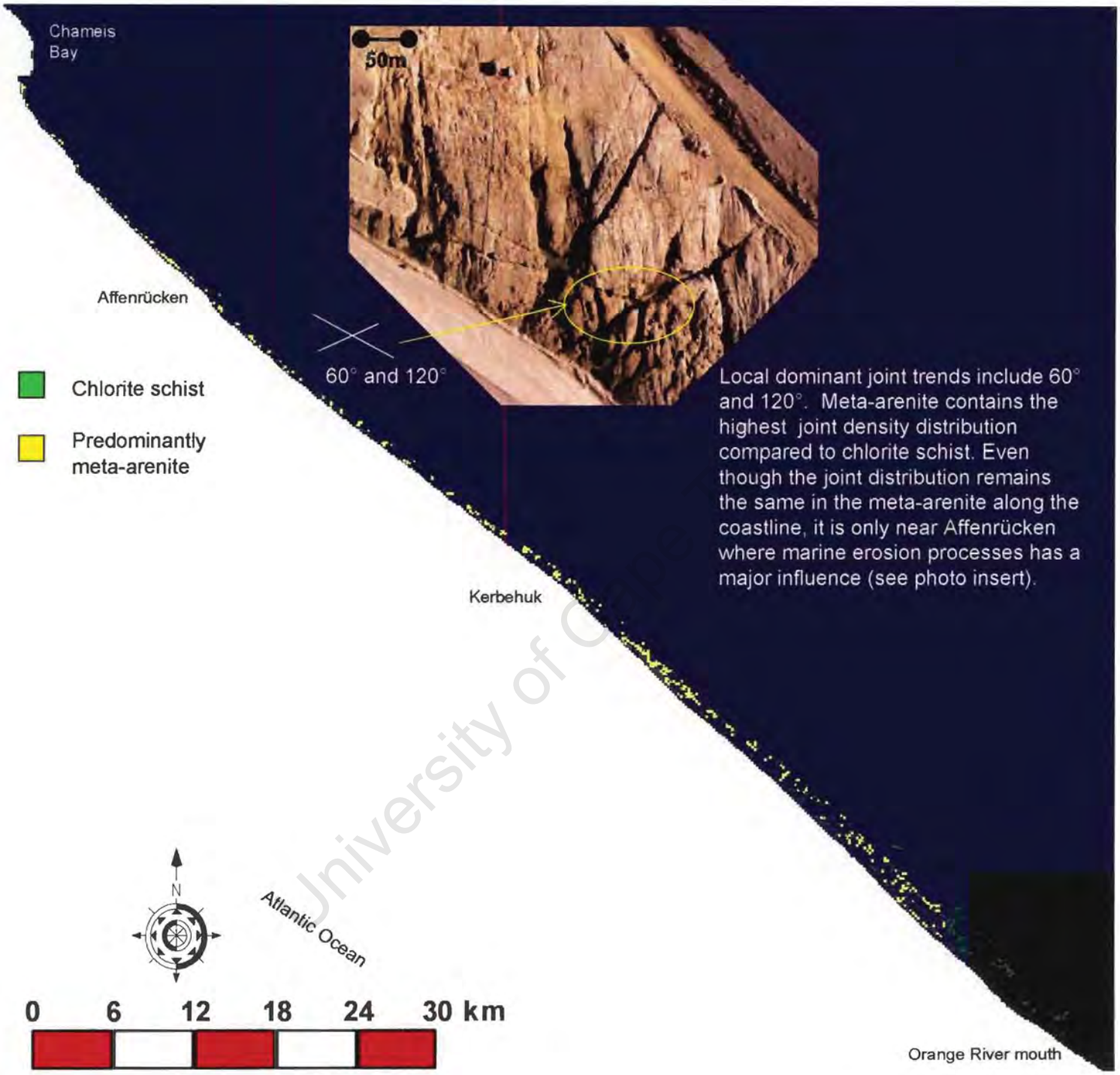

Figure 4.19 Distribution of joints in meta-arenite and chlorite schist between the Orange River mouth and Chameis Bay. The yellow areas represent meta-arenite and the green areas represent chlorite schist mapped on outcrop scale.

CHAPTER 5 - GEOCHEMISTRY

The detrital components of the clastic sediments of the Oranjemund Group contain element ratios representing the source material. In trying to determine tectonic and provenance settings for sediments previous workers (e.g. Holland, 1978 and McLennan *et al.*, 1983) found that La, Ce, Nd, Y, Th, Zr, Hf, Nb, Ti and Sc are most suited because of their relatively low mobility during sedimentary processes and their low residence time in sea water. The above mentioned elements are quantitatively transported into clastic sedimentary rocks during weathering and their concentration would thus reflect the signature of the parent material. Floyd *et al.* (1991) found that the full range of elemental composition for graywackes in different tectonic environments could be more adequately compared utilising upper continental crust-normalised multi-element patterns. These diagrams do not replace specific discrimination diagrams employing diagnostic ratios. However, they have the advantage of showing the effect of variable mafic and heavy mineral input within a sedimentary suite as well as providing a pointer to the tectonic environment.

5.1 Sample description

In total 39 samples (meta-arenite and chlorite schist) from the Oranjemund Group and 10 samples (metabasites) from the Grootderm Formation were used in this study. The major element concentrations of the 10 samples from the Grootderm Formation have been determined previously (Frimmel et al., 1996a) and were supplemented by trace element and REE analyses. All samples were collected from outcrops, avoiding rock with obvious signs of veining or chemical weathering (Figure 5.1). Sampling profiles across the Oranjemund Group were taken across strike at intervals of about 30m. Large-scale tight folding complicated the sampling profiles in the Oranjemund Group and there is a possibility that the same layer could have been sampled more than once in a profile. For the exact sample localities see Figure 5.1 and Appendix 5.

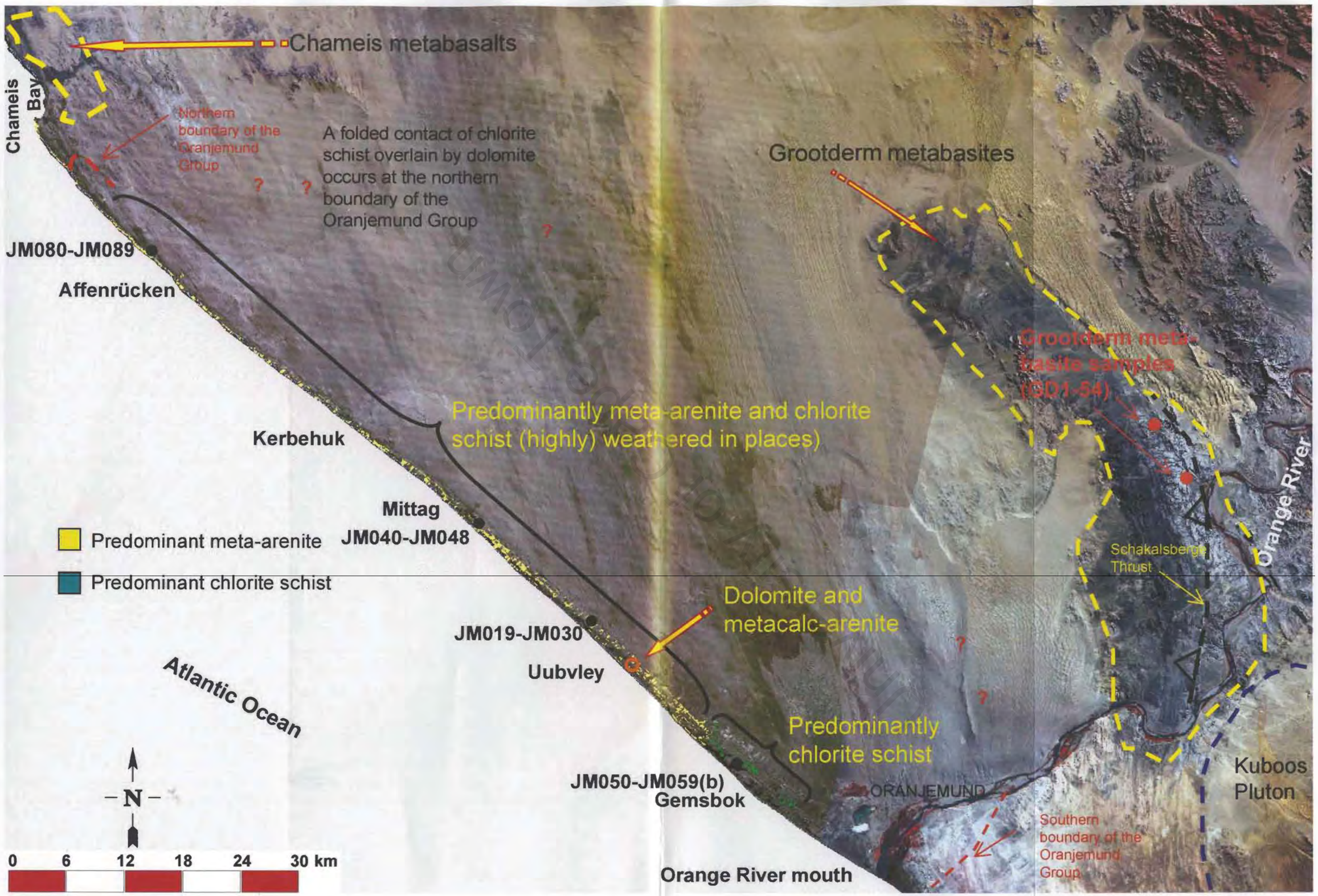

Figure 5.1 Satellite image showing the distribution of the main rock types of the Oranjemund Group in MA1 (in yellow and green) and sample positions of the 39 Oranjemund Group samples (JM019…JM089) and the 10 Grootderm meta-basite samples (GD1-54).

5.2 Analytical techniques

Major- and trace element data, excluding rare earth elements (REE) analyses, were determined by conventional X-ray fluorescence techniques at the Department of Geological Sciences, University of Cape Town. A Philips PW1400 and X'Unique or Siemens SRS303AS XRF spectrometer was used for the analysis. The REE analyses were also done at the Department of Geological Sciences, University of Cape Town using a Perkin Elmer/Sciex Elan 6000 Inductively Coupled Plasma – Mass Spectrometer (ICP-MS). For analytical details see Appendix 4.

5.3 Results

The chemical composition of the Oranjemund Group chlorite schist and meta-arenite can be seen in Appendix 7. The weight percentages of the Oranjemund Group meta-sedimentary rocks ranges as follows: SiO_2 from 43.49 to 77.14 (average 66.74%), Al_2O_3 from 8.34 to 19.30 (average 14.31%), Fe_2O_3 from 3.41 to 9.93 (average 6.18%), MgO from 0.88 to 5.15 (average 2.85%), Na_2O from 0.69 to 2.69 (average 1.96%). The chemical index of alteration (CIA: $[Al_2O_3/[Al_2O_3+ Na_2O + K_2O + CaO]]$), (Nesbit and Young, 1982) for the Oranjemund Group chlorite schist and meta-arenite equals 63-78. This range can be described as moderately to highly weathered, as the CIA for fresh granite equals 45-55. The high CIA is an indication that feldspar was altered to clay minerals in the original sediment and/or in the source area (Figure 5.2). Bathia and Crook (1986) used La/Y and Sc/Cr ratios for geochemical discrimination. La represents the LREE and Y mirrors HREE (Dy-Ho). La/Y ratios would therefore represent enrichment of LREE *versus* HREE. Sc/Cr is the ratio of two compatible elements with Cr being more compatible than Sc. Sc also behaves similar to Cr, Ni, V and Co. The Sc/Cr ratios range from 0.02 to 0.20 and La/Y ratios range from 0.65 to 4.31 for the Oranjemund Group meta-sedimentary rocks.

Progressive metasomatic/metamorphic alteration which affects a rock can be considered as a combination of chemical (Figure 5.3) and volume changes, the formula used to calculate the net gain or loss is as follows (Gresens, 1967; Babcock, 1973 and Kerrich *et al.*, 1977).

$$X_n = 100*[F_v * (g_B/g_A) * (c_n^B - c_n^A)]$$

F_v – Volume factor; $g_{A(initial)}$ and $g_{B(final)}$ – Specific gravity of mineral/rock; $c_n^{B(final)}$ and $c_n^{A(initial)}$ weight fraction of component n in mineral/rock (known from chemical analysis); x_n – total amount of material lost or gained (in 100 g per initial reactants)

Figure 5.4 shows the net gain and loss for elements in sample JM042 (most intensely altered) relative to sample JM046 (least altered).

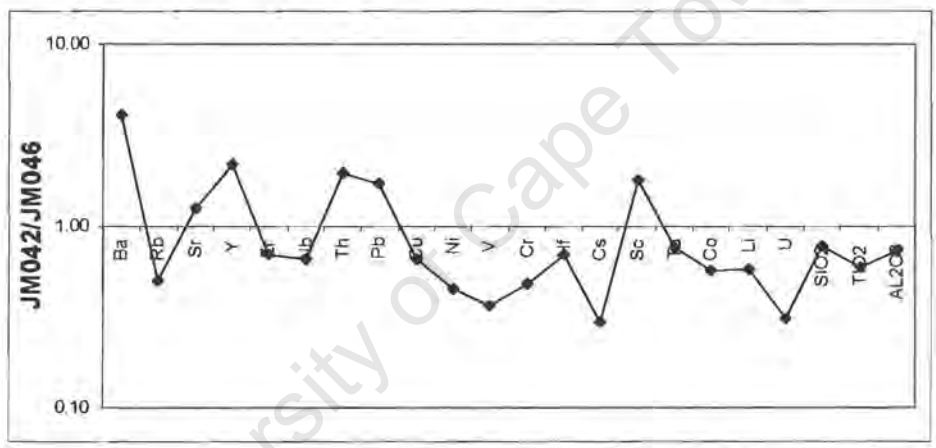

Figure 5.3 Diagram showing the most intensely altered sample JM042 normalised against the least altered sample JM046 in the vicinity of Mittag.

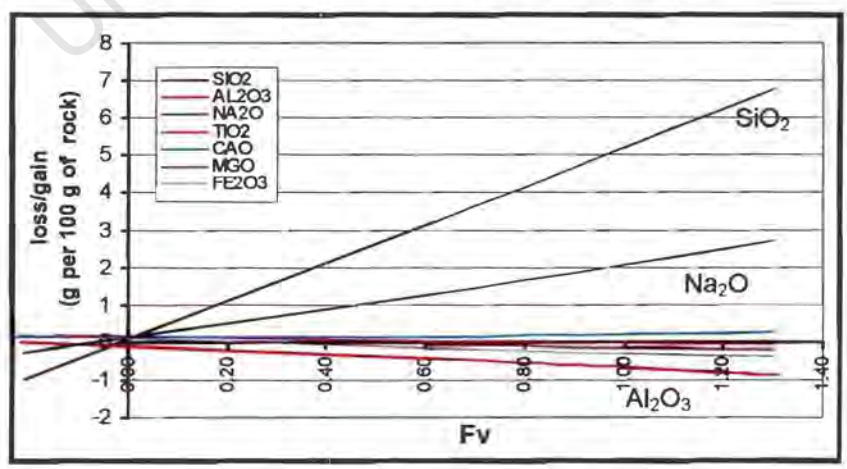

Figure 5.4 Net gain and loss for elements in sample JM042 relative to sample JM046. Na_2O and SiO_2 display a slight gain whereas Al_2O_3 display a slight loss (F_v represents the volume factor).

5.4 Interpretation of geochemical data

The CIA of 63-78 (section 5.3) for the meta-sedimentary rocks of the Oranjemund Group indicates that there was a high degree of weathering in the original sediment and/or source area and therefore major elements are not suitable to use for characterising the source rocks. The ternary Al_2O_3-(Na_2O +CaO)x2-K_2O plot (Figure 5.2) shows a trend towards the Al_2O_3 apex. The southern chlorite schist clusters closer to the Al_2O_3 apex than the northern chlorite schist. Removing CaO from the plot does not influence the trend (Figure 5.2B). The southern chlorite schist display a lesser trend towards the (Na_2O+CaO)x2 apex than the northern chlorite schist. The higher Na content for some of the samples could be related to Na-metasomatism. It therefore seems that the northern chlorite schist is more likely to have undergone Na-metasomatism. Redistribution of Ca and Sr values due to albitization of their initial plagioclase host renders these elements not suitable for geochemical discrimination.

5.4.1 Trace elements

High Cr, Ni, V and Ti contents are indicative of mafic input. Low Zr and Hf contents indicate that there was no major felsic input. In discrimination plots using Zr/Y *vs.* Zr (Figure 5.5) (Pearce and Cann, 1973) samples from the Oranjemund Group plot in the field of within plate basalts. The trace element characteristics of the meta-sedimentary rocks of the Oranjemund Group and the Grootderm Formation are clearly different to island arc basalts and mid oceanic ridge basalts having a much higher Zr/Y ratio (Figure 5.5). It is therefore highly likely that the meta-sedimentary rocks of the Oranjemund Group were sourced from the meta-basites such as those from the Schakalsberge Sub-terrane and posibly Chameis Sub-terrane.

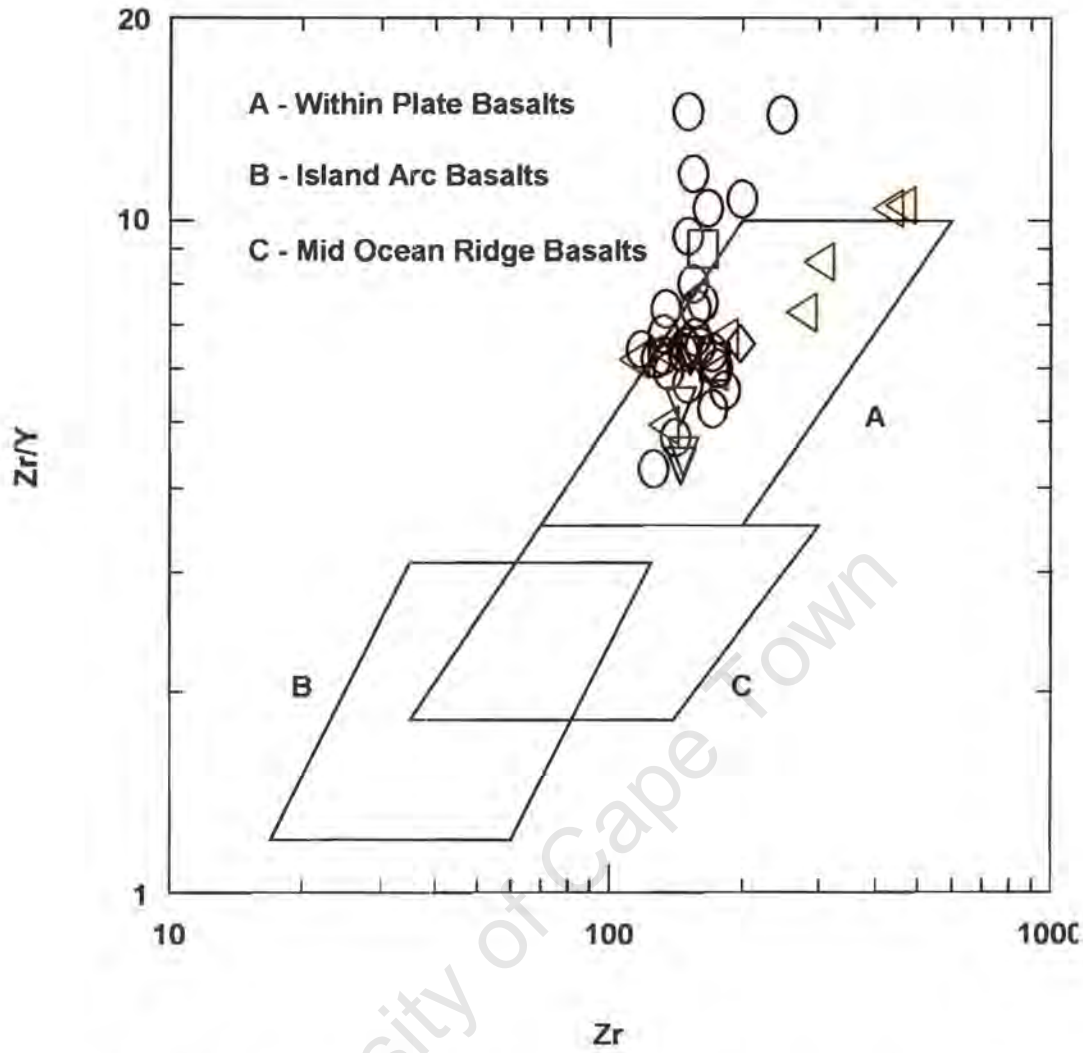

Figure 5.5 Zr/Y vs. Zr plot (Pearce and Cann, 1973) of the meta-arenite (circles), chlorite schist south (triangle) and chlorite schist north (square) from the Oranjemund Group and the meta-basites (left pointing triangles) from the Grootderm Formation, Schakalsberge Sub-terrane.

5.4.2 REE

During continental weathering and transport REE can be mobilized during both warm, humid weathering and temperate weathering. Balashov and Girin (1964) found that argillaceous and arenaceous rocks formed under arid conditions contain similar abundances of REE, and that their associated carbonates, although having a lower REE content, have similar LREE/HREE ratios. The overwhelming concentration of REE in the detrital fraction of transported material, rather than the dissolved portion, must mean that the REE pass from weathering to deposition almost exclusively without taking part, en route, in any significant chemical processes (Henderson, 1989).

Haskin and Gehl (1962), amongst others, established that the REE contents of most pelitic rocks are very similar to each other being enriched in LREE relative to HREE when normalised to chondrites. The similarities in REE content of sediments in general and "shales" in particular led to the idea that the average REE content of the upper crust could be represented by the average abundance of REE in sedimentary rocks. Sedimentary rocks could therefore be seen as causing homogenization of the REE fractionation that occurs during the formation of igneous rocks. The bulk of REE resides in silt and clay size fractions (no direct correlation with clay mineralogy). Sand fractions tend to have lowest REE abundances and they commonly display lower La/Yb ratios than finer grain sizes (Hakin and Gehl, 1962). The low abundances can be attributed to the quartz dilution effect as displayed by a negative correlation between total REE and sum of SiO_2 (Figure 5.6). Both the chlorite schist and the meta-arenite display a scattered distribution on the sum of REE *versus* SiO_2 (wt %) plot. The range of sum of REE (ppm) transitional basalts is 90 to 610 (Henderson, 1989). This is an indication that the chlorite schist is also of sedimentary origin, whereby the detrital material is largely derived from a mafic source such as the meta-basites of the Schakalsberge Sub-terrane. Enrichment in HREE is likely the result of the heavy mineral content. Eu anomaly is similar for all grain sizes (McLennan, 1983). Detrital grains of minerals known to concentrate REE like apatite and zircon could cause sandstone to have an abnormal REE content (Fleet, 1984). The

normalized REE patterns of the Oranjemund meta-sedimentary rocks show a similar REE pattern to the Grootderm meta-basites (Figure 5.7).

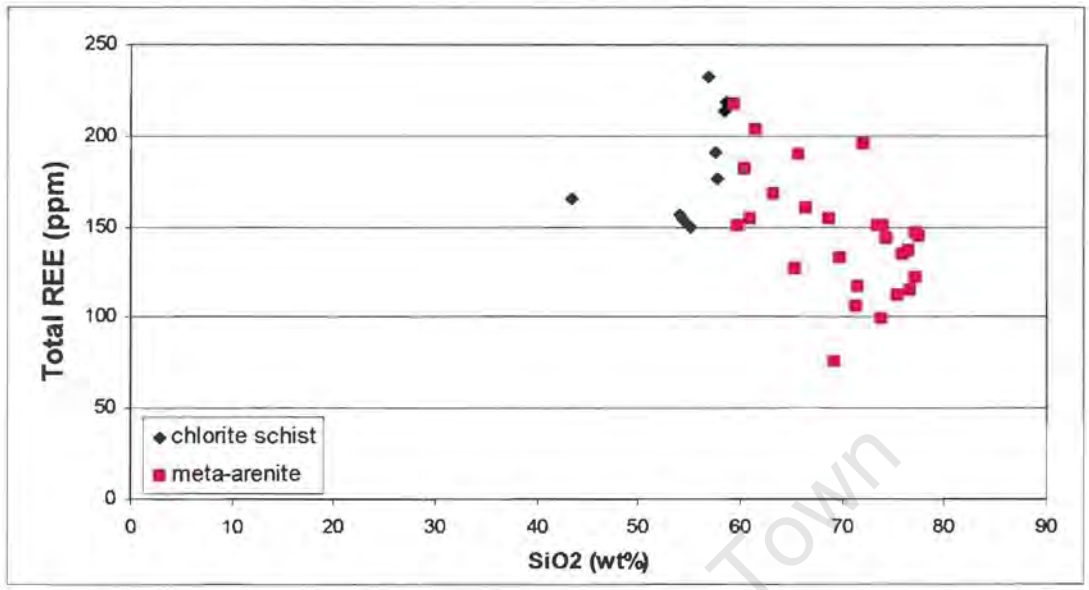

Figure 5.6 The total REE content (sum in ppm) and sum of the SiO_2 weight % of the chlorite schist and meta-arenite from the Oranjemund Group.

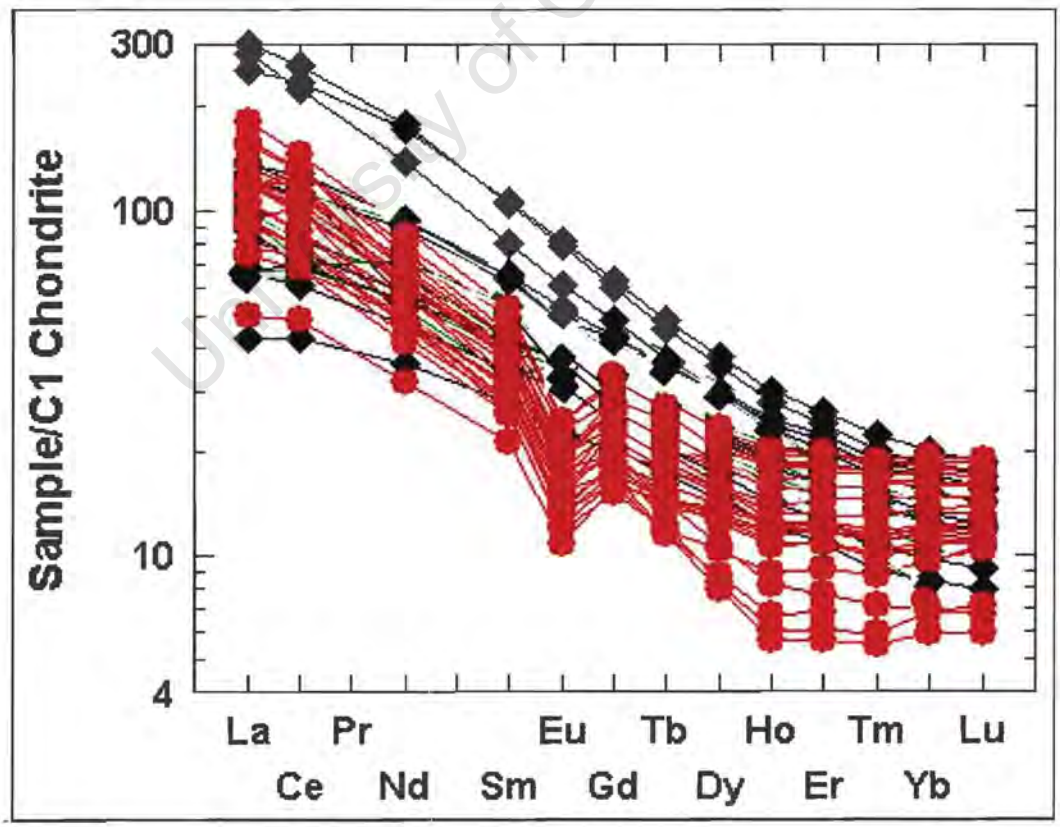

Figure 5.7 REE plot of the Oranjemund Group meta-sedimentary rocks (red circles) and Grootderm Formation, Schakalsberge Sub-terrane, meta-basites (blue diamonds).

5.5 Tectonic setting

Bathia and Crook (1986) used Sc/Cr ratios to plot against La/Y ratios (Figure 5.8) to discriminate between graywackes of different tectonic settings. The La/Y ratios give the enrichment of LREE over HREE. The LREE are represented by La and the HREE represented by Y. The Sc/Cr is the ratio of two compatible elements (Cr being more compatible than Sc). By using the Sc/Co ratio instead of Sc/Cr (Figure 5.9 – not directly comparable with Figure 5.8) better discrimination was obtained in this study. Oceanic island arc rocks are characterised by low La/Y (<0.5) and low Sc/Cr (<0.6) ratios. Continental island arc graywackes are discriminated by La/Y ratios between 0.2 and 0.4. Active continental margin graywackes can be discriminated from the continental island arc type, by their high La/Y ratios (1 to 1.5 generally). Passive margin graywackes have La/Y ratios similar to those of active continental margins. They can however be discriminated by their low Sc/Cr (<0.2) ratio (Bathia and Crook, 1986).

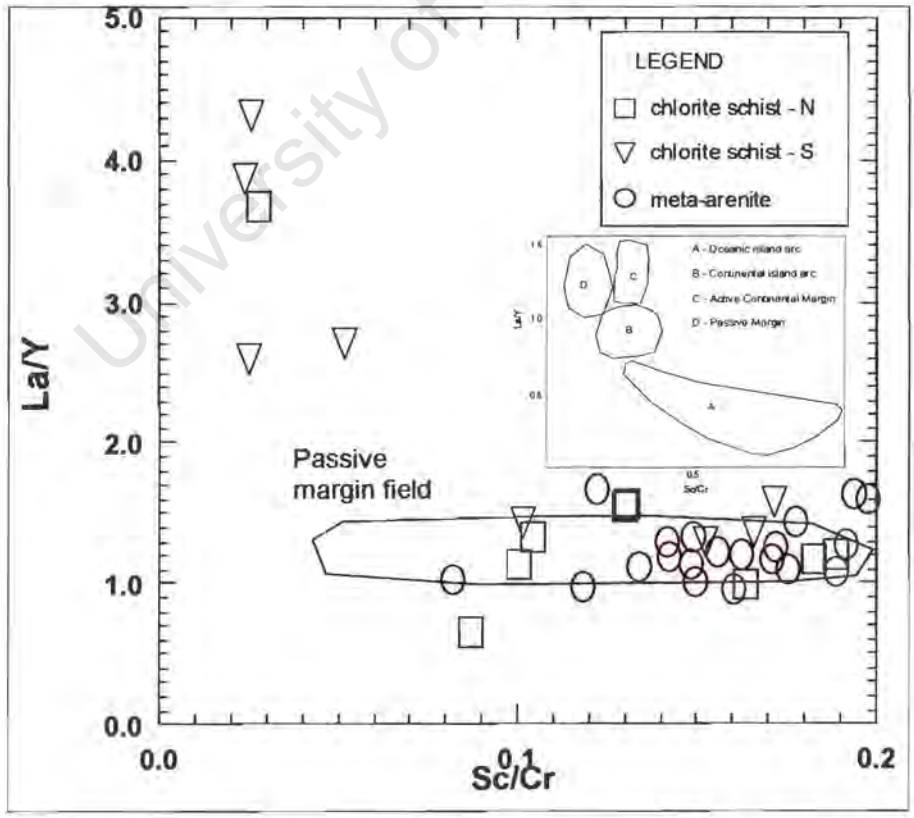

Figure 5.8 La/Y *vs* Sc/Cr of meta-arenite (circles), chlorite schist south (triangles) and chlorite schist north (squares) from the Oranjemund Group. Tectonic setting data fields from Bathia and Crook, 1986.

The Sc/Cr ratios for the meta-sedimentary rocks from the Oranjemund Group are between 0.02 and 0.2, the La/Y ratios are between 0.65 and 4.3. These values falls in the passive continental margin field (Figure 5.8).

Th-Co-Zr/10 and Th-Sc-Zr/10 plots (Bathia and Crook, 1986) (Figure 5.10) place the Oranjemund Group meta-sedimentary rocks (meta-arenite and chlorite schist) in a continental island arc setting. The position of the data point of the Grootderm meta-basites overlaps with the field for oceanic island arc rocks.

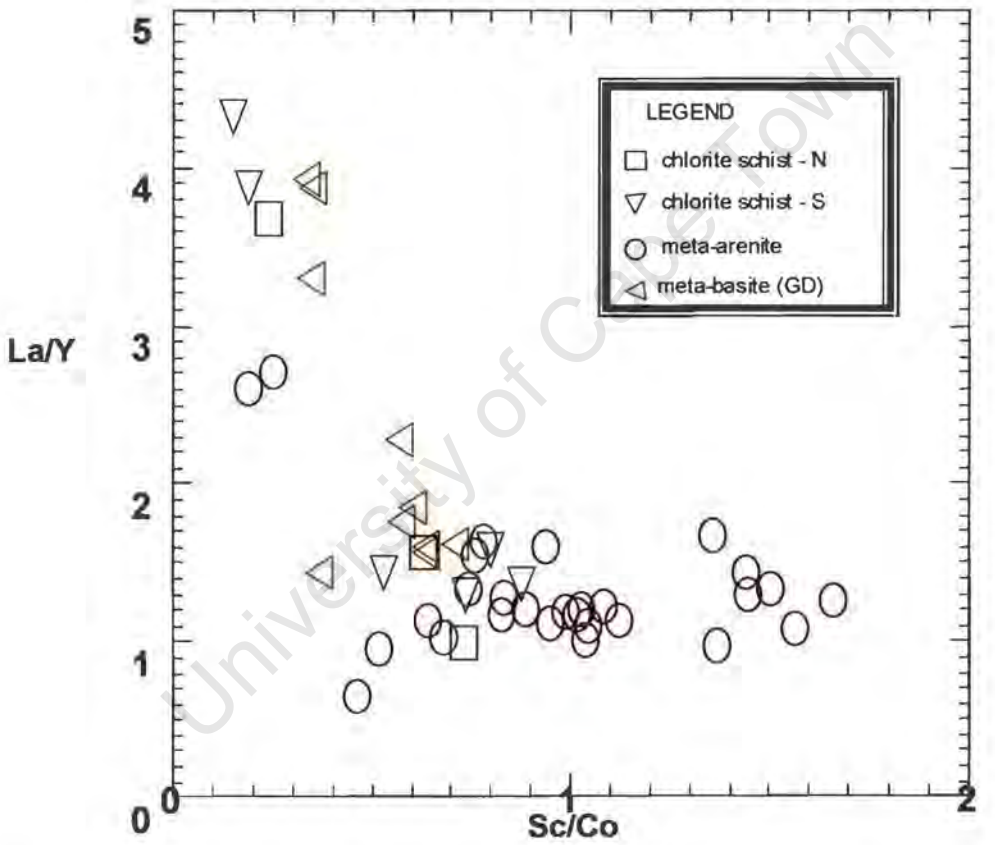

Figure 5.9 La/Y vs Sc/Co the meta-arenite, chlorite schist south and chlorite schist north from the Oranjemund Group and the meta-basites from the Grootderm Formation Schakalsberge Sub-terrane.

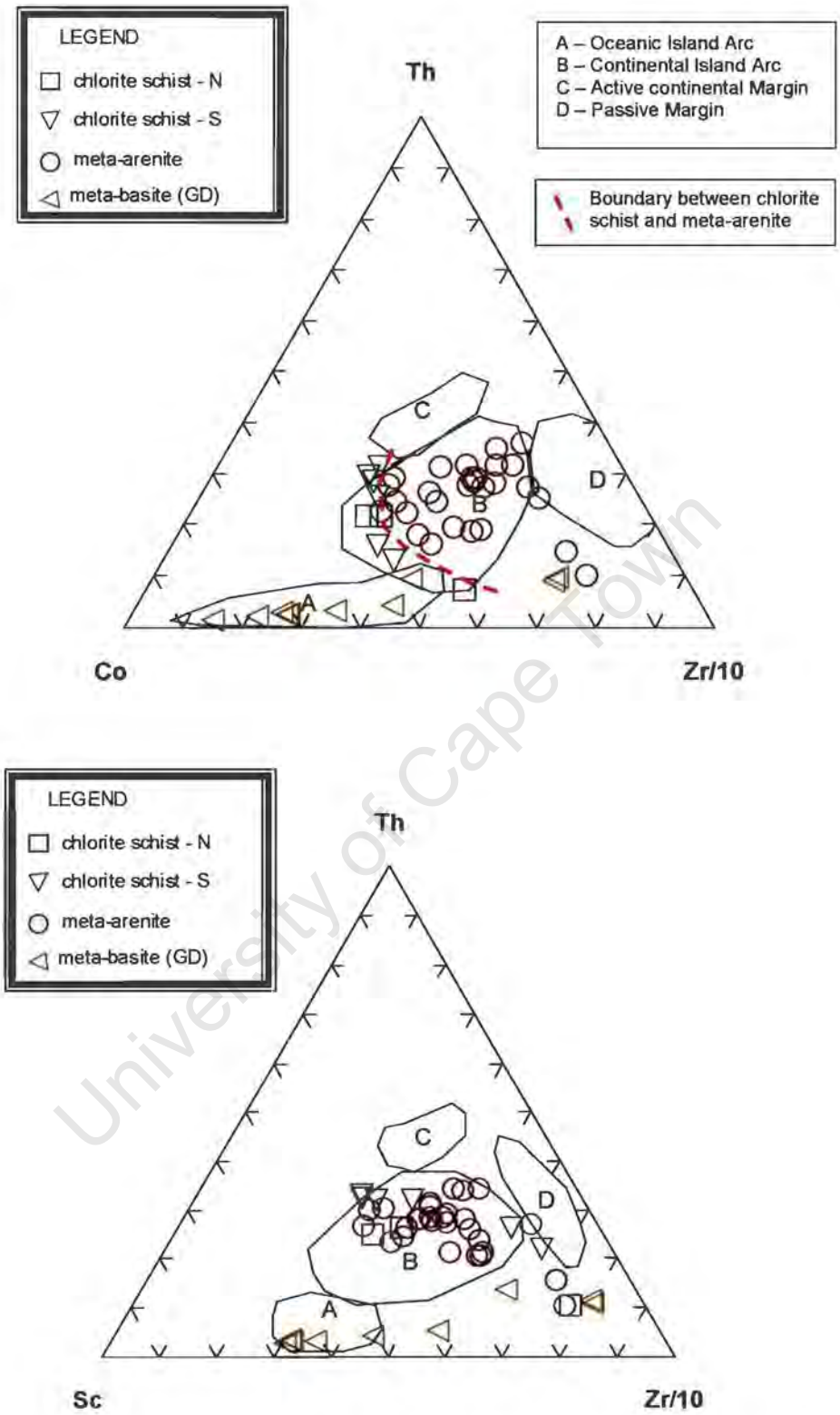

Figure 5.10 Th-Co-Zr/10 and Sc-Th-Zr/10 plots of the meta-arenite, chlorite schist (near the Orange River mouth) and chlorite schist north (Kerbehuk area) from the Oranjemund Group, the meta-basites from the Grootderm Formation, Schakalsberge Sub-terrane (data fields from Bathia and Crook, 1986).

The multi-element pattern for the Oranjemund Group meta-sedimentary rocks has a close correlation to continental arc or active margin (CAAM) setings (Figure 5.11). There is a similarity between the pattern of the passive margin (PM) and the Oranjemund Group meta-sedimentary rocks. Values that deviate from the PM pattern are higher V, Cr, Ni and lower Hf and Zr values. These could be explained by the mafic influence. Deviating values from the CAAM pattern include Rb, Sr and Sc. Due to the mobility of Rb and Sr during metamorphism these elements are not suitable for discrimination in the case of the Oranjemund meta-sedimentary rock.

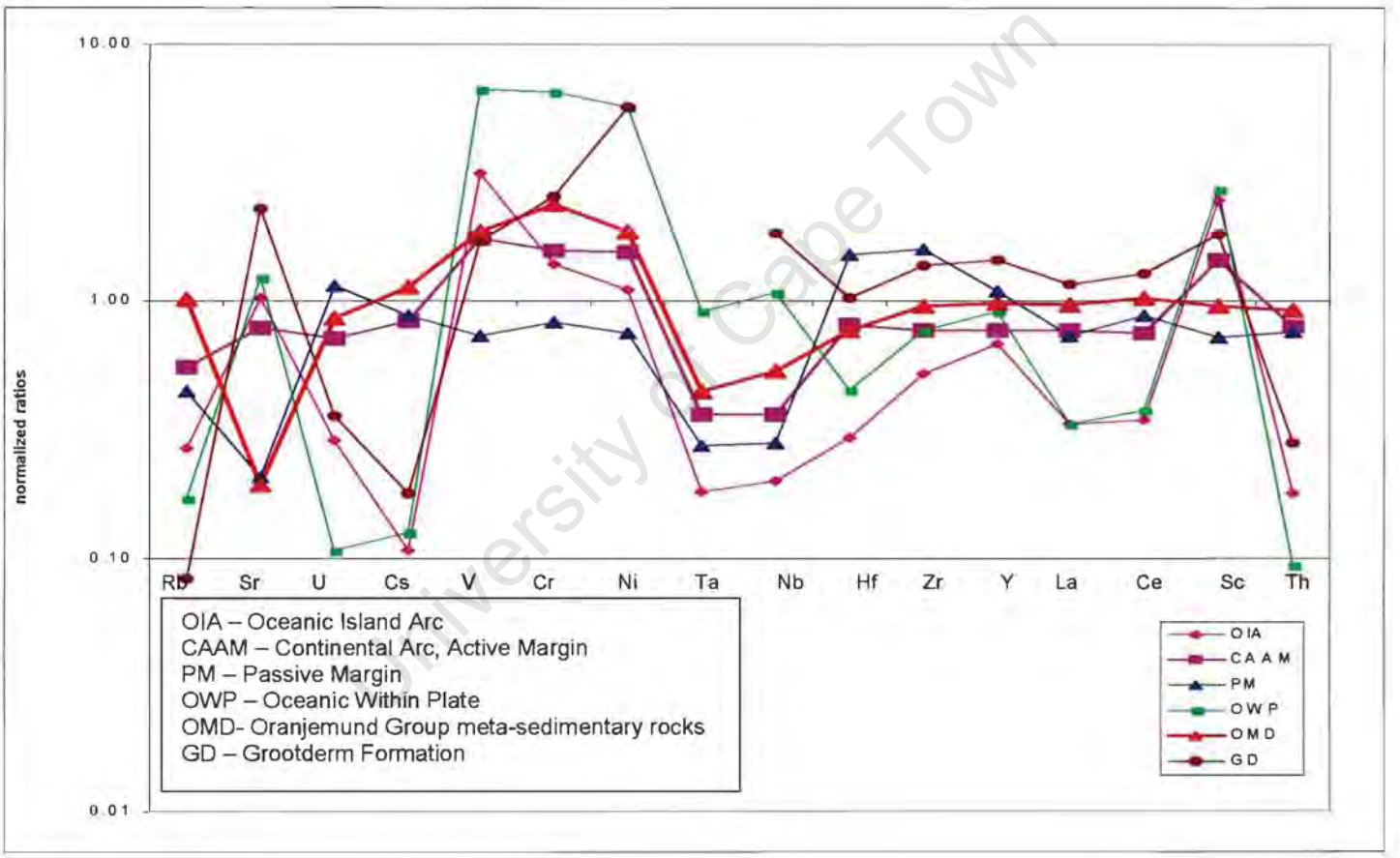

Figure 5.11 Normalised multi-element patterns using averaged graywacke data (from Appendix 3) for different tectonic environments (after Floyd *et al.* 1991), the Oranjemund Group and the Grootderm Formation meta-basites.

CHAPTER 6 – INTERPRETATION OF BEDROCK GEOLOGY

The original detrital mineralogy of the chlorite schist and meta-arenite of the Oranjemund Group was influenced by metamorphism and microtextural deformation. The development of phyllosilicates and recrystallization of quartz can be seen in variable amounts in the samples. The CIA index (Nesbit *et al.* 1982) for these rocks indicates a high degree of weathering. The use of major elements for geochemical discrimination is therefore not suitable. Samples with higher Na content could be related to Na-metasomatism (Figure 5.2). Na-metasomatism could also be a possible explanation for the metamorphic zonation of albite grains in both the chlorite schist and meta-arenite (Figure 3.5).

The meta-calcarenite adjacent to the dolomite (30 km north of the Orange River mouth) is very Na (and Mg) rich and was originally perhaps an evaporite. The Na is now in albite and some Mg is incorporated in phlogopite. A formerly possible evaporite could then have acted as source of the Na for the Na-metasomatism. A Na-rich sedimentary precursor of the dolomite is postulated due to the high occurrence of albite.

The sedimentary rocks of the Oranjemund Group carry a trace element signature (Zr *vs.* Zr/Y) (Pearce and Cann, 1973) of within plate basalts (Figure 5.5). REE patterns of the Oranjemund meta-sedimentary rocks are very similar to that of the Grootderm Formation meta-basites (Figure 5.7). La/Y *vs.* Sc/Cr ratios places the Oranjemund meta-sedimentary rocks in a passive margin setting (Figure 5.8) due to the low < 0.2 Sc/Cr ratio. These values compare well with values for meta-basites from the Chameis Sub-terrane determined by Frimmel *et al.*, 1996a). The data points of the Oranjemund Group meta-sedimentary rocks overlap the field of continental island arc rocks (Th-Co-Zr and Th-Sr-Zr plots - Figure 5.10, Bathia and Crook, 1986). Better discrimantion, for the rocks of the Oranjemund Group, was obtained when Co was used (in the place of Cr) (Figures 5.8 and 5.9). In Figure 5.10A the chlorite schist and meta-arenite fall in the

oceanic island arc field. However, there is a clear boundary between these two rock types. The chlorite schist has tendency towards the Co apex and it is therefore highly likely that it has been deposited when an oceanic influence was dominant. The meta- arenite has a tendency towards the Th and Zr apexes and were therefore most likely deposited when a continental influence was dominant. A possible change in depositional environment during the period of deposition of the Oranjemund Group meta-sedimentary rocks is therefore highly likely. Bathia and Crook (1986) based their classifications of rocks from Australia. Different geological conditions on the African/South American continents put a question mark on the reliability of these discrimination plots for the rocks in the study area. The multi-element patterns (Floyd, 1991) of the Oranjemund meta-sedimentary rocks display a close correlation to average Proterozoic greywackes in continental arcs of active margin setting (Figure 5.11). There is also a close correlation to a passive margin tectonic setting. The passive margin setting for the over all Marmora Terrane (Frimmel, 2001a) agrees with placing the Oranjemund Group meta-sedimentary rocks in a passive margin setting. The close correlation with an active margin setting could be explained by the possibility that the sedimentary rocks were deposited as basin closure started, changing the tectonic environment from a passive margin to an active margin.

SEM-CL did not assist in distinguishing between detrital and recrystallized quartz, and an origin of the detritial quartz grains from a terrain of similar low metamorphic grade as in the Oranjemund Group is inferred. Low-temperature quartz displays low cathodoluminescence and in this case the recrystallization of quartz took place at a low temperature (lower greenschist facies). The recrystallized quartz in the study area therefore has low luminescence. Detrital quartz grains formed at high temperatures should have high luminescence (Anders, 1988).

The chlorite schist (near the inferred thrust contact with the Chameis Sub-terrane) 6 km south of Chameis Bay contains epidote. Epidotisation is typically

related to areas where there was influx of H_2O into Fe- and Ca-rich rocks such as meta-basalts. The localised influx of water can then, in turn, be interpreted as being related to the inferred thrust (because thrust planes provided very effective conduits). On the other hand no satisfying field evidence could be found for the inferred thrust fault and it is possible that foliation could have acted as an effective conduit. The quartzite/chert marker zone, near the inferred thrust, changes into a silicified banded iron stone. The banded iron stone (iron rich chert) could be interpreted as a local phenomenon associated with the inferred thrust.

Intense isoclinal folding with virtual axial plane parallel foliation makes it difficult to calculate the thickness of the Oranjemund strata on the basis of the average orientation of laminated beds. The Oranjemund Group underwent two main deformation events (D_1, D_2). Firstly, the Chameis Sub-terrane was juxtaposed next to the Oranjemund Sub-terrane through southeastward transport (D_1). Evidence (refolded NE-SW trending hinges) for the southeasterly transport direction could only be found near the contacts with the Chameis and Schakalsberge Sub-terranes. This was followed by an intense E-W compressional event (D_2). This compressional event caused the original bedding planes (s_0) of the sedimentary rocks in the Oranjemund Group to be transposed into bedding parallel foliation (s_2). Remnants of s_1 can be seen in inclusions in albite (Figure 3.6). The strike of s_2 is nearly N-S throughout the whole study area. Large-scale tight parasitic folds are visible in the outcrop along the 120 km coastal strip. The hinges of these parasitic folds trend north-south mimicking the host fold orientation. A late stage buckling (D_3) gave rise to NW-SE striking F_3 folds.

CHAPTER 7 – REVISED STRATIGRAPHY OF THE ORANJEMUND SUB-TERRANE AND ITS TECTONOTHERMAL EVOLUTION

In spite of some similarities between the three sub-terranes of the MT, differences between them warrant different stratigraphic names for their individual successions (Frimmel, 2001a). Previously, the now Oranjemund Sub-terrane comprised the Oranjemund Formation. Mapping done in this study revealed lithologies, previously not known to be part of the Oranjemund Formation. It is therefore proposed that the Oranjemund Formation should be upgraded to the Oranjemund Group which comprises the newly defined Gemsbok Formation, the Affenrücken Member and the Mittag Formation (Figure 7.1). The Gemsbok Formation comprises chlorite schist derived from the Grootderm meta-basites (Schakalsberg Sub-terrane) and the Chameis Sub-terrane meta-basalts (Chapter 5). The Affenrücken Member comprises a thin (1 metre thick) laterally extensive dolomite layer (Chapter 3). The Mittag Formation comprises dominant meta-arenite with intercalated chlorite schist. Graded bedding resembling that of turbidite deposits can be seen in the meta-arenite.

The Affenrücken Member is not found in the south of the study area but is only found in the north near the contact with the Chameis Sub-terrane. The Gemsbok Formation chlorite schist is the oldest exposed unit in the Oranjemund Group and comprises reworked volcanics. No lava flow structures were observed in the field.

Frimmel *et al.* (2001c) propose three megasequences (M1,M2 and M3) for the sedimentary fill of the Gariep Basin. The first megasequence (M1) is recorded in the lower part of the Port Nolloth Group, PNZ. M1 (770 – 750 Ma) comprises the up to 800 m thick Lekkersing en Vredefontein Formations (Stinkfontein Subgroup) (Figure 7.2). The Lekkersing Formation is interpreted as an alluvial fan deposit in an emerging continental rift graben (Von Veh,

1993). The Vredefontein Formation is interpreted as an alluvial plain and delta deposit in a widening continental rift graben (Frimmel *et al.*, 2001c).

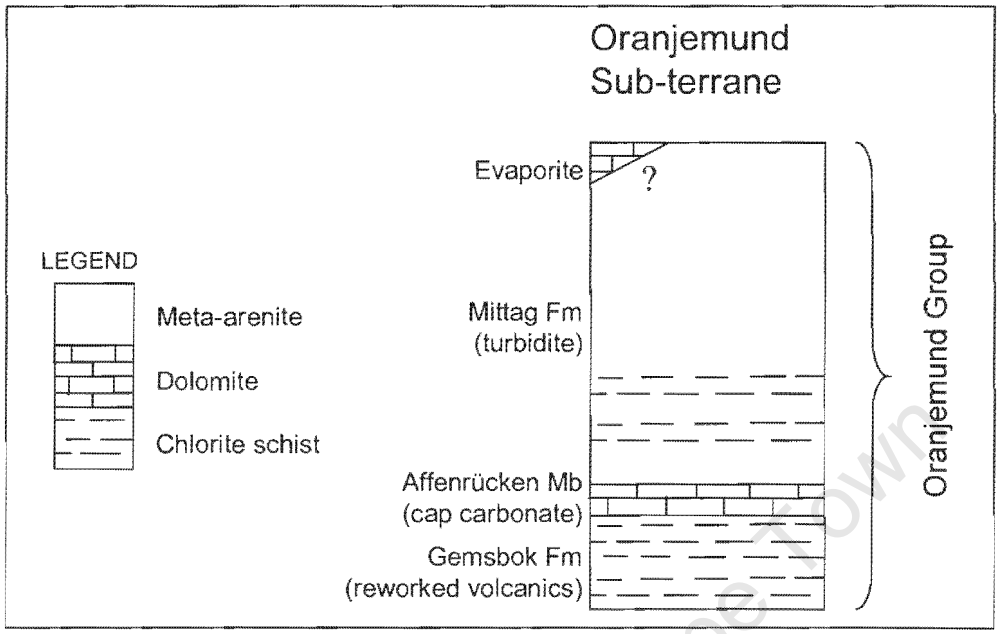

Figure 7.1 Proposed revised stratigraphy of the Oranjemund Sub-terrane

M2 (750 – c. 580 Ma) starts by the drowning of the continental rift deposits (Frimmel *et al.,* 2001c). The Kaigas Formation comprises diamictite, and intercalated upward-fining arkose and greywacke beds. These, along with dolomitic olistostromes (derived from an eastern source, shallow water carbonate platform or lacustrine carbonates) are interpreted to represent debris flow sediments, proximal to medial turbidity fan deposits and large slump masses laid down adjacent to the drowned rift shoulders (Frimmel, *et al.*, 2001c).

The Kaigas Formation is overlain by the Hilda Subgroup. The Hilda Subgroup comprises the Pickelhaube, Wallekraal, Dabie River and Rosh Pinah Formations (Frimmel, 2001a). By this stage a basement high that separated the failed Rosh Pinah Graben in the east from the Gariep Basin proper in the west was submerged and marine deposits were laid down throughout the basin (Frimmel, *et al.*, 2001c). The Wallekraal Formation represents a fluvial/lacustrine pelite deposited near the continental margin, but also shows evidence for a submarine fan environment. The Pickelhaube

Formation represents low-energy turbidity-current argillite, calcareous arenite and dolomite laid down in the more distal regions. The bimodal volcanism of the Rosh Pinah Formation (Frimmel *et al.*, 1996b) took place contemporaneously with the drowning of the rift. Peak of volcanism was reached during the Wallekraal/Pickelhaube times. This marks the time of the start of the formation of oceanic crust in the MT, changing from rifting to drifting (Frimmel *et al.*, 2001c). A Pb-Pb age of 741±6 Ma (Frimmel *et al.*, 1996b) correlates well with a Pb-Pb age of 728±32 Ma for the Pickelhaube Formation (Fölling *et al.*, 2000).

A second-order basin developed between the basaltic oceanic islands of the Grootderm Formation, Schakalsberge Sub-terrane and the Dernberg Formation, Chameis Sub-terrane. This second-order basin was filled with the Oranjemund Group (Figure 7.3), derived from the adjacent oceanic islands (Chapter 5). Due to a drop in sea level during this time, stromatolitic reef carbonates of the Dabie Formation formed on the previously relatively deep water sediments of the Pickelhuabe Formation (Frimmel *et al.*, 2001c).

Stromatolitic dolomite (Gais Member) found on the basaltic seamounts of the Schakalsberge Sub-terrane may be equivalent to the Dabie River Formation. In the same way, the former evaporite deposit associated with reef dolomite (Scholtzberg Member) within the basaltic Dernberg Formation (Chameis Sub-terrane) may be equivalent to the Dabie River Formation (Frimmel and Jiang, 2001).

The Hilda Subgroup is overlain by a thin banded-iron-formation (Jakkalsberg Member) intercalated at the base of the up to 500 m thick Numees Formation diamictite (Frimmel *et al.*, 2001c).

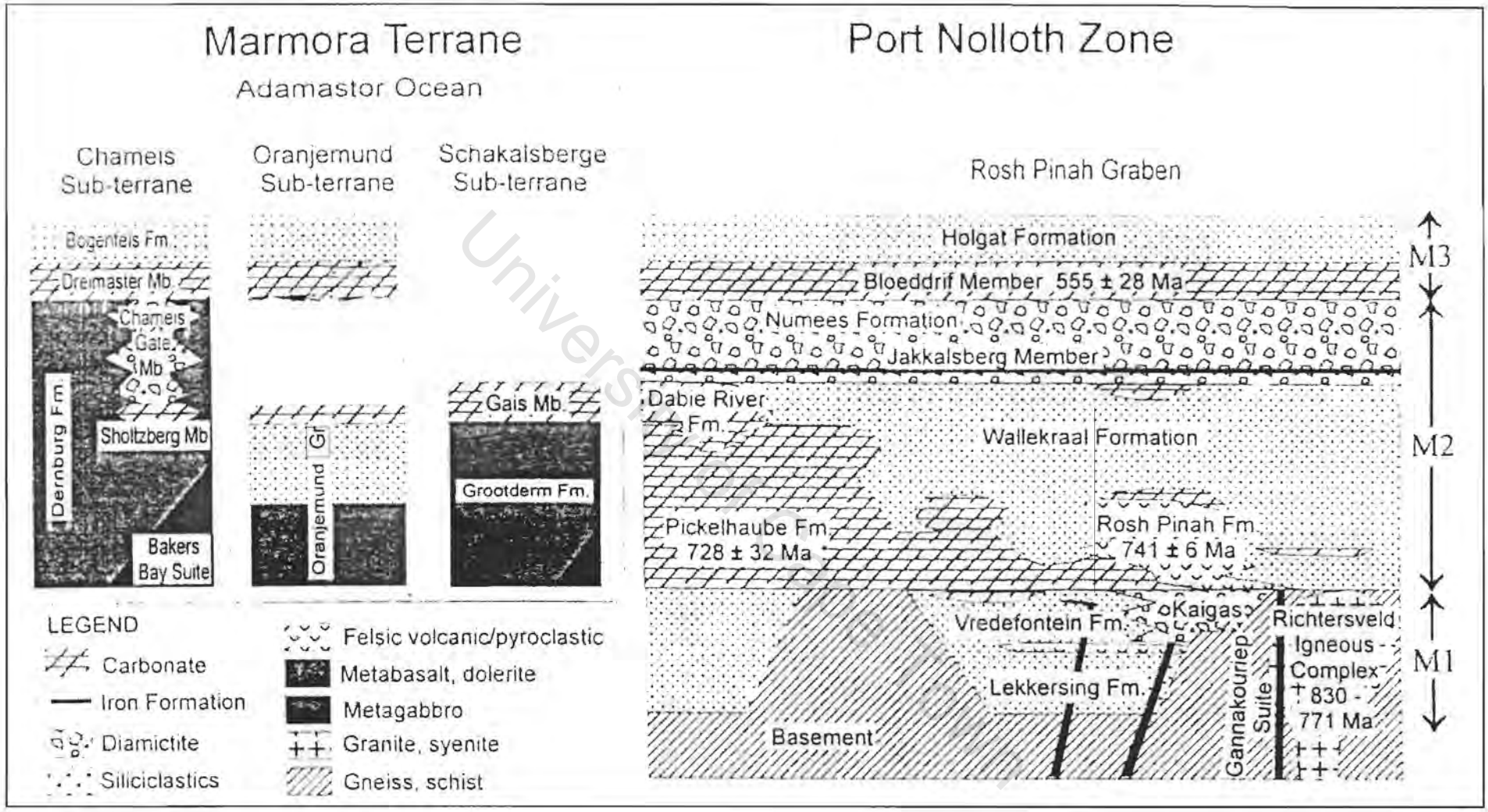

Figure 7.2 Stratigraphic correlation for the main tectonic units of the Gariep Belt (after Frimmel *et al.*, 2001c)

A sequence of cap carbonates (Bloeddrif Member) and siliciclastic rocks (Holgat Formation) occur above the glaciogenic Numees Formation M3 (580-550 Ma). These rocks are very similar throughout the whole Gariep Basin.

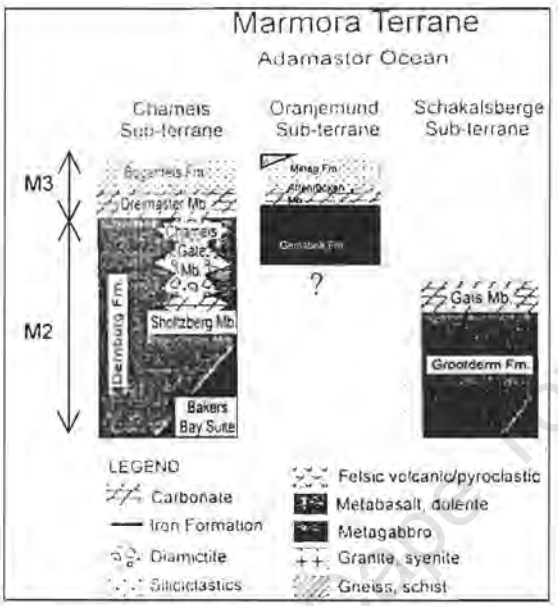

Figure 7.3 Proposed stratigraphy for the Marmora Terrane (modified after Frimmel *et al.*, 2001c).

The term Oranjemund Group is proposed to embrace all Pan-African rocks in the Oranjemund Sub-terrane. The oldest exposed unit is the reworked volcanics of the Gemsbok Formation. The Affenrücken Member overlies the Gemsbok Formation described here. The Affenrücken Member is interpreted as a cap carbonate due to its lateral distribution and could therefore be correlated with the Bloedrif Member (PNZ) and the Dreimaster Member (Chameis Sub-terrane) (Figure 7.2). The Gemsbok Formation must therefore have been deposited prior to the start of M3 (Figure 7.3).

The Mittag Formation (overlying the Affenrücken Member) could be correlated with the Holgat Formation (PNZ) and the Bogenfels Formation (Chameis Sub-terrane) (Frimmel *et al.*, 2001c). The Holgat Formation displays graded bedding from which a turbiditic origin (relatively proximal to the source) could be inferred (Frimmel, 2001a).

An isolated dolomite outcrop (Chapter 3) occurs within the Mittag Formation. The stratigraphic position of this dolomite is unknown (Figure 7.3) but it is interpreted as a former evaporite (Chapter 3). This former evaporite could be similar to the Duruchaus Formation evaporite in the southern Damara Belt (Behr *et al.,* 1983) formed in a playa-lake or sabkha environment.

This study has shown that the rocks of the Oranjemund Group, Oranjemund Sub-terrane (MT) first underwent southeastward transport (D_1), followed by intense E-W compression (D_2). A late-stage D_3 event generated buckling with NW-SE trending F_3 open folds. The Schakalsberge Thrust separates the PNZ and the MT and records top-to-southeast tectonic transport (Davies and Coward, 1982; Von Veh, 1993). The metamorphic grade for all three sub-terranes of the MT falls in the lower greenschist facies (Frimmel, 1995). Continent collision at 545±2 Ma (Frimmel and Frank, 1998) is characterised by intense southeast and eastward folding and thrusting.

The three sub-terranes of the MT could be allochthonous or autochthonous. If the sub-terranes were allochtonous, a difference in metamorphic grade would be expected, but this is not the case. The assumption therefore has to be made that the Sub-terranes were either autochthonous or para-autochthonous ("piggy back" model suggested by Hartnady and Von Veh, 1990).

The metamorphic grade for the whole of the MT is similar and falls in the lower greenschist facies (temperature about 340 °C) (Frimmel, 1995). The peak of metamorphism in the PNZ was at about 500 °C. The required thickness of the MT to make up the PT difference of 160 degrees celsius can be calculated as follows. The density for mafic rocks can be taken as 3 and 2.5 for siliciclastic rocks (average 2.75). Using the geothermal-gradient curve (Frimmel, 1995) and assuming a pressure and density, an average thickness of 6 km for the MT can be calculated ($P = \rho.g.d$ with ρ-density, g-gravity and

d-depth). Assuming that the three sub-terranes are equal in thickness, an estimated thickness of 2 km per sub-terrane can be deducted. Each sub-terrane has its own crustal thickening and therefore it is estimated that the original strata of the Oranjemund Group may have been only a few hundred metres thick. Using the geothermal-gradient curve estimation (Frimmel, 1995) the difference in temperature for the metamorphism in the three Sub-terranes is less than 10 °C. The Schakalsberge Sub-terrane, placed at the bottom of the "piggy back" stacking is expected to have a slightly higher temperature than the Oranjemund Sub-terrane overthrusted in turn by the Chameis Sub-terrane.

The meta-sedimentary rocks of the Oranjemund Group have most likely been derived from the meta-basites of the Schakalsberge Sub-terrane and possibly from the meta-basites of the Chameis Sub-terrane. The Oranjemund Group is therefore stratigraphically higher than the meta-basites (Schakalsberge Sub-terrane) and possibly higher than the meta-basites (Chameis Sub-terrane) (Figure 7.3).

CHAPTER 8 – DIAMOND TRAPSITES IN A MARINE ENVIRONMENT

Diamond Area No. 1, more commonly referred to as the Sperrgebiet (Figure 1.1), on the southwestern coast of Namibia (Hallam, 1964), hosts one of the world's largest diamond placer deposits. To date, the bulk of the diamonds mined from this placer deposit have been sourced from Late-Cenozoic marine deposits (Hallam, 1964), lying onshore in Mining Area no. 1 (MA1). These marine deposits rest unconformably on the Late-Proterozoic rocks of the Pan-African Gariep Belt. The width of the marine platform in the study area on which the diamond deposits rest varies from 3000m at the Orange River mouth to less than 500m in the north near Chameis Bay (Figure 1.2).

A fundamental parameter controlling the distribution of alluvial diamonds in the mining area is the marine erosion pattern on the bedrock surface (Figure 1.3). Oosterveld *et al.* (1987) recognised the significance of statistical evaluation parameters for diamondiferous marine deposits in a complex geological environment. There are a number of factors influencing the complexity of the geological environment in the study area. Firstly, the diamonds were delivered to the marine environment via the 100 Ma old Orange River system (see Chapter 2.2). The bulk of the diamonds were delivered to the Atlantic coast during the early mid-Miocene (19-17Ma ago, Pickford, 1987), while another contribution from the Orange River is considered to have come during the Plio-Pleistocene (Jacob *et al.*, 1999). Secondly, the diamonds were reworked by the marine system and concentrated and trapped in gravel beaches (Spaggiari *et al.*, 1999). Thirdly, the marine erosion platforms, which contain diamond trapsites (variable potholes and gullies), underlie the diamondiferous beaches. The distribution of the diamonds is therefore directly related to the presence of a diamond-carrying gravel and to the quantity and quality of the trapsites and the degree of reworking which has taken place (Kalbskopf, 1978).

Previous workers (eg. Kalbskopf, 1978 and Wright, 1964) worked in portions of the study area, but to date no quantitative assessment of the marine erosion pattern over the whole study area has been done. The newly acquired structural and lithological data now makes possible investigation by the control of local structural features and lithology on erosion patterns over the whole study area.

8.1 Climate

The study area lies in the Namib Desert and has a low annual rainfall of 40-50 mm. The average water temperature of the northward flowing Benguela current is 10 °C and the average maximum daily air temperature is 23 °C. Prevailing winds from the south (Figure 8.1) have an average daily maximum velocity of 8-9 knots between the Orange River mouth and Mittag (Murray *et. al*, 1970). Winter months are characterised by sporadic hot east winds from the interior. A north wind occasionally brings rain and when there is no wind, mist creeps in from the sea providing life-giving moisture in this arid environment.

The coast is exposed to swells with a height of > 3m for about 8 days per month in the summer and up to 14 days per month in the winter. Upwelling of the cold waters of the Benguela and the strong winds are due to the proximity of the South Atlantic anticyclonic system (Figure 8.1). The tidal range is less than 2m and therefore falls into the micro-tidal range.

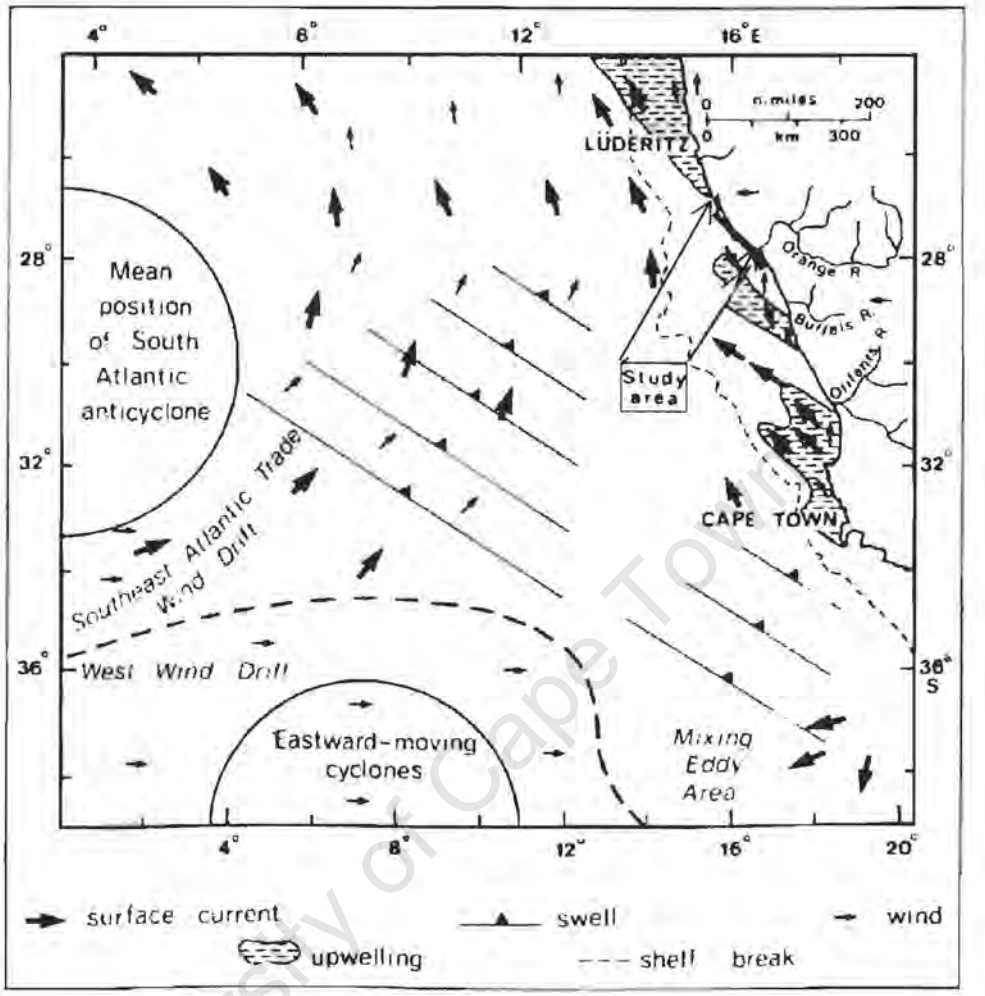

Figure 8.1 Synoptic map: Meteorology and hydrology of the South Atlantic (after De Decker, 1986).

8.2 Previous work

8.2.1 The nature of the marine diamond deposits in MA1

The marine (abrasion) erosion platform was cut by several major river channels, but is now completely filled with silty clays and quartz rubble (Murray *et al.*, 1970). This reflects low stands of sea level prior to the deposition of the diamondiferous beach sediments. A total of six raised beaches (Figure 1.4) have been divided into younger (lower) terraces (A, B and C beaches) and older

(upper) terraces (D, E and F beaches) (Stöcken, 1978). The beaches of the upper (late Plio- to early Pleistocene) terrace all hosts a warm-water fossil fauna *Donax rogersi.* The younger (mid-Pleistocene to Holocene) beaches are characterised by modern cold water fauna (Pether, 1986). All the beaches of the upper terrace underwent down-warping towards the north and this can be seen in their changing elevations and the change at the base of the main cliff at +25m a.m.s.l. near the Orange River mouth (Figure 1.4) and +9m a.m.s.l. in the Affenrücken area (Hallam, 1964). The younger beaches maintain a constant elevation all along the coast and gradually overstep the older beaches, which have been down warped towards the north. The C-beach maintains a constant elevation of +8m, a.m.s.l. all along the coast. Emplacement of the C-beach is associated with the world-wide high stand of sea-level during the interglacial period about 120 000 years (oxygen isotope) ago (Shackleton and Opdyke, 1973). This makes it possible to set a maximum age for the emplacement of the lower terraces (Stöcken, 1978).

The degree of reworking of diamondiferous gravel influences diamond concentration. The degree of reworking during deposition is, in turn, controlled by the degree of turbulence and length of sea level standstill and will be discussed further later in this chapter. This implies that high concentrations of diamonds can be found on both smooth wave-cut platforms, as a result of lengthy still stand, as well as on gullied bedrock where vigorous turbulence has taken place. Therefore, the distribution of diamonds is different for each of the six recognised raised beaches; the F- and B-beaches being the two richest beaches (Hallam, 1964). The older platforms (Figure 1.4) host higher diamond concentration than the younger marine platforms, but in all cases diamond concentration remains a function of the amount of reworking.

Marine erosion platforms in the study area are under the influence of the following:

(a) Coarse sediments brought down by the Orange River provide the materials needed to cut the platforms. This sediment, up to 800mm in grain size, comprises abundant, tough Nama Group quartzite, which has clearly persisted through the many cycles of accumulation and erosion of previous beaches spread onto the continental shelf. In this respect this shelf differs from many other shelves of the South Atlantic coastline.

(b) Although the tidal range is small, the wave energy is great. This part of the African coast has been regarded as one of the most energetic in the world.

(c) The Late Proterozoic bedrock varies considerably throughout the study area. There are a number of factors known to control the nature and rate of platform cutting:

- Lithology. The bedrock ranges from hard meta-arenites to very soft highly weathered meta-sedimentary rocks in places. The chlorite schists and meta-arenites occur in alternating bands of different thickness (Chapter 3).
- Dip and Strike of the meta-sedimentary rocks. The strike remains roughly N-S throughout the study area. The dip varies from 45 degrees to the west to 60 degrees to the east. In some places the dip is between 80 to 85 degrees (Chapter 4).
- Jointing. The dominant local joint directions are 060-070 degrees and 120-140 degrees (Chapter 4). These joints are in places exploited by erosion.

The inner shelf off the coast of Namibia has been subject to transgression and regression since mid-Eocene (Figure 8.2). Murray *et al.* (1970) found diamondiferous beach deposits on the shelf, drowned by the present Holocene highstand that only reached its present level a mere 6000 years ago. The most prominent low stand is at –20m and this can be traced over a distance of 550km from Kerbehuk northwards. The platform varies in width and slopes seaward at about 1 in 70. A cliff that ranges in height from 1.5 to 5m (below sea-level) has been mapped for about 20 km of its length in the Kerbehuk - Affenrücken area. The cliff generally runs parallel to the present day coastline. The strike of s_2 in

the Kerbehuk area is between 0º and 10º. The regional joint direction in this area has a trend of 110º and a second locally dominant joint set has a trend of 140º.

These joint sets give the cliff a zig-zag pattern, but the general trend of the coastline remains parallel to present-day coastline (Murray *et al.*, 1970). Acoustic profiling found break in slope at –38m, -44m, -50m, -60m, -75m and –100m. The –75m break in slope could be traced for several hundred kilometres southwards from Bogenfels.

The type of trapsite (gully) formed is dependant on the amount of boulder material available (Figure 8.3) (Oosterveld *et al.*, 1987 and Kalbskopf, 1972). If few boulders are available structural features will be exploited, while an abundance of boulders will increase the erosive action of the waves and "Consequent" gullies (Kalbskopf, 1987) (Figure 8.4) will form, irrespective of the competence of the bedrock (Oosterveld *et al.*, 1987).

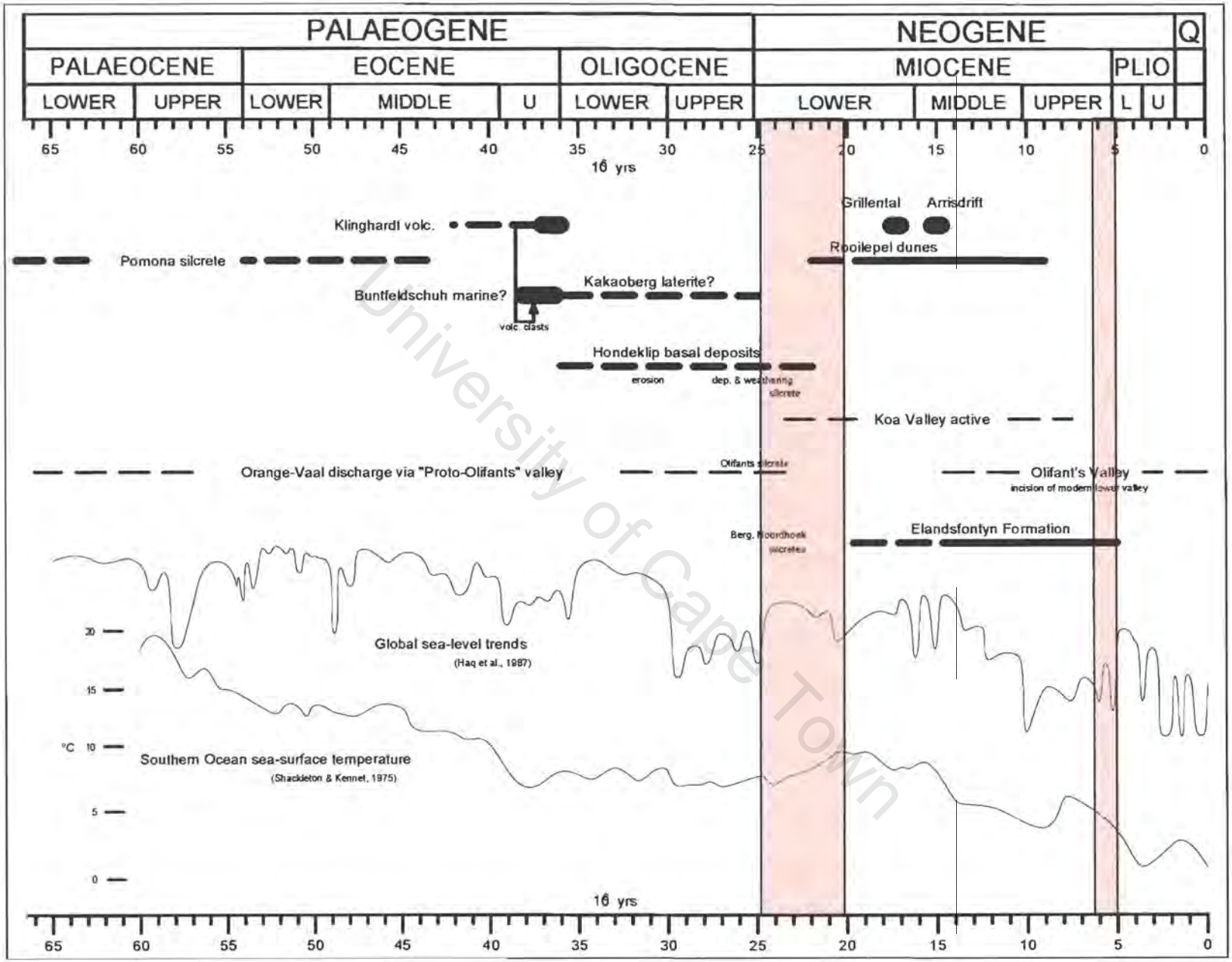

Figure 8.2 Sea-level trends and the geological evolution related to the diamondiferous deposits along the west coast of southern Africa (after Pether, 1986). The arrival age of diamonds in the study area is projected as an age just older than the age of the fluvial diamond terrace deposits in the vicinity of the Orange River mouth (Jacob et al. 1999).

Figure 8.3 A. Boulders and cobbles in a 2 m deep gully. **B.** Boulders and cobbles, predominantly Nama Group quartzite in this photo, act as abrasive agents. **C.** A modern day equivalent (Terrace Bay, northern Nambia) of boulders and cobbles acting as abrasive agents at the time when the gullies were cut, predominantly parallel to swash direction. At present the study area comprises a sandy system.

8.2.2 Previous gully classifications

The majority of diamond concentration takes place below bedrock peaks where maximum turbulence occurs. Kalbskopf (1978) classified 3 types of gullies according to their genesis (Figure 8.4):

i. A "Consequent or Slope gully" is formed as a consequence of the steeper inclination of the local shelf slope.

ii. A "Subsequent gully" follows the strike of the bedding or foliation and forms as a result of differential weathering of harder and softer units.

iii. A "Joint gully" is formed by exploitation of local structural features in the footwall.

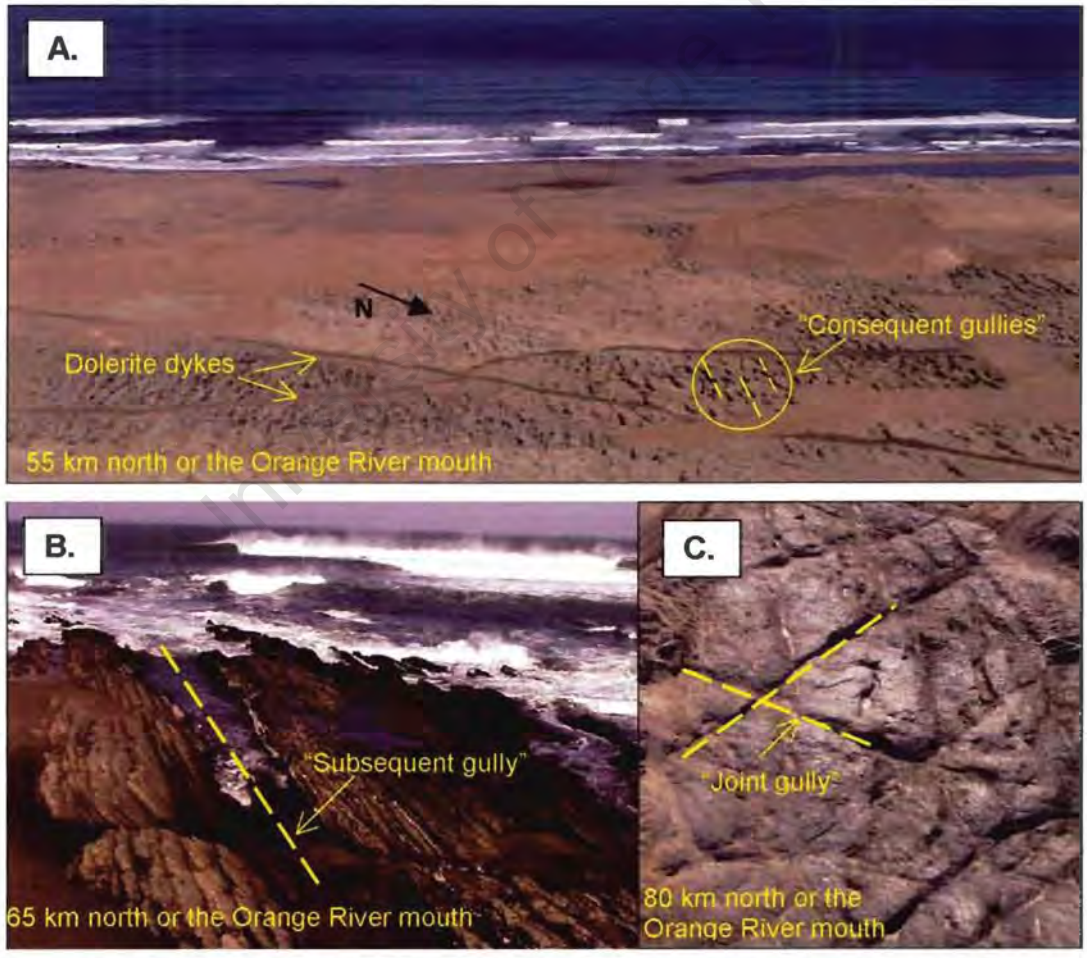

Figure 8.4 Kalbskopf's (1978) gully classification. **A.** "Consequent or Slope gully", **B.** "Subsequent gully" and **C.** "Joint gully"

Wright (1964) found that gullies in a part of the study area are generally independent of bedrock structural planes. The structural planes may have influenced gully trends especially on gently inclined platforms. The dominant gully trend is normal to former coastlines. An ideal cycle of gully evolution proposed by Wright (1964) is summarised as follows (Figure 8.5)

- **Incipient:** Isolated potholes and aligned potholes in very variable resulting trends. Little of bedrock surface dissected, perhaps less than 10 percent.
- **Youthful:** Coalescence of potholes into closed gullies. Some uniformity of trend. Up to 50 percent of bedrock surface dissected.
- **Mature:** Coalescence of closed gullies to form an integrated drainage system of open gullies following a definite trend line. Up to 80 percent of the bedrock surface dissected. Maximum gully depth reached at the onset of maturity.
- **Post-mature:** Reduction of inter-gully area so that islands of bedrock shelf mark the direction of alignment.

For the purpose of this study the following genetic gully classification (Figure 8.6) will be used. "Swash gullies" are orientated parallel to the swash direction ("Consequent gully" of Kalbskopf, 1978). "Strike gullies" are formed due to differential weathering of harder and softer lithological units ("Subsequent gully" of Kalbskopf, 1978). "Joint gullies" are formed due to the exploitation of local joint features in the bedrock. Kalbskopf used the term "Consequent gully" for "Swash gully" and "Subsequent gully" for "Strike gully".

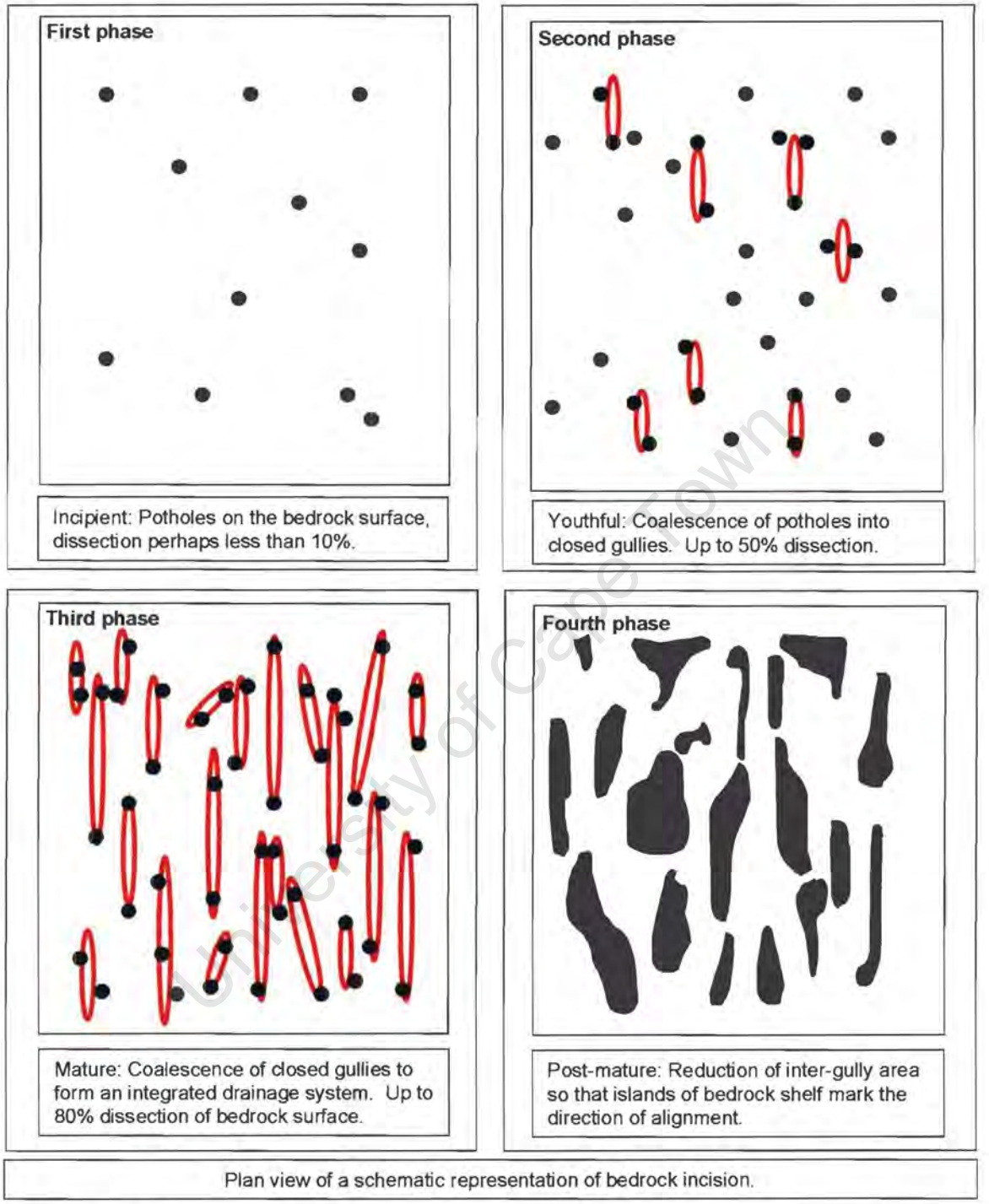

Figure 8.5 An ideal cycle of gully evolution (after Wright, 1964).

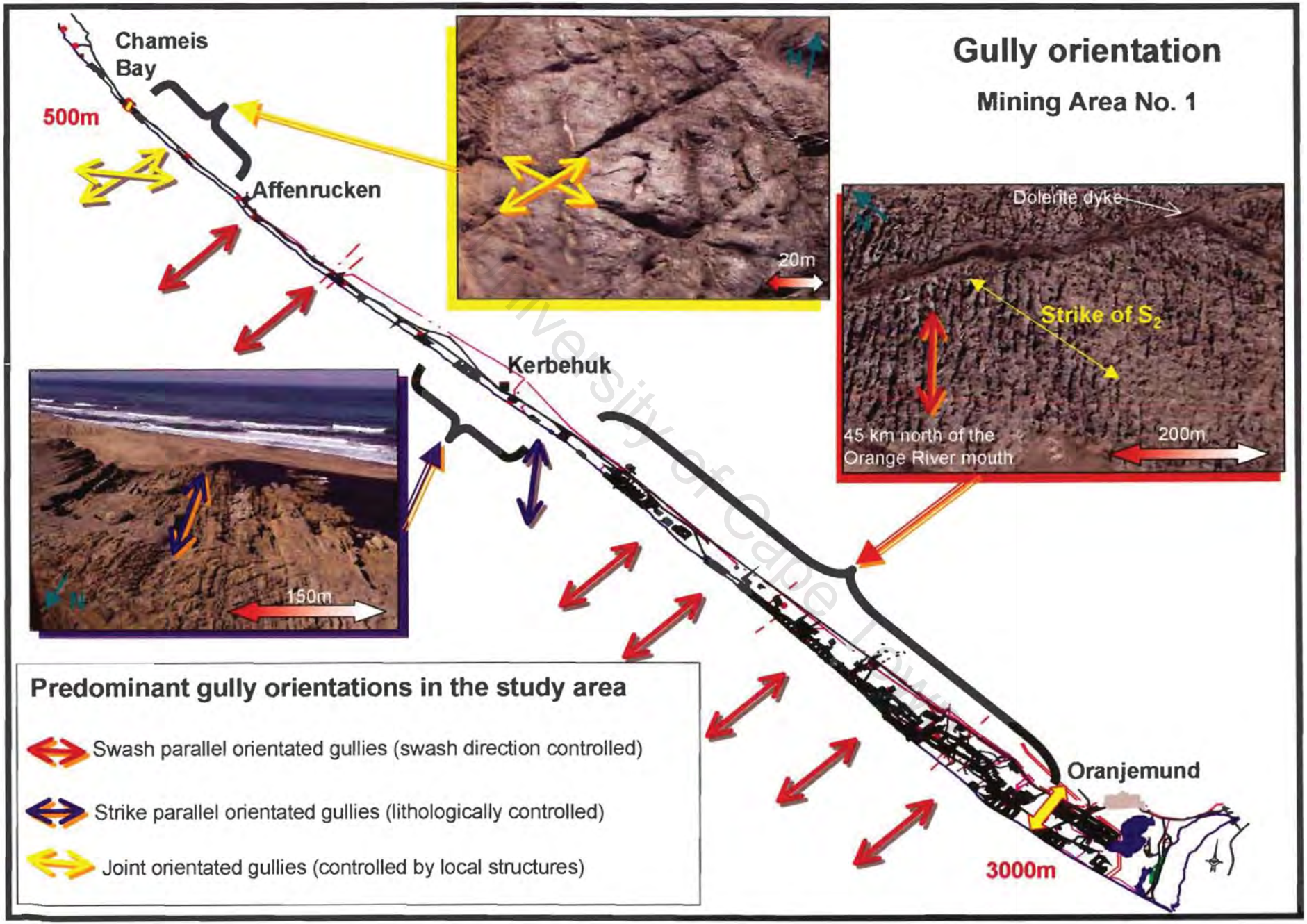

Figure 8.6 Genetic gully classification and distribution in MA1. All photographs are oblique aerial photographs.

8.2.3 Statistical evaluation of the deposit in MA1

Oosterveld *et al.* (1987) recognised that two models are necessary for evaluating an ore deposit. The first is the geological model, which provides an understanding of the distribution of ore minerals and takes many complex geological parameters into account. The second is the statistical model which is obtained from samples taken from the deposit. To obtain optimum evaluation of a deposit the relationship between the statistical and the geological parameters must be found.

Statistical parameters are used when the grade (G) is calculated:

$$G = D \times S \qquad (1)$$

D - estimate of the average number of diamonds per unit
S - estimate of the mean value of diamonds size

$$D = \alpha\theta/2\sqrt{(1-\theta)}$$

$$= \beta/\sqrt{(1-\theta)} \qquad (2)$$

α,θ - distribution parameters
β - function of α and θ

The α and θ parameters are estimated by means of a joint maximum likelihood estimation method with both α and θ unknown. Sichel (1972) derived a model which represents diamond density distribution (the compound Poisson distribution). For derivation of this model and estimation of the parameters see Sichel (1972).

Addition of components can be obtained by converting (2) to logs.

$$\log D = \log \beta + \log (1/\sqrt{(1-\theta)})$$

where log β and log $(1/\sqrt{(1-\theta)})$ are called the Beta and Theta contributions. Oosterveld *et al.* (1987) found that an increase in the Beta contribution could be related to an increase in the supply of diamonds, which is a function of the rate of the marine transgression and availability of diamonds at the time of deposition. A higher Theta contribution implies more diamonds in trapsites and it can be said that the "quality" of these trapsites is improved.

There are similarities in the scale and trend of the Beta contribution. These similarities in trap "quantity" can be expected when dealing with beaches in the same ore body with similar bedrock characteristics. For example, the erosion platform on which these beaches lie might have been developed during earlier marine transgressions. It is therefore possible for two or more beaches to lie on one old abrasion platform thus having similar trapsite development.

Cliffs produced by marine transgression back both the F and the B beaches (Figure 1.4). The Theta contribution is the highest on these two beaches. The high Theta contribution for the B beach is related to both the influence of the cliff and the high degree of reworking of older deposits. An increase of coastal slope in the north caused the beach width to decrease and the amount of reworking to increase.

Oosterveld *et al.* (1987) make the assumption that there is a uniform diamond supply related to the rate of marine transgression. Diamonds have been in the marine environment since the early mid-Miocene. In addition, more diamonds were added to the marine environment during the Plio-Pleistocene. The area of transgression is a function of the slope of the transgression surface and the magnitude of sea-level rise (pers. com. B. J. Bluck). It is not correct to

assume that the rate of marine transgression is related to an increase in the Beta contribution (amount of diamonds available).

A higher Theta contribution is assumed by Oosterveld *et al.* (1987) when there are more diamonds in trapsites, e.g. higher "quality" of trapsites. An example is used that if two diamondiferous beaches were to be deposited on the same platform the trapsite development would be similar underneath both beaches. Field observations and aerial photographs, however show that variation in trapsite development on a single platform is common and to assume that the "quality" of trapsites remains the same throughout one platform creates a false impression.

8.2.4 Physical characteristics of marine platforms

Wright (1964) postulated an ideal gully cycle with four stages: incipient, youthful, mature and post-mature. In order to understand these erosion patterns one must first look at wave energy. The following questions need to be answered: how do platforms form; what forces play a role in causing marine erosion patterns, and why does the depth of incision into these marine platforms differ?

Heydorn and Tinley (1980) noted that the difference between the highest and lowest tidal range on the West Coast is 60 cm and that the tidal range at Port Nolloth (100km south of the Orange River mouth) is 1.6m. Erosional features at depths shallower than –20m could have formed since the time sea-level reached its present level (De Decker, 1987). Tankard (1976) quoted evidence for a sea-level elevation within a metre of the present elevation between 5.5 and 6 ky before present. Another sea-level stillstand close to present day sea-level took place 120-130 ky before present during substage 5e of the last interglacial (Shackleton and Opdyke, 1973). Below, a more detailed investigation of platforms possibly related to sea-level stillstands is undertaken.

Sunamura (1994) argued in favour of wave action as the formative process in the development of shore (marine) platforms based on observations of visually impressive waves impinging on platforms. Stephenson and Kirk (1998) argued that platforms result from sub-aerial weathering. Morphological change data, rather than direct investigation of processes operating on shore platforms, was the basis for their argument. Morphology is however an ambiguous indicator of process (Mii, 1962).

Sunamura (1992) defined the resisting force of rock (F_R) as the mechanical strength of rock. The mechanical strength is strongly influenced by lithology, structure and weathering. The assailing force of waves (F_W) was represented using deep water wave energy. If F_W is greater than F_R, erosion will occur. No erosion will occur if F_R is greater than F_W. As waves impinge on a platform or cliff, a number of forces can cause erosion. Breaking wave shock, water hammer, air compression in joints, hydrostatic pressure, cavitation and abrasion are all causes of erosion on shore platforms (Saunders, 1968). The most effective wave erosional processes require frequent interplay of air and water. Abrasion is dependent upon the degree of agitation of the water and sediment and is therefore probably most effective in the swash zone and in shallow water.

The rock coast of south-western Africa has been classified on a global classification scale in terms of wave environment, tidal range, and late Holocene sea level history, as follows. West coast swell environments are subject to long waves with high energy in the higher latitudes. Energy levels are less in the lower latitudes (Davies, 1972). Clark (1980) classified the south-western coast of Africa as a zone consisting of all the continental margin types.

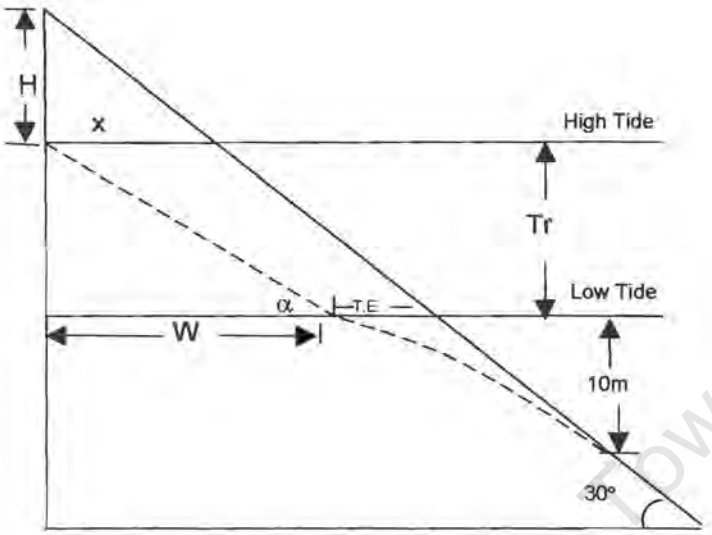

Figure 8.7 Model by Trenhaile and Bryne (1985) to illustrate the development of shore platforms. The dashed line shows the position of the subtidal and the intertidal shore platforms after time T, following one period of cliff undercutting, collapse and debris removal.

Trenhaile and Bryne (1985) developed a model (Figure 8.7) to simulate the development of shore platforms under stable sea level conditions. The model is based upon the assumption that cliff recession results from alternations of periods of undercutting and debris removal at the high tidal level. The time needed to undercut a cliff is given by:

$$T1 = Rx/A\tan\alpha$$

T1 – time needed to undercut the cliff

x – maximum depth of the undercut before collapse

R – wave energy needed to cut one unit depth

A – annual deep water wave energy

α - gradient of the intertidal platform.

W – width of the intertidal corridor

Tr – tidal range ($\tan\alpha$ = Tr/W)

H – total height of cliff

The subtidal erosion rate was made proportional to the water depth so that:

$$E2 = E1.h1/h2$$

E1,h1 – rate of erosion and water depth at level 1

E2, h2 – rate of erosion and water depth at level 2

The model suggests that rising sea levels are normally more erosive than falling sea-levels. The erosive efficiency of the waves usually increases with the rate of sea-level rise and decreases with the rate of sea-level fall (Trenhaile and Bryne, 1985).

Hallam (1964) and Gurney *et al.* (1982) found that along the West Coast, diamondiferous deposits are more likely to occur along the base of a wave-cut cliff, within gullies and potholes, on the southern side of reefs that trend north-eastward and the northern side of south-facing bays, as well as along palaeo-channels scoured by fluvial action.

According to Wright's (1964) ideal gully cycle with its four stages, the first stage begins with a marine platform. Potholes form in weaker zones of the platform (e.g. joint intersections, parallel joints and weaker lithological spots) and dissect the shore platform. Wedges of bedrock are sometimes removed from the platform at joint intersections by wave shock, water hammer, or air compression

in joints. These potholes and joint intersection wedges then become interconnected to form a network of gullies (Figure 8.6).

8.3 Trapsite cutting mechanisms in MA1

8.3.1 Lithologically controlled erosion patterns

Alternation of chlorite schistose and meta-arenite units (or layers) occurs on different scales throughout the study area. Where the alternating layers are between 0.5m and 3m thick, differential erosion of the layers is most likely to occur (Figure 8.8). Differential erosion does not take place where the alternating layers are less than 0.5m thick.

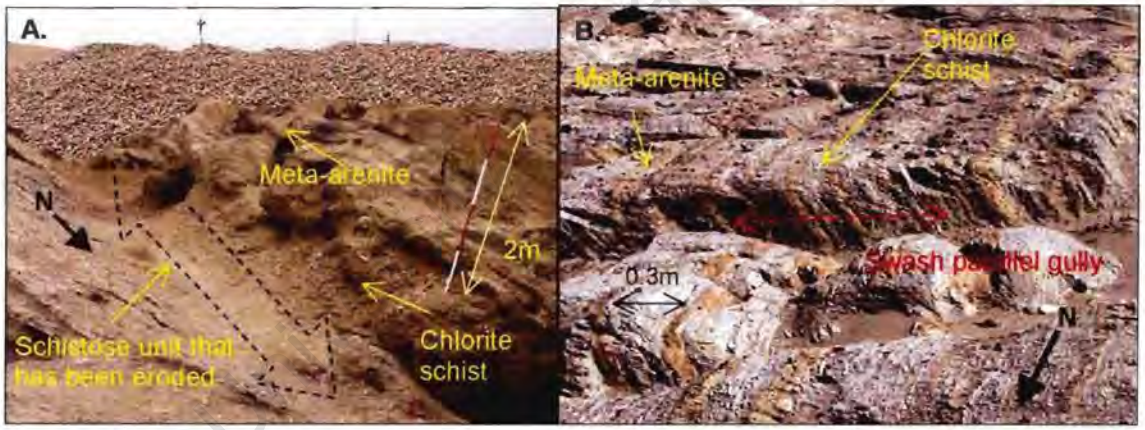

Figure 8.8 Differential erosion of harder and softer lithological units. **A.** The softer schistose unit (about 2m thick) has been eroded creating a high-potential diamond trapsite (35 km north of the Orange River mouth). **B.** The width of the lithological layers is less than 0.5m in this case and differential erosion did not take place. The only erosion that occurs here is a swash-parallel gully (red dashed line) (80 km north of the Orange River mouth).

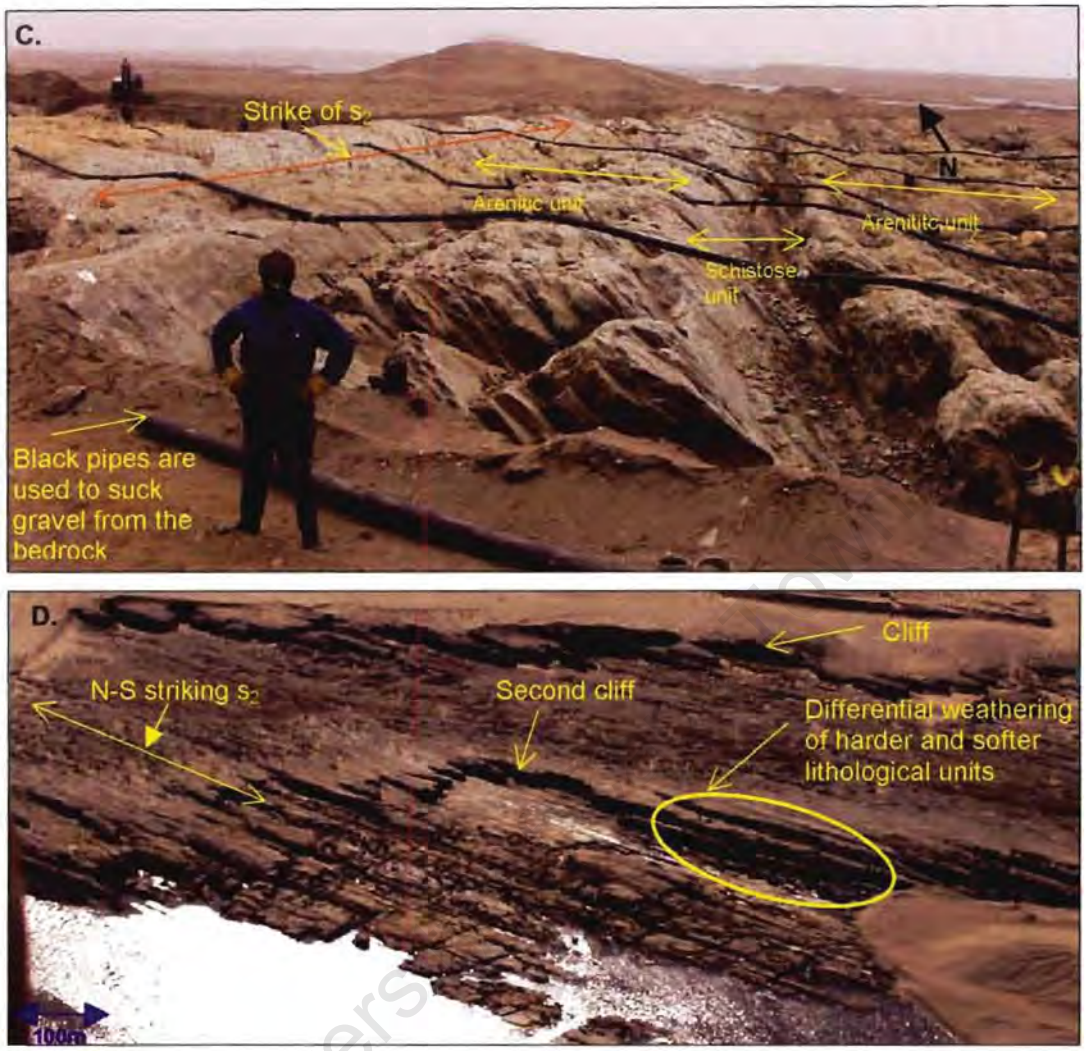

Figure 8.8 (continued) **C.** Differential erosion of the softer schistose unit, parallel to the strike of s_2 (12 km north of the Orange River mouth). The zigzag course of the cliffline is controlled by jointing. **D.** Differential erosion is most spectacular where s_2 dips between 80 – 89 degrees to the west in the Kerbehuk area (60 km north of the Orange River mouth).

8.3.2 Factors controlling the type and distribution of gullies

Gully distribution and genetic classification along the coast can be seen in Figure 8.6. Accepting the theory that "Swash parallel gullies" are formed when there is an abundance of abrasive agents (boulders) available (Kalbskopf, 1978), then the dominant occurrence of "Swash parallel gullies" from the Orange River mouth to Mittag can be easily explained due to this area's close proximity to the

source (the Orange River) of the abrasive agents (eg. boulders and cobbles). As the abundance of boulders and cobbles decreases away from the source, sand increases to the north. The fact that the two younger platforms in the area from the Orange River mouth to Mittag contain more structurally controlled gullies could be due to a lack of abrasive agents during their formative period. The structural features exploited mostly are joints (Chapter 4). The cliff-line has a characteristic zigzag pattern due to the exploitation of the 140 degrees and 110 degrees striking joint sets. Around the Kerbehuk area "Strike gullies" dominate. This is directly related to the dip of the s_2 bedding-parallel foliation of between 80 to 85 degrees west. Differential erosion of the softer schistose units dominates here where the harder arenitic units do not require the support of the schistous units (Figure 8.8). North of Affenrücken the dominant gully type is the structurally-controlled "Joint gully". These gullies are the furthest removed from the source of the abrasive agents and are therefore not as influenced by wave energy (i. e. swash parallel direction). All three of these gully types can be up to 100m long and 4m wide in places.

The depth of the gullies is controlled by factors, which will be discussed at a later stage (Section 8.4). Swash-controlled gullies ("Slope Gullies") are abundant on present-day outcrop between the Orange River mouth and Mittag. Divers have found that these gullies are far less common beneath the sea (Murray *et al.* 1970). This could be due to the fact that the equivalent stretch at sea is covered with sediment, implying that divers could not realistically observe the bedrock in this area.

Previous workers, e.g. Wright (1964), postulated an ideal gully cycle (Figure 8.5 and Figure 8.9). To date there has been no attempt to predict where the deepest incision on a platform could take place. Therefore a closer examination should be made of cutting mechanisms. In order to gain a better understanding of how gullies are cut, a detailed survey of a 40 m long and up to 7 m deep gully (20 km north of the Orange River mouth) was undertaken in the

field (Figure 8.10). The surveyed "Swash controlled" gully is blind on the seaward end and opens out on the landward end (Figure 8.10).

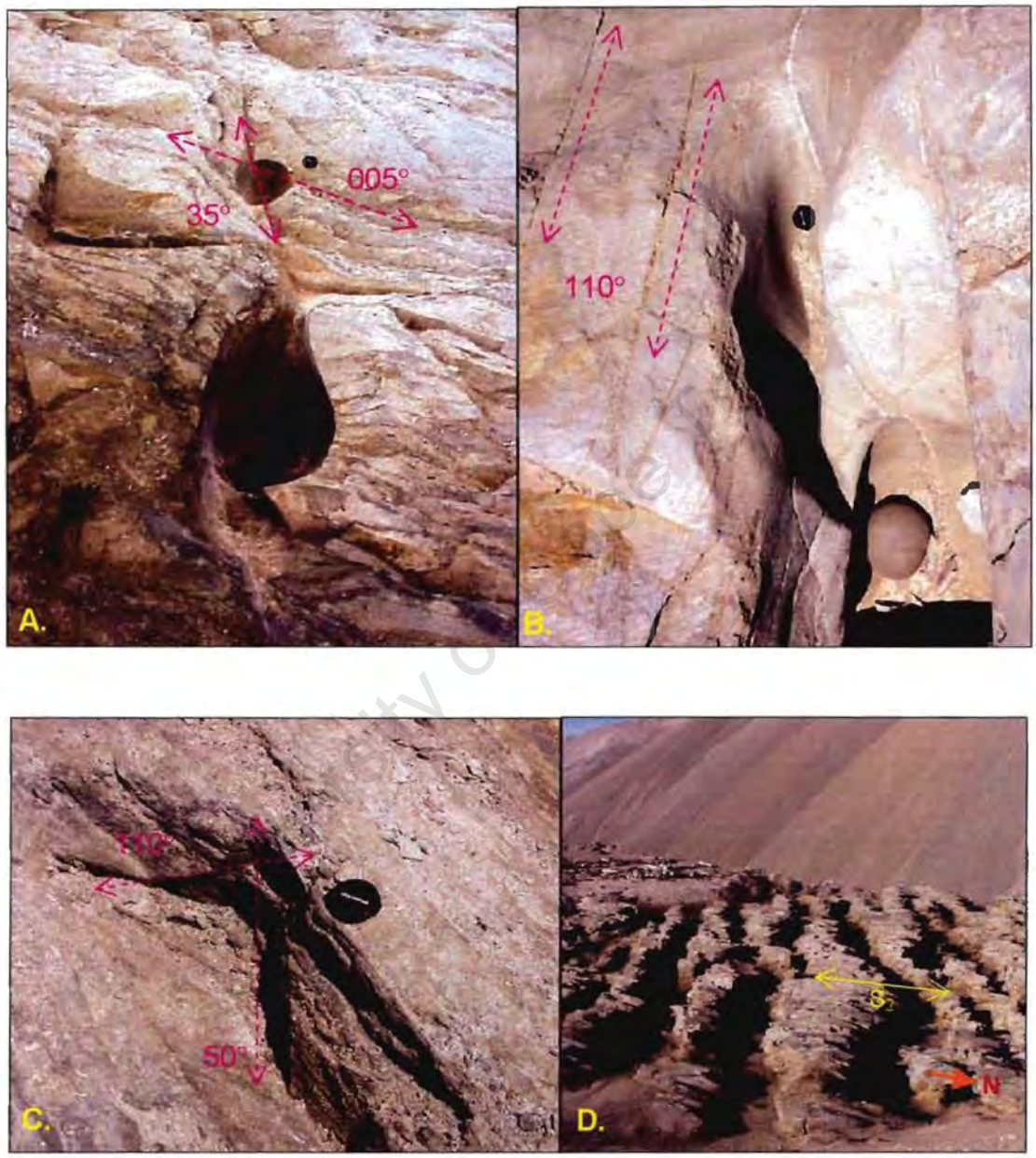

Figure 8.9 Potholes form along **A.** Joint intersections and **B.** zones of parallel jointing. **C.** A wedge of bedrock removed at a joint intersection. **D.** The series of potholes and removed wedges of bedrock are then interconnected to form a network of gullies, parallel to swash direction. A. and B. are 10 km north of the Orange River mouth, C. is 55 km north of the Orange River mouth and D. 18 km north of the Orange River mouth.

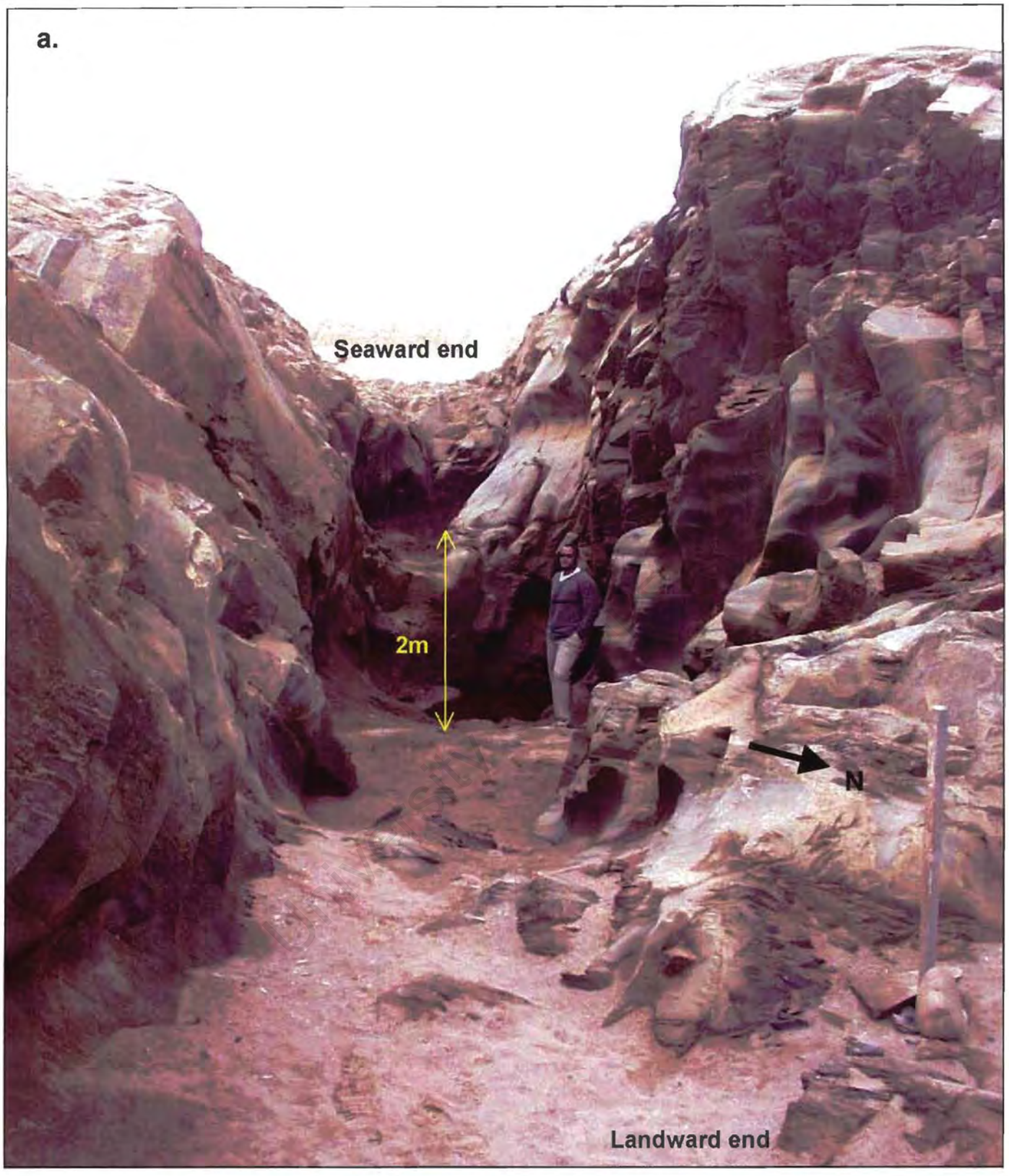

Figure 8.10a The "Swash parallel" gully (20 km north of the Orange River mouth) which was surveyed in the field. An Electronic Distance Meter (EDM) was used for this tacheometric survey. This gully is 40m long and up to 7m deep and incised into meta-arenite, which dips 45 degrees to the west (thus dipping towards the energy source).

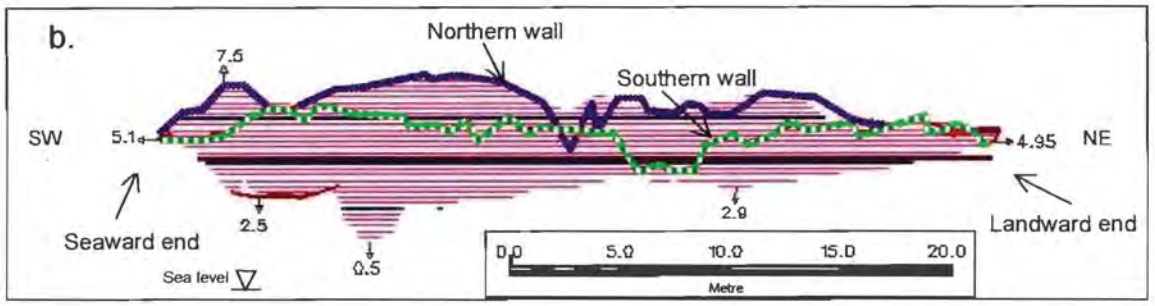

Figure 8.10b. A morphological section along the long axis of the gully shown in Figure 8.10a, showing both the northern and southern wall (with elevation m.a.s.l).

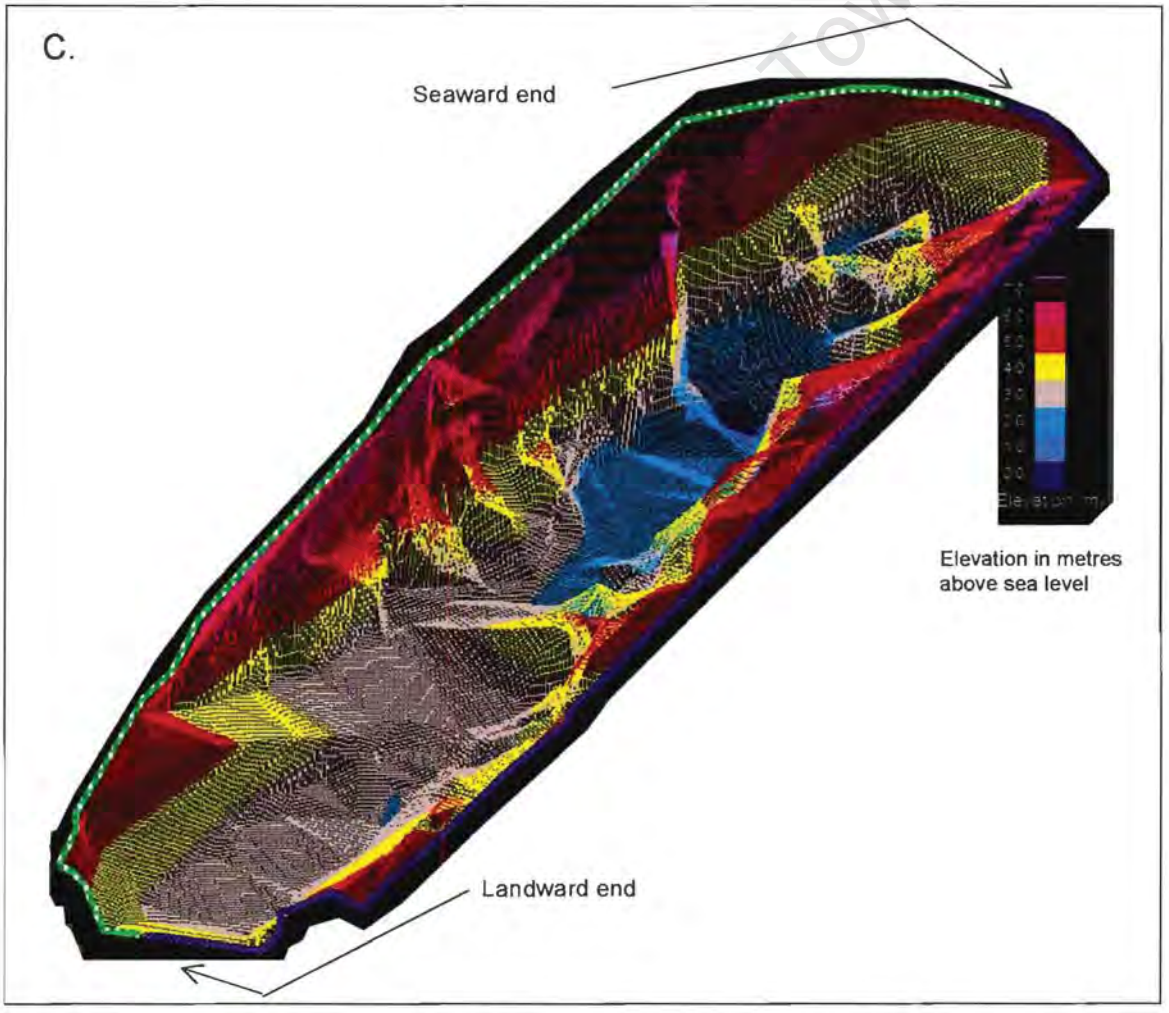

Figure 8.10c A three-dimensional computer generated model of the surveyed gully (Figure 8.10a), showing deepest incision into bedrock on the landward side.

The first observation which can be made is that the difference in depth of the two most seaward elevations of well defined potholes in this gully is 2.0m (Figure 8.11). It is interesting to note that the tidal range for the study area is 1.8m. This would imply that incision of a gully took place at different elevations at the same time during high water and low water cycle, forming a tidal gully. Another observation is that the deepest incision has taken place on the seaward end.

This gully forms part of a series of gullies (up to 7m deep) on the seaward edge of a platform. On the landward side of the series of "7m deep gullies" shallower gullies, blind on the seaward side and opening up on the landward side can be found (Figure 8.11). On the seaward side of these "7m deep gullies" (Figure 8.11), a lower elevation platform containing the same "Swash parallel" gullies, open to the landward side and blind to the seaward side are found. Why then do we find the deepest gullies (all swash parallel in this case) with their deepest ends parallel to the present-day coastline on the seaward edge of a platform?

At the beginning of 2000 new data was acquired by Namdeb with an "Airborne Laser Survey" (ALS). A complete data set of corrected ortho-photos for the whole MA1 became available as company proprietary data (elevation accuracy: +/-30cm). Elevations for the outcrop in the study area were obtained using the ALS data. These elevations were then contoured utilising the "Surfer" software. Individual platforms could then be identified from the contoured outcrop data. The seaward edges of these platforms were then scrutinised to see if the deepest incision had in fact taken place on the seaward extremities.

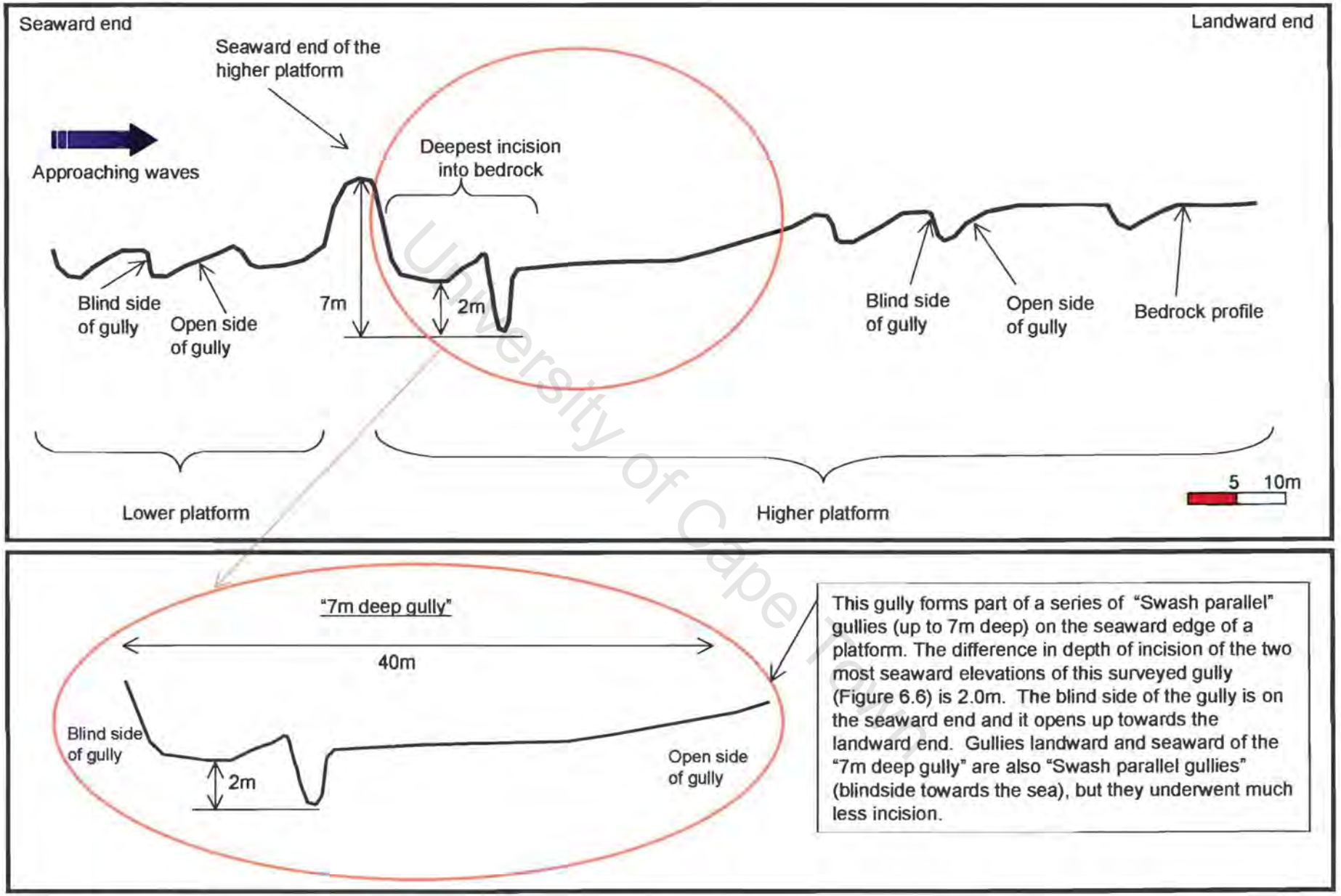

Figure 8.11 Schematic NE-SW section of platforms and gullies incised into bedrock.

8.4 Results and Discussion

The accuracy of the ALS survey provided, for the first time, the opportunity to compare the bedrock morphology with the historical sampling trench results. This was done by overlaying the sampling results on present-day outcrop exposed by mining activities, to visualise the influence of change in bedrock morphology on diamond concentration. Taking only the basal gravel sampling results into account and not looking at terrace gravel, positive results were found on the interface between platforms and in gullied areas (Figure 8.12a-d). The smoother parts of the platforms are less likely to yield positive results. Positive results of course are all dependent on the availability of diamondiferous gravel.

Historical sampling data are made up of the results obtained from one-metre trenches. The one-metre trenches (normal to the present day coastline) were divided into paddocks (1 metre wide and 5 metres long). Using the images (corrected ortho-photos) taken during the ALS survey, the outcrop over the whole study area was digitised. The points, which fall on outcrop, were then contoured (at 1m intervals) using the "Surfer" software package. The contoured images (Figure 8.12a) were then used to identify transitions between platforms. These transitions between platforms were subsequently overlayed over the corrected ortho-photos obtained from the ALS survey (Figure 8.12a-d).

Figure 8.12a shows the +8m bedrock contours combined with the sampling results. Positive results were found on the transition between platforms. "Swash controlled gullies" dominate on the older +4m to +12m platforms (Figure 8.12b) whereas "Strike gullies" and "Joint gullies" dominate on the younger +2m platform. The older platforms (+2m to +12m) were formed during a period when there was an abundance of abrasive agents (boulders). The younger +2m platform was formed during a time when there was a relative lack of abrasive agents (boulders). In the sand-covered areas between outcrop, transitions between platforms can be inferred (Figure 8.12c). The inferred

transitions are as a rule sub-parallel to the present day coastline. Kalbskopf (1978) suggested that the down-warping of the older beaches started in the Mittag area. The inferred transitions between platforms in Figure 8.12d are not sub-parallel to the present day coastline and it is therefore highly likely that this is the point of inflection for the down-warping of the older beaches.

The breaker zone is known to be the highest energy zone in a near shore marine wave system (Martinez and Harbuagh, 1993) (Figure 8.13). A wave breaks when its amplitude (wave height) is roughly equal to water depth. The type of breaking wave is related to the steepness and the gradient of the shore (Summerfield, 1991). As a wave front approaches the coast, the water depth decreases. At the point where the wave breaks (point of resistance where the water depth is less than the wave amplitude) the wave has the highest potential to carry the most abrasive material (Figure 8.13). This point could correspond with the seaward end of a platform (Figure 8.14). The most likely place on a platform for the deepest incision to take place would therefore be the seaward extreme of the platform, since wave energy decreases in the post-breaker zone. After a long swash-run-up backwash energy will also affect further incision due to creating turbulence within gullies. This is of particular importance in pothole development where rotating clasts drill holes into the bedrock and these potholes later become linked up as described in Section 8.3.2.

The best place for diamond concentration is an area with a high quality and quantity of trapsites and where diamond-carrying gravel (Figure 8.15) which has undergone extensive reworking (Figure 8.16) is present. Deepest incision into bedrock (best quality of trapsite) was found at the seaward extreme of platforms (Figure 8.17). The relation of wave energy and its capacity to incise into bedrock during a sea level still stand (in the breaker zone and pre- and post-breaker zone) is represented in Figure 8.18.

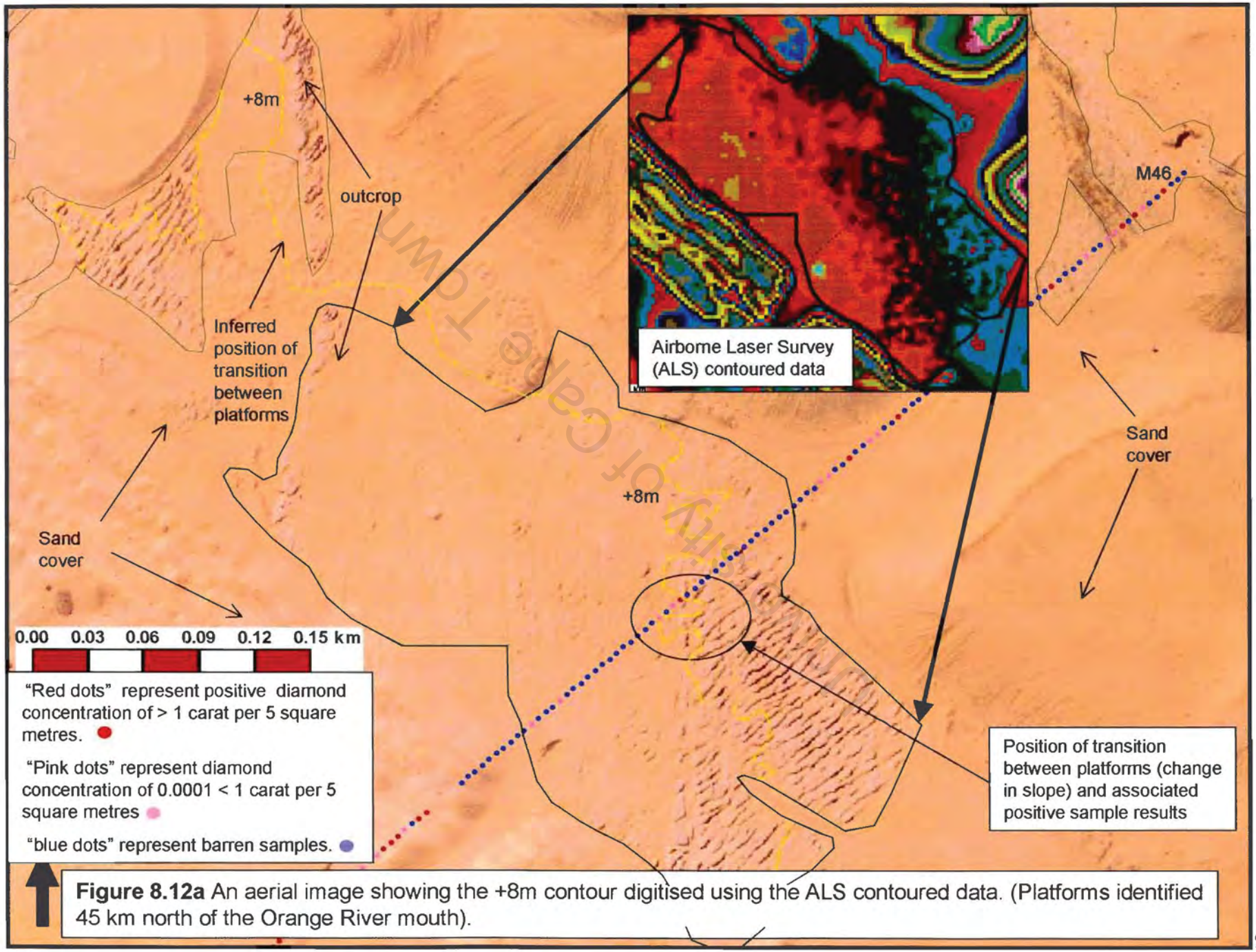

Figure 8.12a An aerial image showing the +8m contour digitised using the ALS contoured data. (Platforms identified 45 km north of the Orange River mouth).

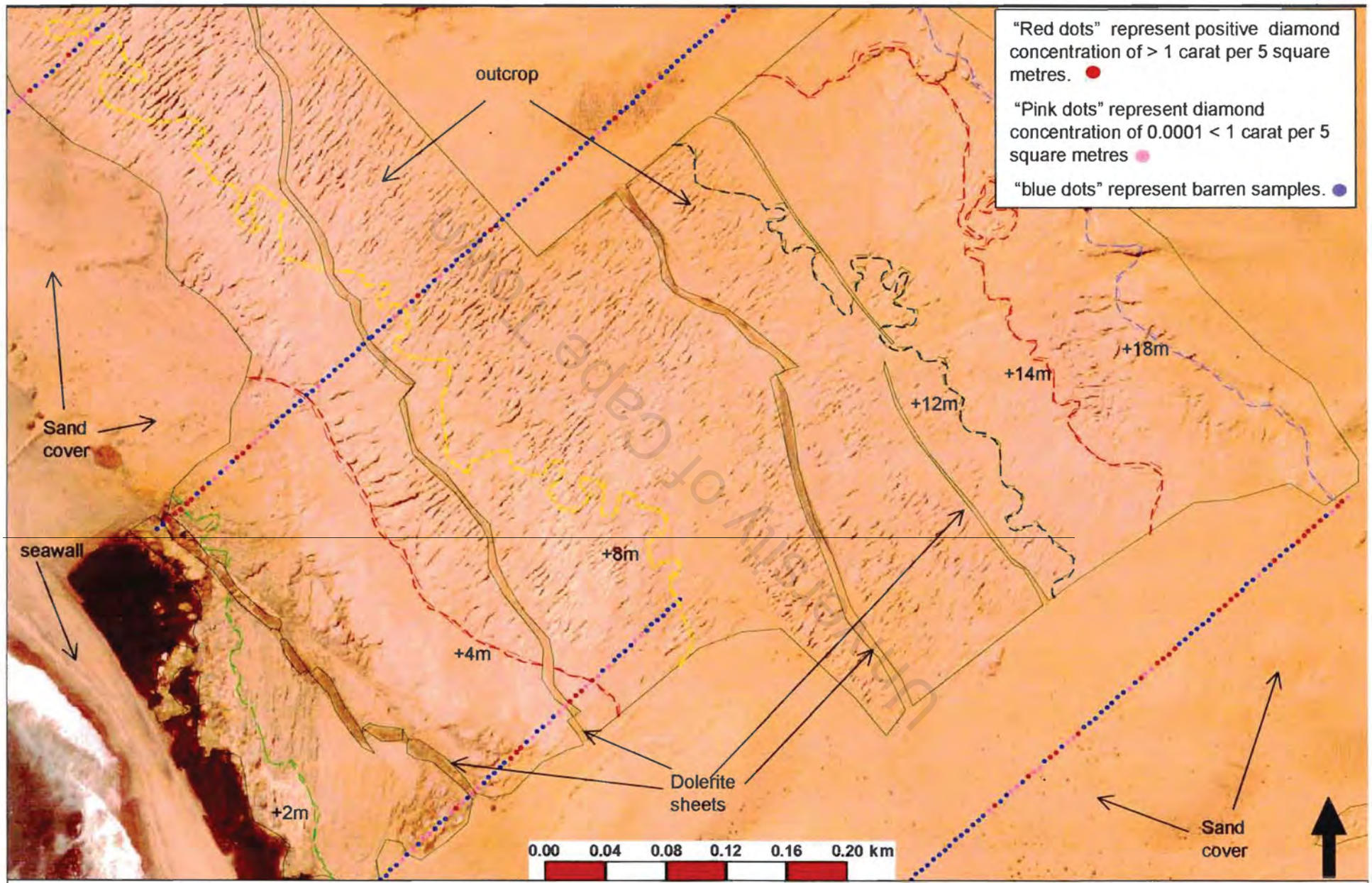

Figure 8.12b An aerial image showing the +2m to +18m contours digitised using the ALS contoured data. Note the structural and lithological controlled gullies on the +2m platform *vs* the "Swash controlled gullies" on the +4m to +12m platforms. (50 km north of the Orange River mouth)

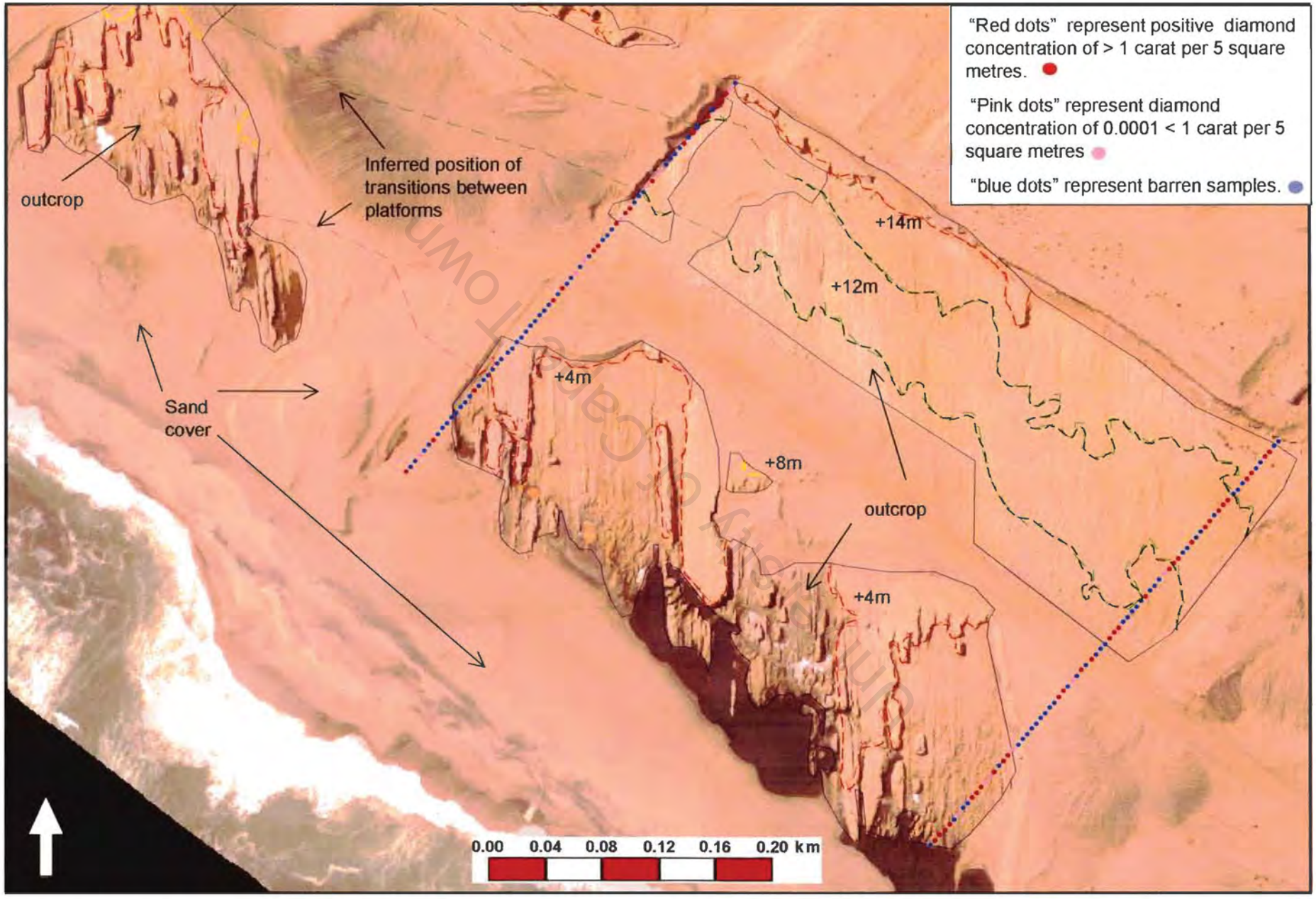

Figure 8.12c An aerial image showing the +4m to +14m contours digitised using the ALS contoured data. S_2 dips between 80-89 degrees towards the west here. The dominant gully type here is strike controlled. (60 km north of the Orange River mouth)

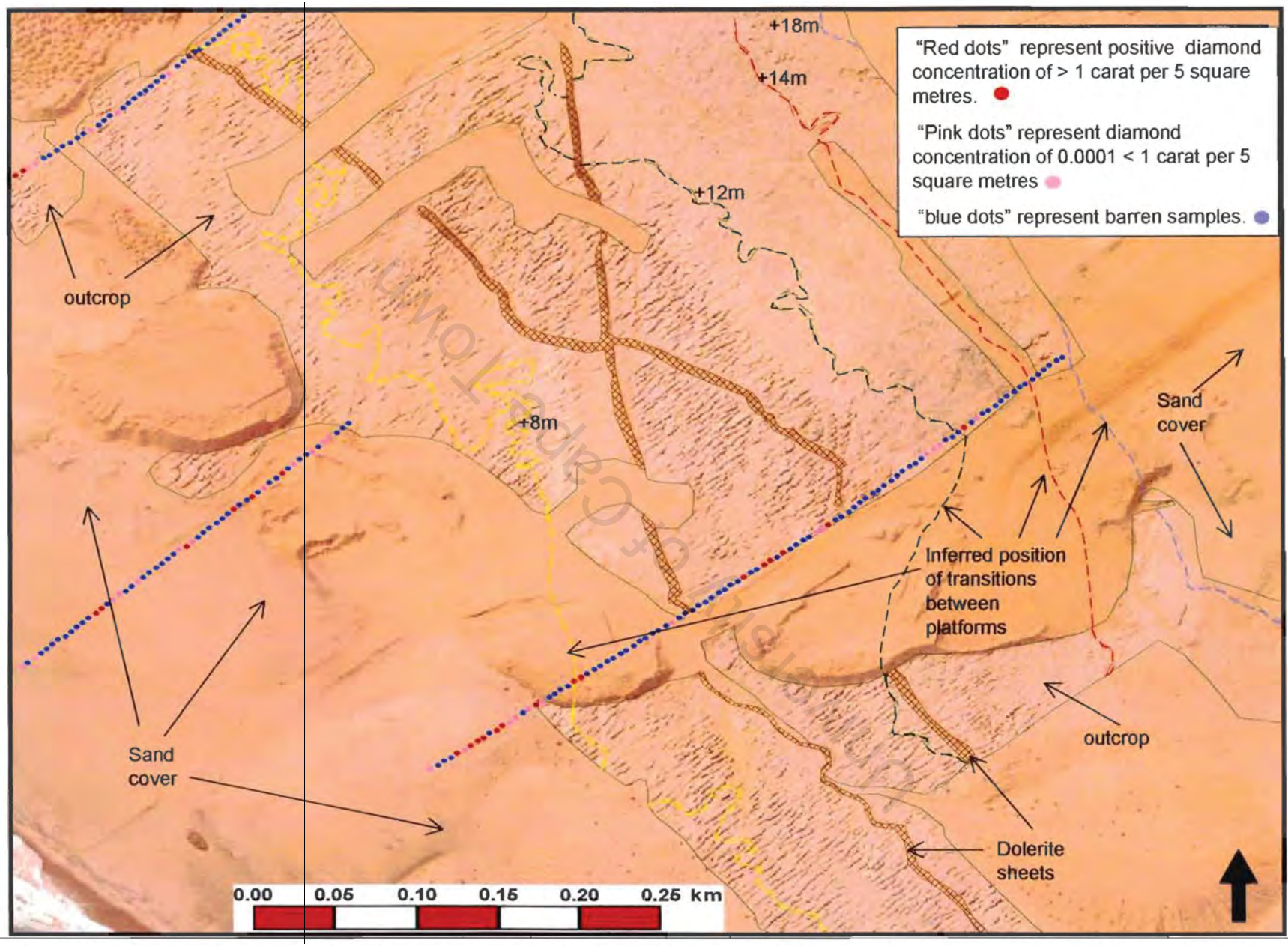

Figure 8.12d An aerial image showing the +8m to +18m contours digitised using the ALS contoured data. Kalbskopf (1978) proposed that the down-warping of the D,E and F beaches (Figure 1.4) started in the Mittag area. The inferred transitions between platforms here are not sub-parallel to the present day coastline. It is therefore highly likely that this is the point of infliction.

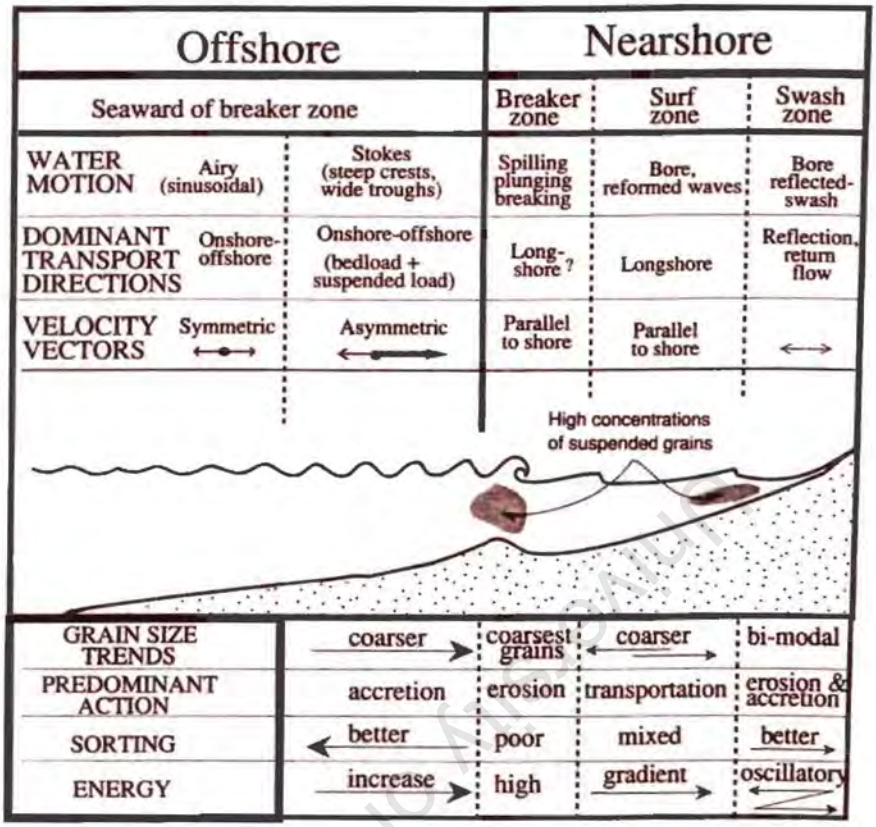

Figure 8.13 Classification of waves and sediment transport in nearshore and offshore areas (after Martinez and Harbuagh, 1993).

Figure 8.14 A wave breaking against bedrock in the Chameis Bay area. At the point where it breaks the wave has the highest potential to carry the most suspended material (refer Figure 8.13).

Figure 8.15 Diamondiferous gravel **a.** trapped in a gully. **b.** Exotics present in the diamondiferous gravel include jasper, epidote and banded iron stone (BIF).

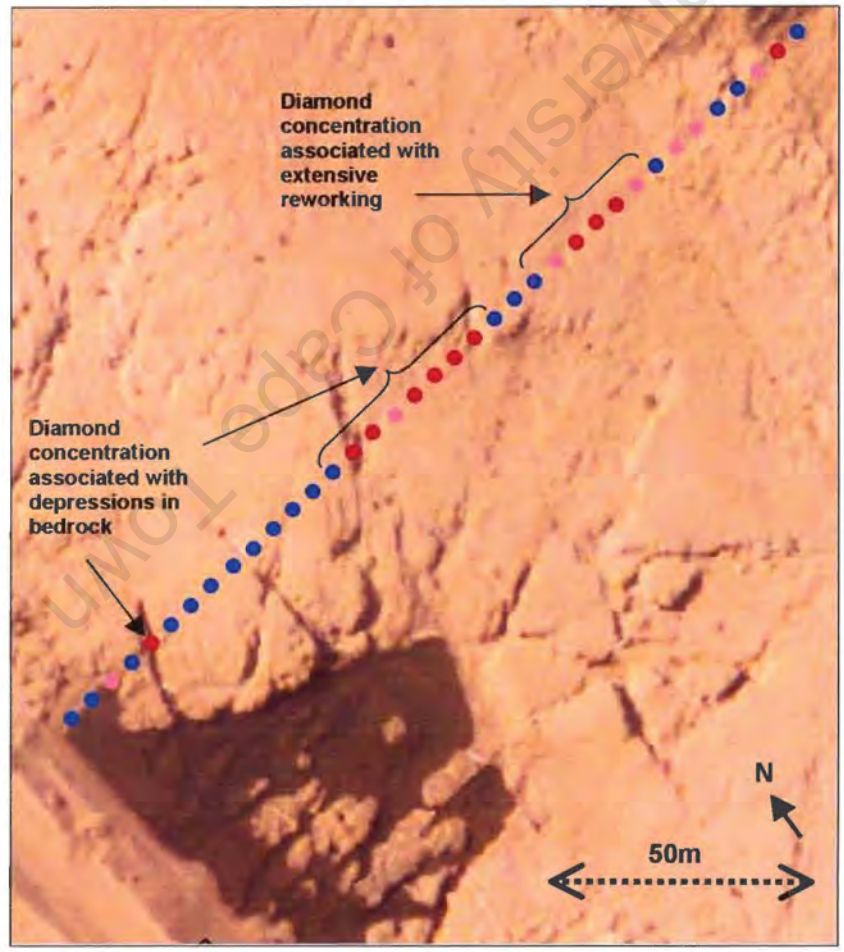

Figure 8.16 ALS image 45 km north of the Orange River mouth. Sampling data from trenches are represented by different colour dots. The red dots represent a grade of >1 carat per 5 square metres. Highest concentrations of diamonds are associated with depressions in the bedrock.

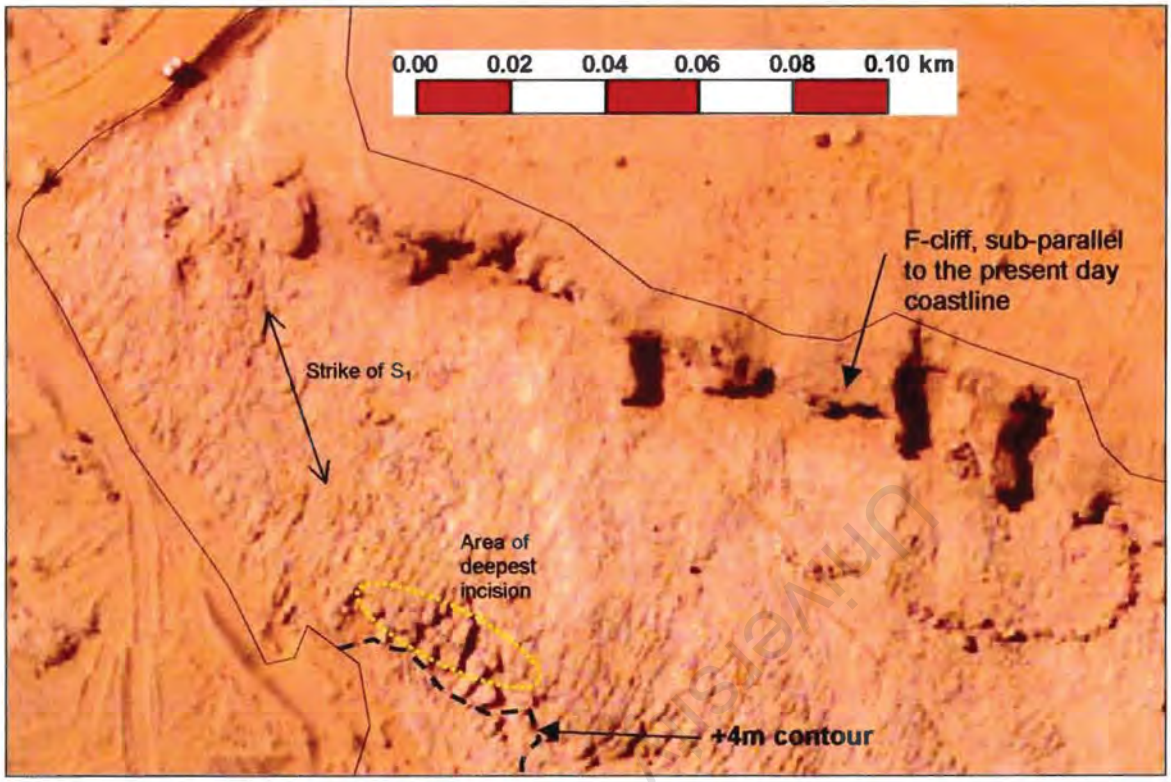

Figure 8.17 An aerial photograph showing bedrock exposed due to mining activities. The deepest incision into the bedrock can be seen on the seaward end of the +4m platform.

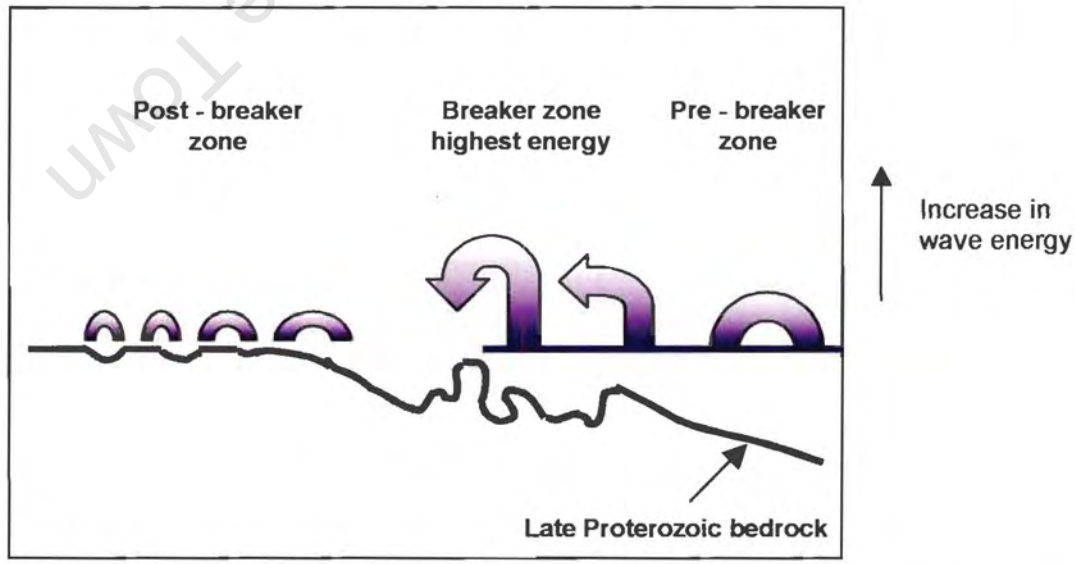

Figure 8.18 Schematic representation of wave energy and its relation to depth of incision into bedrock during a sea level still stand.

CHAPTER 9 - CONCLUSIONS

The Sperrgebiet, on the southwestern coast of Namibia hosts the world's largest known diamond placer deposits. The distribution of diamonds in these placer deposits is directly related to the presence of diamond-carrying gravel, the degree of reworking of the gravel and the quantity and quality of the diamond trapsites.

Structural and lithological features in the bedrock control the forming of diamond trapsites. The bedrock in the study area forms part of the now redefined Oranjemund Group of the MT, Pan-African Gariep Belt. Previously the MT has been subdivided into three complexes. Field mapping demonstrates that in spite of differences in the lithology, correlation of the major lithostratigraphic units between these three complexes is possible, and they may have been deposited contiguously. New geochemical data provided in this study indicate that the meta-sedimentary rocks of the Oranjemund Group carry a trace element signature of within-plate basalts. It is therefore highly likely that these sediments have been derived from meta-basalts of the adjacent Chameis Sub-terrane and the Grootderm Formation meta-basites of the Schakalsberge Sub-terrane. Further lithostratigraphic similarities with the Holgat Formation, PNZ and Chameis and Schakalsberge Sub-terranes has shown in this study that the three Complexes are not different terranes, but should be seen as three Sub-terranes of the MT.

The nature of the Oranjemund Sub-terrane is thus lithostratigraphically determined by the contributions from the Grootderm Formation metabasites and Chameis metabasalts and structurally determined by a southeastward transport direction followed by east-west compression (Figure 9.1).

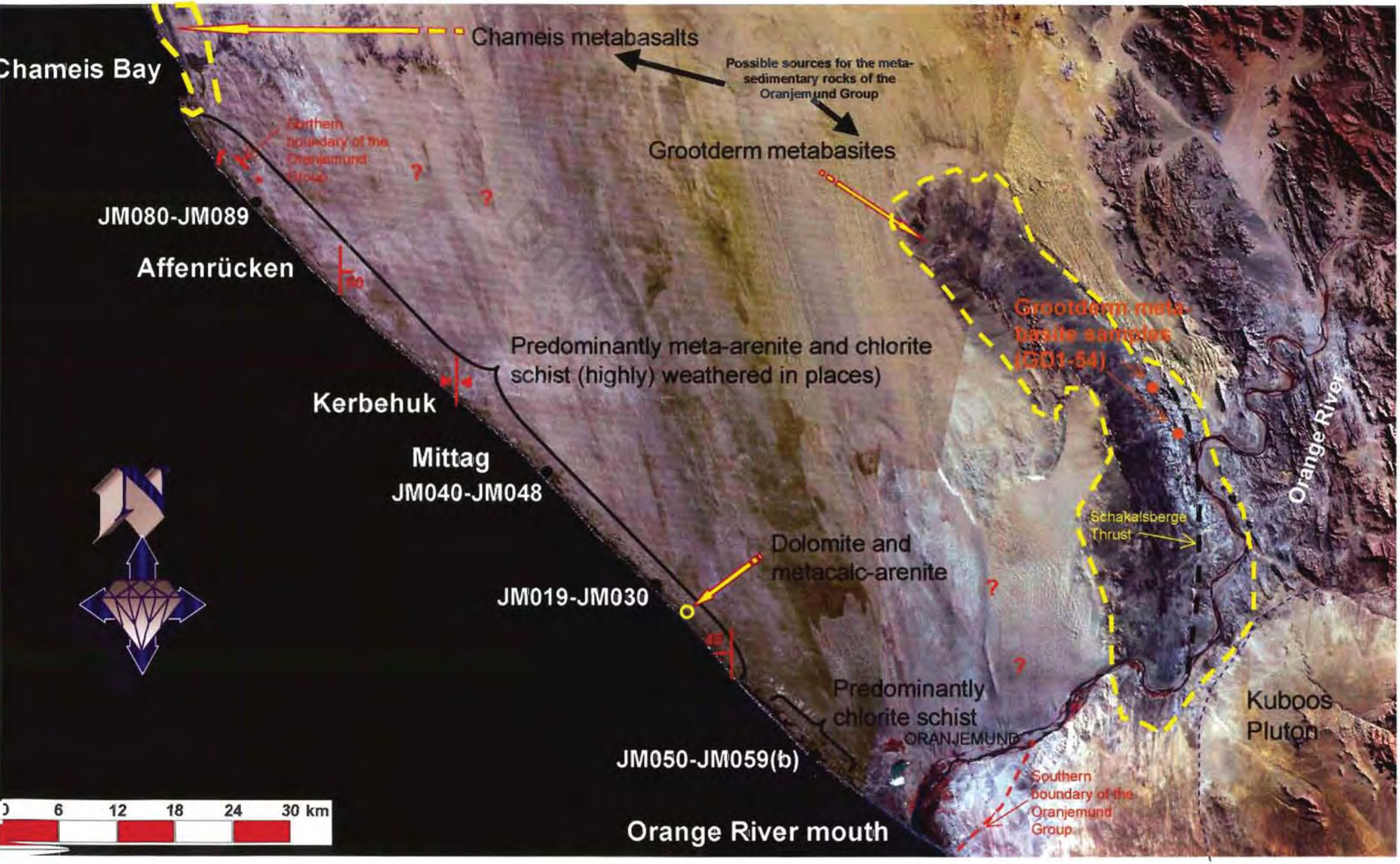

Figure 9.1 Satellite image of the south westem Sperrgebiet, displaying lithology and structural geology of the Oranjemund Sub-terrane as well as sample positions.

The Oranjemund Group consists predominantly of chlorite schist and meta-arenite. Alternation of lithological layers of chlorite schist and meta-arenite (section 8.3.1) occur on different scales. Differential weathering took place depending on the thickness of the harder and softer lithological units. The gullies or trapsites formed in this way are called "Strike gullies".

A gradation of the type of diamond trapsites found from the Orange River mouth northwards is evident (Figure 8.4). Near the Orange River mouth, where abrasive agents (boulders) were most abundant, "Swash parallel gullies" were the dominant gully formed, over-riding structural and lithological controls in the bedrock. In the Kerbehuk area 60km north of the river mouth, the abundance of boulders declined and "Strike gullies" are most prominent. North of Affenrücken where the structural features in the bedrock are the dominating factor controlling the type of trapsite formed and abrasive agents were least abundant, "Joint gullies" are most prominent. The gradation of the gully types is also linked to the large-scale synclinal structure of the bedrock (Figure 4.2 and 4.3). "Strike gullies" dominate in the Kerbehuk area where bedding parallel S_2 dips 80-89 degrees to the west. There differential weathering takes place and the softer lithological bands have been eroded out while the harder lithological units stand proud (Figure 8.8). Where S_2 dips 45 degrees to the west "Strike gullies" are less common. The harder units require the softer units for support and when the softer units are eroded out, the harder units tend to collapse.

The quality of a trapsite is directly linked to the depth of incision into the bedrock. Using new data acquired by an "Airborne Laser Survey" (ALS) the bedrock outcrop could be contoured. The contoured outcrop was used to identify platforms formed during different sea-level stillstands. Deepest incision into palaeo-platforms was found to be on the seaward side (Figure 8.14). The greatest likelihood for diamond concentration is therefore related to the seaward extreme of these palaeo-platforms. Due to the large-scale structural characteristics of the bedrock and the marine erosion processes to which the

bedrock has been exposed, the same should apply to the direct offshore area between the Orange River mouth and Chameis Bay, depending on diamondiferous gravel being present.

A comparison of diamond sample results from areas in the present day offshore where the interface between platforms can be identified should be used to test this model. If positive results are obtained, this model can be directly implemented as a new tool to identify areas with a very high likelihood for diamond concentration in the present-day nearshore environments.

LIST OF FIGURES

Figure 3.8 A photograph of the graded contact between the chlorite schist and the meta-arenite, 8 km north of the Orange River mouth.

Figure 3.9 Back scatter SEM image. Minerals identified: 1. quartz; 2. zircon, 3. biotite; 4. chlorite.

Figure 3.10 A. Meta-arenite (20 km north of the Orange River mouth) in outcrop highly weathered in places. **B**. Graded laminae of meta-arenite. **C**. Photomicrograph of meta-arenite (JM020) with orientated chlorite and mica minerals and detrital quartz, crossed polars.

Figure 3.11 A meta-arenite 80 km north of the Orange River mouth .In places evenly spaced, continuous, homogeneous layers (cm scale) occur. This is interpreted as metamorphic differentiation aligned parallel to axial planes.

Figure 3.12 A. A single white-pink dolomite outcrop about 30km north of the Orange River mouth. **B.** Quartz and calcite veins (with random orientation) cross cut the highly brecciated dolomite in places.

Figure 4.1 Photomicrograph of a thin section (crossed polars) of chlorite schist (JM050) showing s_1 and chlorite aligned along bedding parallel s_2 (8 km NW of the Orange River mouth).

Figure 4.2 Map of MA1 with equal area stereoplots of the poles to S_2.for different areas.

Figure 4.3 Plan view of the strike and dip of s_2 along the study area. The value of each dip and strike direction in this figure has been calculated by using the average of 10 readings 10 metres apart.

Figure 4.4 SEM Backscatter image showing tight folding on micro-scale (in yellow), sample JM053.

Figure 4.5 Tight folding (meter scale) about 8 km north of the Orange River mouth.

Figure 4.6 Aerial photograph of the Kerbehuk area showing large-scale tight folds, with fold axes striking about N-S.

Figure 4.7 N-S trending hinges on the contact between chlorite schist and dolomite 6 km south of Chameis Bay.

Figure 4.8 Detailed map of the inferred contact between Oranjemund and Chameis Sub-terranes

Figure 4.9 F_3 open fold with hinge trending NW-SE.

Figure 4.10 Different responses of a meta-arenitic unit and a chlorite schist unit to deformation.

Figure 4.11 A class 2 (similar) Ramsay fold, formed in mixed sediment folding. The schistose unit shows greater axial thickening.

Figure 4.12 Equal area stereoplot of the fold axes. Black dots (F_1) show W to SSW plunging axes and red dots (F_2) show NNW plunging axes.

Figure 4.13 Equal area stereoplot of the poles to the co-planar s_2 with the position of the main fold axis, striking N-S dipping slightly towards the north.

Figure 8.8 Differential weathering of harder and softer lithological units. **A.** The softer schistose unit (about 2m thick) has been eroded creating a high-potential diamond trapsite (35 km north of the Orange River mouth). **B.** The width of the lithological layers is less than 0.5m in this case and differential weathering did not take place. The only erosion that occurs here is a swash-parallel gully (red dashed line) (80 km north of the Orange River mouth). **C.** Differential weathering of the softer schistose unit, parallel to the strike of s_2 (12 km north of the Orange River mouth) **D.** Differential weathering is most spectacular where s_2 dips between 80 –95 degrees to the west in the Kerbehuk area.

Figure 8.9 Potholes form along **A.** Joint intersections and **B.** zones of parallel jointing. **C.** A wedge of bedrock removed at a joint intersection. **D.** The series of potholes and removed wedges of bedrock are then interconnected to form a network of gullies, parallel to swash direction.

Figure 8.10a The "Swash parallel" gully (20 km north of the Orange River mouth) which was surveyed in the field. This gully is 40m long and up to 7m deep. **b.** A morphological section along the long axis of the gully shown in Figure 8.10a, showing both the northern and southern wall (with elevation m.a.s.l). **c.** A three-dimensional computer generated model of the surveyed gully (Figure 8.10a), showing deepest incision into bedrock on the landward side.

Figure 8.11 Schematic NE_SW section of platforms and gullies incised into bedrock.

Figure 8.12a The +8m contour digitised using the ALS contoured data.

Figure 8.12b The +2m to +18m contours digitised using the ALS contoured data. Note the structural and lithological controlled gullies on the +2m platform vs.the "Swash controlled gullies" on the +4m to +12m platforms.

Figure 8.12c The +4m to +14m contours digitised using the ALS contoured data. S_1 dips between 80-95 towards the west here. The dominant gully type here is strike controlled.

Figure 8.12d The +8m to +18m contours digitised using the ALS contoured data. Kalbskopf (1978) proposed that the down-warping of the D,E and F beaches (Figure 1.4) started in the Mittag area. The inferred transitions between platforms here are not sub-parallel to the present day coastline. It is therefore highly likely that this is the point of infliction.

Figure 8.13 Classification of waves and sediment transport in nearshore and offshore areas (after Martinez and Harbuagh, 1993).

Figure 8.14 A wave breaking against bedrock in the Chameis Bay area. At the point where it breaks the wave has the highest potential to carry the most suspended material (refer Figure 8.13).

Figure 8.15 Diamondiferous gravel **a.** trapped in a gully. **b.** Exotics present in the diamondiferous gravel include jasper, epidote and banded iron stone (BIF).

Figure 8.16 Sampling data from trenches are represented by different colour dots. The red dots represent a grade of >1 carat per 5 square metres. Highest concentrations of diamonds are associated with depressions in the bedrock.

Figure 8.17 An aerial photograph showing bedrock exposed due to mining activities. The deepest incision into the bedrock can be seen on the seaward end of the +4m platform.

Figure 8.15 Diamondiferous gravel **a**. trapped in a gully. **b**. Exotics present in the diamondiferous gravel include jasper, epidote and banded iron stone (BIF).

Figure 8.16 Sampling data from trenches are represented by different colour dots. The red dots represent a grade of >1 carat per 5 square metres. Highest concentrations of diamonds are associated with the depressions into bedrock.

Figure 8.17 An aerial photograph showing bedrock exposed due to mining activities. Deepest incision into bedrock can be seen on the seaward end of the +4m platform.

Figure 8.18 Schematic representation of wave energy and its relation to depth of incision into bedrock during a sea level still stand.

Figure 9.1 Satellite image of the south western Sperrgebiet, displaying lithology and structural geology of the Oranjemund Sub-terrane as well as sampling positions.

REFERENCES

Anders, M. H., 1988. Evidence from cathodo-luminescence for non-volcanic origin of shocked quartz at the Cretaceous/Tertiary boundary. *Nature,* **334**, 145-146.

Babcock, R. S., 1973. Computational models of metasomatic processes. *Lithos,* **6**, 179-190.

Balashov, Yu. A. and Girin, Yu.P., 1969. On the reserve of mobile rare earth elements in sedimentary rocks. *Geochem. Int.,* **7**, 649-659.

Bathia, M. R. and Crook, K. A., W., 1986. Trace element characteristics of graywackes and tectonic setting discrimination of sedimentary basins. *Contrib. Mineral. Petrol.,* **92**, 181-193.

Behr, H. J., Ahrendt, H., Porada, H., Röhrs, J. and Weber, K., 1983. Upper Proterozoic playa and sabkha deposits in the Damara orogen, SWA/Namibia. *Spec. Publ. Geol. Soc. S Afr.*, **11**, 1-20.

Blatt, H., Middleton, G. and Murray, R., 1972. Origin of sedimentary rocks. *Prentice-Hall, Inc., Englewood Cliffs, New Jersey.*

Chemale, F., 1998. Assembly of West Gondwana in southern regions of Africa and Brazil. *J. of Afr. Earth Sci.*, **27/1A**, 44-45.

Clark, J. A., 1980. A numerical model of worldwide sea level changes on viscoelastic Earth. In *Morner, N. A. (ed.), Earth rheology, isostasy and eustasy. John Wiley, Chichester England.* 525-534.

Condie, K.C., 1983. Plate Tectonics and Crustal Evolution 2nd edition. *Pergamon Press, New York*. 310pp.

da Silva, L. C., McNaughton, N. J., Hartmann, L. A., Fletcher, I. R., Gresse, P. and Scheepers, R., 1997. U-Pb (SHRIMP) isotopic constraints for the evolution of southern Brazilain granitic province, and some correlated South African, Pan –African plutons. *In Ferreira, V. P. and Sial, A. N. (eds.) Second Internation Symposium on Granites and Associated mineralizations, Superintendecia de geologi e recursos minerais – SGM, Salvador*, 276-277.

Davies, C. J., 1972. Geographical variation in Coastline Development. *Oliver and Boyd, Edinburgh*. 204pp.

Davies, C.J. and Coward, M.P., 1982. The Structural Evolution of the Gariep Arc in Southern Namibia. *Precam. Res.*, **17**, 173-198

De Decker, R. H., 1986. The Geological setting of deamondiferous depositson the inner shelf between the Orange River and Wreckpoint, Namaqualand. *Bull. Geol. Surv. of S. Afr.*, **86**, 99 pp.

De Villiers, J. and Sönhge, P. G., 1959. The Geology of the Richtersveld. *Memoirs of the Geol. Surv. of S. Afr.*, **48**, 1-295.

Dingle, R. V. and Hendey, Q.B., 1984. Late Mesozoic and Tertiary sediment supply to the eastern Cape Basin (SE Atlantic) and palaeo-drainage systems in southwestern Africa. *Marine Geol.*, **56**, 13-26.

Dingle, R.V., Birch, G.F., Bremner, J.M., De Decker, R.H., Du Plessis, A., Engelbrecht, J.C., Fincham, M.J., Fitton, T., Flemming, B.W., Gentle, R.I., Goodlad, S.W., Martin, A.K., Mills, E.G., Moir, G.J., Parker, R.J., Robson,

S.H., Rogers, J., Salmon, D.A., Siesser, W.G., Simpson, E.S.W., Summerhayes, C.P., Westall, F., Winter, A. and Woodborne, M.W., 1987. Deep-sea sedimentary environments around southern Africa (South-East Atlantic and South-West Indian Oceans). *Ann. S. Afr. Museum* **98** (1): 1-27.

Duncan, A. R., Erlank, A. J. and Betton, P. J., 1984. Appendix 1: Analytical techniques and database descriptions. In*: Petrogenesis of the volcanic rocks of the Karoo Province, (ed. A. J. Erlank),* **13**, 389-395.

Fernandes, J.A.D., Tommasi, A. and Porcher, C.C., 1992 Deformation patterns in the southern Brazilian branch of the Dom Feliciano Belt, a reappraisal. *J. S. Amer. Earth Sci.,* **5**, 77-96

Fleet, A. J. 1984. Aqueous and sedimentary geochemistry of the rare earth elements. In: *Rare Earth Element Geochemistry Elsevier Science Publishers B. V.,* **2**, 343-373.

Floyd P.A., Shail, R., Leveridge, B.E. and Franke, W., 1991. Geochemistry and provenance of Rhenohercynian synorogenic sandstones: implications for tectonic environment discrimination. In: Morton et al. (eds): Developments in Sedimentary Provenance Studies. *Geol. Soc. (London) Spec. Publ.* **57**, 173-188.

Frimmel, H. E., 2000a. The Pan-African Gariep Belt in southwestern Namibia and western South Africa. *Comm. Geol. Survey of Namibia*, **13**, in press.

Frimmel, H. E., 2000b. The stratigraphy of the Chameis Sub-terrane in the Gariep Belt in southwestern Namibia. *Comm. Geol. Survey of Namibia, Henno Martin commemorative,* **13**, in press.

Frimmel, H. E., Fölling, P. G. and Eriksson, P., 2000c. Neoproterozoic tectonic and climatic evolution recorded in the Gariep Belt, Namibia and South Africa. *Basin Res.*, submitted.

Frimmel, H. E., Zartmann, R. E. and Späth, A., 2000d. Dating Neoproterozioc continental break-up in the Richtersveld Igneous Complex, South Africa. *J. Geol.,* in press.

Frimmel, H. E. and Jiang, S.-Y., 2001. Marine evaporites from an oceanic island in the Neoproterozoic Adamastor ocean. *Precam. Res.*, **105**, 57-71.

Frimmel, H.E. and Frank, W., 1998. Neoproterozoic tectono-thermal evolution of the Gariep Belt and its Basement, Namibia and South Africa. *Precam. Res.,* **90**, 1-28.

Frimmel, H.E., Hartnady, C.J.H and Koller, F., 1996a. Geochemistry and tectonic setting of magmatic units in the Pan-African Gariep Belt, Namibia. *Chem. Geol.* **130**, 101-121.

Frimmel, H. E., Klötzli, U. and Siegfried, P. 1996b. New Pb/Pb single zircon age constraints on the timing of Neoproterozoic glaciation and continental break-up in Namibia. *J. Geol.,* **104**, 459-469.

Frimmel, H. E., 1995. Metamorphic evolution of the Gariep Belt. *S. Afr. J. Geol.*, **98**, 176-190.

Frimmel, H.E. and Hartnady, C.J.H., 1992. Blue amphiboles and their significance for the metamorphic history of the Pan-African Gariep belt, Namibia. *J. metamorphic Geol.* **10**, 651-669.

Germs, G. J. B. and Gresse, P. G., 1991. The foreland basin of the Damara and Gariep Belt and its basement, Namibia/South Africa. *Precam. Res.*, **90**, 1-28.

Gresse, P. G., 1994. Strain partitioning in the southern Gariep Arc as reflected by sheath folds and stretching lineations. *S. Afr. J. of Geol.*, **94**, 159-169.

Gressens, R. L., 1967. Composition-volume relationships of metasomatism. *Chem Geol.*, **2**, 47-65.

Gurney, J. J., Walker, C. S. H., Prinsloo, K., Borchers, R. and Flemming, B. W., 1982. Diamond discoveries from the surf zone of the Namaqualand coast near the Olifant River. *Abstr. 3rd Symp. Sedim. Div. Geol. Soc. S. Afr.*, 84-87.

Haack, U., Gohn, E. and Hartmann, O., 1983. Radiogenic heat generation in Damaran rocks. *In:* Miller, R. McG. 1983 Evolution of the Damara Orogen of South West Africa/Namibia. *Special Publication, Geol. Soc. of S. Afr.* **11,** 225-231.

Haskin, L. and Gehl, M. A., 1962. The rare-earth distribution in sediments. *J. Geophys. Res.*, **67**, 2537-2541.

Hallam, C. D., 1964. The Geology of the Coastal Diamond Deposits of Southern Africa. *The Geology of some Ore Deposits of Southern Africa,* **2**, 671-728.

Hanson, R. E., Wilson, T. J. and Munyanyiwa, H., 1994. Geological evolution of the Neoproterozoic Zambezi orogenic belt in Zambia. *J. Afr. Earth Sci,* **18**, 135-150.

Haq, B.U., Hardenbol, J. and Vail, P.R. 1987. Chronology of fluctuating sea levels since the Triassic. *Science,* **235,** 1156-1167.

Hartnady, C. J. H., Joubert, P., and Stowe, C., 1985. Proterozoic crustal evolution in southwestern Africa. *Episodes*, **8**, 236-244.

Hartnady, C. J. H. and Von Veh, M. W. 1990. Tectonostratigraphic and structural history of the Late Proterozoic – Early Palaezoic Gariep Belt, Cape Province, South Africa. *Geol. Soc. of S. Afr., Cape Town, Excursion Guidebook PO1*, 1-49.

Henderson, P, (Editor), 1989. Rare Earth Element Geochemistry, *Developments in Geochemistry* **2**, *Elsevier. Amsterdam*, 510 pp.

Heydorn, A. E. F. and Tinley, K. L., 1980. Synopsis of the Cape Coast: Natural features, dynamics and utilization in Estuaries of the Cape. Part I: *Res. Rep;. Nat. Res. Inst. Oceanol. S. Afr. Counc. Sci ind. Res., Stellenbosch,* **380**, pp96.

Hoffman, P. F., Hawkins, D. P., Isaachsen, C. E. and Bowirng, S. A., 1996. Precise U-Pb zircon ages for early Damaran magmatism in the Summas Mountains and Welwitchia inlier, northern Damara Belt, Namibia. *Comm. Geol. Survey of Namibia*, **11**, 47-2.

Hoffman, P. F., 1999. The break-up of Rodinia, birth of Gondwana , true polar wander and the snowball earth. *J. Afr. Earth Sci.*, **28**, 17-33.

Holland, H. D., 1978. The chemistry of the atmosphere and oceans. *John Wiley Chichester England,* 351 pp.

Hoyt, S. H., Smith, D. D. and Oostdam, B. L., 1969. Offshore sediments and valleys of the Orange River (South and South West Africa): *Mar. Geol.*, **7(1),** 69-84.

Jacob, R. J., Bluck, B. J., and Ward, J. D., 1999. Tertiary-Age diamondiferous fluvial deposits of the lower Orange River valley, Southwestern Africa. *Economic Geol.*, **94,** 749-758.

Kaiser, E., 1926. Die Diamantenwüste Süd West-Afrikas. 2 Vol. *Dietrich Reimer, Berlin.* 241pp.

Kalbskopf, S., 1978. Bedrock gullies, their patterns, morphology and relationship to the major wave-cut shelves at CDM. *CDM, (PTY) LTD. Inhouse report*

Kalsbeek, F., Pulvertaft, T.C.R. and Nutman, A.P., 1998. Geochemistry , age and origin of metagreywackes from the Palaeoproterozoic Karrat Group, Rinkian Belt, West Greenland. *Bul. Precam. Res., University of Cape Town,* **91**, *383-399.*

Kerrich, R., Fyfe, W. S., Gorman, B. E. and Allison, I., 1977. Local modification of rock chemistry by deformation. *Contrib. Mineral. Petrol.*, **65**, 183-190.

Kröner, A., 1974. Late-Precambrian Formations in the Western Richtersveld, Northern Cape Province. *Bul. Precam. Res., University of Cape Town,* **13**, 115 pp.

Le Roex, A. P. and Dick, H. J. B., 1981. Petrography and geochemistry of basaltic rocks from the Conrad fracture zone on the America-Antarctica Ridge. *Earth and Plan. Sci. Letters*, **54**, 117-138.

Martinez, P. A. and Harbuagh, J. W., 1993. Simulating nearshore environments. *Pergamon Press Ltd. Headyton Hill Hall, Oxford*. 265pp.

McLennan, S. M., Taylor, S. R., Kröner, A., 1983. Geochemical evolution of Archaean shales from South Africa I. The Swaziland and Pongola Supergroups. *Precam. Res. Unit*, **22**, 93-124.

Mii, H., 1962. Coastal geology of Tanabe Bay. *Science Reports of the Tohoku University, Series 2: Geology,* **34(1),** 1-96.

Miller, R. McG., 1983. The Pan-African Damara Orogen of South West Africa/Namibia. *Special Publ., Geol. Soc. SA* **11,** 431-515.

Murray L. G., Joynt, R. H., O'Shea, D. O'C..Foster, R.W. and Kleinjan,L., 1970. The Geological environment of some diamond deposits off the coast of South West Africa. *ICSU/SCOR Working Party 31 Symposium,Cambridge 1970: The geology of the East Atlantic Continental Margin. Edited by F. M/ Delany, 1970. Institute of Geol. Sci. Report* **70/3**, 110-141.

Nesbit, H. W. and Young, G. M., 1982. Early Proterozoic climates and plate motions inferred from major element chemistry of lutites. *Nature,* **299**, 715-716.

Nisbet, E. G., Dietrich, V. J. and Esenwein, A., 1979. Routine trace-element determination in silicate minerals and rocks by X-ray fluorescence. *Fortschr. Mineral.*, **57**, 264-279.

Norrish, K. and Hutton, J. T., 1969. An accurate X-ray spectrographic method for the analysis of a wide range of geological samples. *Geochim et Cosm. Acta*, **33**, 431-453.

Oosterveld, M. M., Campbell, D. and Hazell, K. R., 1987. Geology related to statistical evaluation parameters for a diamondiferous beach deposit. *Proceedings of the Twentieth International Symposium on the application of computers and mathematics in the mineral industries. Geostatistics*, **3,** 129-136.

Partridge, T.C. and Maud, R.R. 1987. Geomorphic evolution of South Africa since the Mezozoic. *S. Afr. J. Geol.*, **90**: 179-208.

Pearce, J. A. and Cann, J. R., 1973. Tectonic setting of basic volcanic rocks determined using trace element analyses. *Earth Planet. Sci. Letters,* **19,** 290-300.

Pether, J., 1986. Late Tertiary and early Quarternary marine deposits of the Namaqualand coast, Cape Province: new perspectives. *S. Afr. J. Science*, **82,** 464-470.

Pickford, M., 1987. Miocene Suidae from Arris Drift, South West Africa/Namibia. *Ann. SA Museum* **97**, 283-295.

Ramsay, J. G., 1967. Folding and fracturing of rocks. *McGraw-Hill Book Co. London,* 211pp.

Reid, D. L., Ransome, I. G. D., Onstott, T. C. and Adams, C. J. 1991. Time of emplacement and metamorphism of Late Precambrian mafic dykes associated with the Pan-African Gariep orogeny, Southern Africa: implications for the age of the Nama Group. *J. Afr. Earth Sci.*, **13**, 531-541.

Rogers, J., 1977. Sedimentation on the continental margin off the Orange River and the Namib Desert. *Department of Geology, University of Cape Town, Marine Geoscience Group Bul.,* **7,** 162pp.

Rogers, J., 1977a. *PhD thesis, University of Cape Town, South Africa.* 176pp.

Saunders, N. K., 1968. The development of Tasmanian shore platforms. *PhD Thesis, University of Tasmania, Hobart*, 402pp.

Sichel, H. S., 1972. Statistical Valuation of Diamondiferous Deposits. In: *Proceedings of the International Symposium on the Application of Computers in the Mineral Industry. SA Inst. of Mining and Metallurgy, Johannesburg.* 17-25.

Siesser, W. G., 1978. In: *Antarctic glacial history and world palaeo-envirionments* (ed. E. M. van Zinderen Bakker). *Balkema, Roterdam*, 105.

Shackleton, N. J. and Kennet, J. P. 1975. Paleotemperature history of the Cenozoic and the initiation of Antarctic glaciation: oxygen and carbon isotope analyses in DSDP sites 277, 279 and 281. In: Kennet, J.P. *et al.* (eds.), *Initial reports of the Deep Sea Drilling Project* **29**:743-755.

Shackleton, N. J. and Opdyke, N. D., 1973. Oxygen isotope and palaeomagnetic stratigraphy of equatorial Pacific core V28-238: Oxygen isotope temperatures and ice volumes on a 10^5 and 10^6 year scale. *Quaternary Res.*, **3**, 39-55.

Spaggiari R. I., Bluck, B. J. and Ward, J. D., 1999. Beaches, barriers and bars: sedimentary facies of Early Pleistocene diamondiferous deposits within the Orange River Mouth, Namibia. *XV International Congress, August 1999, Durban, S. Afr.* 169-170.

Stephenson, W. J. and Kirk, R. M., 2000. Development of shore platforms on Kaikoura Peninsula, South Island, New Zealand. Part One: The role of waves. *Geomorphology*, **32**, 21-41.

Stöcken, C. G., 1978. A review of Cenozoic climatic and geological events in the Sperrgebiet. *CDM, (PTY) LTD. Inhouse report.*

Summerfield, M. A., 1991. Global Geomormphology. *John Wiley & Sons, New York*, 264pp.

Sunamura, T., 1992. Geomorphology of Rocky Coasts. *Wiley, New York,* 302pp.

Sunamura, T., 1994. Rock control in coastal geomorphic processes. *Trans. Jap. Geomorph. Union*, **153**, 253-272.

Tankard, A. J., 1976. Cenozoic sea-level changes: a discussion. *Ann. S. Afr. Mus.*, **71**, 1-17.

Trenhaile, A. S. and Bryne, M., 1985. A theoretical investigation of the Holocene development of rock coasts, with particular reference to shore platforms. *Geogr. Ann. 68 A,* **(1-2)** pp1-14.

Von Veh, M. W., 1993. The stratigraphy and structural evolution of the Late Proterozoic Gariep Belt in the Sendelingsdrif- Annisfontein area, northwestern Cape Province. *Bul. Precam. Res., UCT,* **38**, 174pp.

Ward, J. D., 2000. In *The Cenozoic of Southern Africa.* (Ed. Partridge, T. C. and Maud, R. R.), *Oxford Monographs on Geology and Geophysics*, **40**. ISBN 0195125304

Ward, J. D. and Bluck, B. J., 1997. *Abstracts vol. 6th International Fluvial Conf., Intern. Ass. Sedimentologists, Cape Town.*

Wilson, T. J., Brunow, A. M. and Hanson, R. E., 1997. Gondwana assembly: the view from southern Africa and East Gondwana. *J. Geodynamics,* **23**, 263-286.

White, W. M., 1997. Chapter 7–Basalt calculations. *Course notes on geochemistry, University of Cape Town,* 296pp.

Wright, J. A., 1964. Gully pattern and development in wave-cut bedrock shelves north of the Orange River mouth, South West Africa. *Trans. Geol. Soc. S. Afr.,* **LXVII,** 163-171.

Appendix 1

Major element oxide concentrations (wt%) for meta-arenite (m-arenite) and chlorite schist (chl-schist) of the Oranjemund Group.

Sample	Rock type	SiO_2	TiO_2	Al_2O_3	Fe_2O_3*	MnO	MgO	CaO	Na_2O	K_2O	P_2O_5	H2O-	LOI	Total
JM019	m-arenite	73.47	0.60	11.67	4.09	0.06	1.75	0.48	2.51	2.40	0.14	0.10	1.99	99.26
JM020	m-arenite	63.12	0.73	15.87	6.71	0.06	3.27	0.29	1.34	3.65	0.16	0.12	3.48	98.80
JM021	m-arenite	77.12	0.53	10.38	3.71	0.04	1.27	0.65	1.96	2.11	0.14	0.11	1.83	99.88
JM022	m-arenite	73.87	0.56	11.26	4.12	0.07	1.89	0.64	2.30	1.98	0.14	0.08	2.26	99.17
JM024	m-arenite	73.83	0.55	10.81	4.10	0.05	1.62	0.91	2.24	1.90	0.14	0.13	2.36	98.61
JM025	m-arenite	76.68	0.51	10.85	3.75	0.04	1.42	0.56	2.46	2.14	0.13	0.12	1.75	100.43
JM026	m-arenite	82.24	0.47	8.34	2.90	0.04	0.89	0.78	1.79	2.09	0.11	0.08	1.30	101.05
JM027	m-arenite	75.43	0.59	10.77	3.75	0.04	1.71	0.54	2.69	1.90	0.14	0.05	1.78	99.45
JM028	m-arenite	65.63	0.83	14.99	6.36	0.06	2.83	0.30	1.76	4.13	0.22	0.14	2.53	99.80
JM030	m-arenite	75.35	0.60	10.76	3.79	0.05	1.52	0.61	1.81	3.02	0.15	0.10	1.88	99.64
JM040	chl schist	54.33	0.78	18.13	9.60	0.11	5.20	0.17	0.69	4.88	0.12	0.49	5.35	99.99
JM041	m-arenite	69.25	0.67	12.13	5.53	0.05	2.13	1.47	2.49	2.55	0.20	0.22	3.13	99.87
JM042	m-arenite	71.53	0.73	11.72	4.63	0.09	2.09	1.08	2.99	1.83	0.19	0.15	2.46	99.49
JM043	m-arenite	71.29	0.66	11.30	4.47	0.10	2.12	1.99	2.83	1.61	0.16	0.14	3.21	99.85
JM044	chl schist	54.02	0.88	19.58	7.90	0.08	5.15	0.26	2.72	4.07	0.19	0.24	4.09	99.24
JM045	m-arenite	66.43	0.93	14.13	6.02	0.07	2.63	0.59	2.61	2.93	0.25	0.23	2.66	99.47
JM046	chl schist	43.49	1.16	24.08	10.50	0.10	5.82	0.41	0.42	6.89	0.29	0.37	5.27	98.84
JM048	m-arenite	69.78	0.75	13.08	6.12	0.08	2.70	0.23	2.44	2.41	0.18	0.17	2.41	100.36
JM049	m-arenite	71.97	0.90	12.34	5.86	0.12	2.50	0.26	2.53	2.19	0.20	0.14	2.18	101.23
JM050	chl schist	58.38	0.83	18.08	8.68	0.04	3.36	0.26	2.10	3.86	0.18	0.15	3.41	99.38
JM051	m-arenite	60.92	0.77	16.30	9.11	0.07	3.84	0.25	1.79	2.87	0.18	0.09	3.32	99.56
JM052	m-arenite	59.67	0.93	18.57	8.20	0.09	4.41	0.25	1.43	3.62	0.18	0.13	3.96	101.45
JM053	m-arenite	65.33	0.87	14.88	7.05	0.07	3.72	0.24	1.39	2.71	0.18	0.08	3.12	99.64
JM055	chl schist	57.54	0.83	17.95	9.60	0.06	3.65	0.25	1.67	3.67	0.18	0.11	3.55	99.10
JM058	chl schist	54.99	0.78	19.30	9.94	0.06	4.00	0.23	0.66	4.47	0.16	0.10	4.17	98.88
JM059	chl schist	58.66	0.86	17.93	8.67	0.06	3.88	0.28	2.15	3.55	0.21	0.09	3.44	99.83
JM059B	chl schist	56.80	0.84	18.41	9.11	0.07	4.39	0.32	1.28	4.02	0.17	0.28	3.90	99.62
JM080	m-arenite	59.23	0.80	17.71	7.41	0.13	4.01	0.19	1.34	4.37	0.12	0.21	3.90	99.44
JM081	m-arenite	60.33	0.84	17.40	7.68	0.08	3.46	0.25	1.87	4.07	0.18	0.19	3.47	99.86
JM082	m-arenite	77.41	0.60	10.55	3.97	0.04	1.56	0.24	1.83	2.88	0.15	0.13	1.36	100.74
JM083	m-arenite	75.80	0.58	10.39	3.79	0.06	1.47	1.35	1.82	2.75	0.14	0.13	2.22	100.52
JM084	m-arenite	68.68	0.68	13.49	5.69	0.06	2.65	0.34	1.43	3.88	0.24	0.14	2.25	99.56
JM085	m-arenite	77.06	0.52	10.34	3.42	0.05	1.49	0.32	2.38	2.19	0.13	0.13	1.35	99.40
JM086	m-arenite	57.78	0.78	17.35	7.89	0.11	4.47	0.56	1.15	4.36	0.17	0.14	4.05	98.83
JM087	m-arenite	61.41	0.83	16.31	7.02	0.08	3.56	0.33	2.63	3.30	0.22	0.17	3.02	98.91
JM088	m-arenite	74.34	0.63	11.78	4.17	0.07	1.74	0.27	2.75	2.15	0.17	0.09	1.57	99.74
JM089	m-arenite	76.45	0.58	10.68	3.62	0.05	1.44	0.51	2.40	2.33	0.16	0.09	1.29	99.64

* All Fe expressed as Fe_2O_3

Appendix 2

Trace element and REE concentrations (ppm) for the meta-basites (GD) of the Grootderm Formation, Schakalsberge Sub-terrane.

Sample	GD3	GD4	GD7	GD21	GD25	GD37	GD42	GD51	GD54
Ba	47	22	23	124	57	51	58	376	391
Rb	3	1	0	25	5	4	3	21	23
Sr	308	587	699	527	102	183	427	3277	1115
Y	29	21	27	35	18	44	37	35	41
Zr	171	135	180	299	114	459	272	299	426
Nb	23	19	23	44	15	81	38	86	83
Th	2	1	2	3	1	6	3	6	6
Pb	2	1	1	3	1	1	2	5	4
Cu	72	89	92	48	9	14	147	38	10
Ni	94	79	105	11	661	5	50	20	3
V	149	136	160	107	119	19	171	54	12
Cr	81	67	97	4	512	2	25	19	1
Hf	4	3	4	7	3	10	6	6	9
Cs	0	0	0	5	0	0	0	0	1
Sc	29	28	31	21	25	5	30	11	5
Ta	1	1	1	3	1	4	2	5	4
Co	46	48	48	36	67	15	50	32	14
U	1	0	1	1	0	2	1	2	2
La	19,40	15,50	16,20	31,70	10,20	60,00	28,60	66,80	71,00
Ce	46,30	37,10	41,90	78,30	26,30	144,00	68,80	136,00	159,00
Pr	6,23	4,98	5,82	10,00	3,71	19,20	9,31	16,40	20,30
Nd	27,30	22,00	26,10	43,80	16,90	80,40	41,10	64,50	82,20
Sm	6,58	5,27	6,37	10,00	4,27	16,30	9,65	12,40	15,90
Eu	2,11	1,80	2,14	3,05	1,29	4,74	2,82	3,53	4,61
Gd	6,51	5,05	6,24	8,95	4,17	13,00	8,83	9,95	12,40
Tb	1,01	0,76	0,94	1,32	0,64	1,80	1,33	1,39	1,70
Dy	5,80	4,35	5,46	7,49	3,70	9,62	7,60	7,40	8,95
Ho	1,10	0,81	1,02	1,37	0,69	1,70	1,41	1,32	1,57
Er	2,85	2,10	2,63	3,53	1,79	4,33	3,69	3,34	3,97
Tm	0,38	0,27	0,35	0,46	0,23	0,57	0,48	0,43	0,51
Yb	2,24	1,64	2,11	2,83	1,44	3,38	2,92	2,59	3,08
Lu	0,31	0,23	0,30	0,39	0,20	0,47	0,40	0,36	0,43
La/Y	0,67	0,73	0,60	0,92	0,56	1,38	0,76	1,93	1,73
Sc/Co	0,63	0,57	0,64	0,57	0,37	0,35	0,60	0,33	0,35

Appendix 3

Average composition of late Proterozoic and Phanerozoic greywackes associated with different tectonic environments (Floyd *et al.*, 1991) and the average composition of the Oranjemund Formation meta-sedimentary rocks.

	OIA	CAAM	PM	OWP	OMD	UUC
Rb	30	62	50	19	113.25	112.00
Sr	362	274	72	432	66.91	350.00
U	0.8	2	3.2	0.3	2.41	2.80
Cs	0.6	4.7	4.9	0.7	6.33	5.60
V	188	106	44	400	112.26	60.00
Cr	49	55	29	230	83.08	35.00
Ni	22	31	15	114	37.40	20.00
Ta	0.4	0.8	0.6	2	0.98	2.20
Nb	5	9	7	27	13.29	25.00
Hf	1.7	4.7	8.8	2.6	4.44	5.80
Zr	99	146	302	146	181.50	190.00
Y	15	17	24	20	21.58	22.00
La	10	23	22	10	28.96	30.00
Ce	22	48	56	24	65.61	64.00
Sc	27	16	8	30	10.50	11.00
Th	1.9	8.5	8.1	1	9.89	10.70

OIA – Oceanic Island Arc
CAAM – Continental Arc + Active Margin
PM – Passive Margin
OWP – Oceanic Within Plate
OMD – Oranjemund meta-sedimentary rocks
UUC – Upper Continental Crust

Appendix 4

Analytical techniques

X-Ray Fluoresence (XRF) Spectrometry

The major, minor and selected trace element concentrations of the bulk-rock samples were obtained using a Philips PW1400 and X'Unique or Siemens SRS303AS XRF spectrometer in the Department of Geological Sciences at UCT. The analyses were conducted at operating conditions adopted for routine analysis in the department and sample preparation and analytical procedures followed were these described by Duncan *et al.* (1984). The lithium tetraborate fusion method of Norrish and Hutton (1969) was used to determine all major and minor elements, except Na. Pressed powder briquettes were used for the determination of the trace elements and Na concentrations. A loss-on-ignition (LOI) value was obtained for each sample by heating in a furnace for at least 12 hours at 950 °C. The analytical errors and detection limits are similar to those quoted by le Roux and Dick (1981) and Duncan *et al.* (1984), reported in Table 1.

Inductively coupled plasma mass spectrometry (ICP-MS)

Trace and rare earth element (REE) concentrations were determined by inductively coupled plasma mass spectrometry (ICP-MS) using a Perkin Elmer/Sciex Elan 6000 mass spectrometer in the Department of Geological Sciences at UCT. Fifty milligrams of sample powder were dissolved using HF and HNO_3, diluted in 5% HNO_3 and analysed against five-point calibration curves (origin and four artificial multi-element standards with elemental concentrations of 10, 30, 50 and 100 ppb), with ^{103}Rh (^{45}Sc, ^{59}Co, ^{60}Ni, ^{63}Cu, ^{85}Rb, ^{88}Sr, ^{89}Y, ^{90}Zr, ^{93}Nb), ^{115}In (^{133}Cs, ^{137}Ba, ^{139}La, ^{140}Ce, ^{141}Pr, ^{144}Nd, ^{152}Sm), ^{187}Re (^{153}Eu, ^{160}Gd, ^{159}Tb, ^{163}Dy, ^{165}Ho, ^{166}Er, ^{169}Tm, ^{174}Yb, ^{175}Lu, ^{178}Hf, ^{181}Ta) and ^{209}Bi (^{208}Pb, ^{232}Th, ^{238}U) as internal standards. The instrument operating parameters were as

follows: nebuliser gas flow = 0.84 l.min^{-1}, main gas flow = 15 l.min^{-1}, auxiliary gas flow = 0.75 l.min^{-1}; ICP RF forward power = 1100 V; autolens voltages: ^{9}Be = 7.8, ^{59}Co = 9.0, ^{115}In = 9.8. The number of sweeps and replicates was 20 and 3, respectively, the peak dwell time 35 - 50 ms, the total counting time per peak 2100 - 3000 ms, the total analytical time 101.58 s, and the wash time between samples 180 s. The instrument sensitivity was 30529 cps.ppb^{-1} ^{103}Rh and the background intensity at mass 220 was 3.1 cps. The nebuliser gas flow was optimised to minimise oxide and doubly-charged ion formation, giving ^{156}CeO/^{140}Ce of 0.027 and ^{69}Ba^{++}/^{138}Ba of 0.024. Mathematical corrections were made for isobaric (^{115}Sn, ^{144}Sm, ^{152}Gd, ^{160}Dy, ^{187}Os), oxide (BaO, NdO, SmO, EuO, GdO, TbO, DyO, ErO, HoO) and doubly-charged ion (Er^{++}, Yb^{++}, Lu^{++}) interferences. Procedural blank concentrations were <0.065 ppm for Pb, <0.030 ppm for Ba, Nb, Zr, Sr, Cu, Ni and Sc, and <0.009 ppm for all other elements. Within-run precision was better than 3% (1 σ relative standard deviation) for all elements, as was the precision between duplicate analyses, except for Co (3.36%). Lower limits of detection (based on 3 standard deviations of the procedural blank intensities) were <0.300 ppm for Sc, <0.085 ppm for Sr, <0.050 ppm for Pb, Ta, Ba, Nb, Zr, Rb, Cu, Ni and Co, and <0.0095 ppm for all other elements.

Table 1 Lower limits of detection (LLD) (wt % for major element oxides, and ppm for trace elements) and 2σ errors (wt% for major-element oxides, and ppm for trace elements) for XRF analysis of bulk-rock samples.

	Duncan *et al.* (1984)		le Roex and Dick (1981)	
	2σ errors	LLD	2σ errors	LLD
SiO_2	0.140	0.040		
TiO_2	0.008	0.005		
Al_2O_3	0.080	0.020		
Fe_2O_3	0.038	0.014		
MnO	0.008	0.008		
MgO	0.148	0.070		
CaO	0.028	0.008		
Na_2O	0.032	0.080		
K_2O	0.002	0.002		
P_2O_5	0.012	0.011		
Sc	1.0-1.2	1.2	1.2	1.2
V	2.4-3.7	5.5	3.7	5.0
Cr	1.5-2.1	2.2	2.0	3.4
Co	1.9-2.5	4.5	2.0	3.4
Ni	0.7-1.0	1.2	3.7	5.0
Cu	1.8-2.1	2.9	1.9	2.2
Zn	0.9-1.7	1.4	1.9	2.2
Rb	0.8-1.1	1.5	0.9	1.4
Sr	1.0-1.7	1.5	0.9	1.4
Y	0.8-1.0	1.3	0.9	1.4
Zr	0.9-1.4	1.4	0.9	1.4
Nb	1.0-1.2	1.8	1.0	2.5
Ba	2.1-6.0	3.7	2.0	3.7

Appendix 5

List of samples and sample localities

SAMPLE	Y CO-ORDINATE	X CO-ORDINATE	SAMPLE	Y CO-ORDINATE	X CO-ORDINATE
JM019	79492.594	3142462.544	JM050	61935.874	3160772.008
JM020	79519.628	3142464.062	JM051	61954.034	3160759.900
JM021	79557.857	3142463.872	JM052	61965.075	3160739.231
JM022	79586.834	3142466.410	JM053	61984.226	3160724.867
JM024	79640.191	3142493.947	JM055	62008.187	3160702.003
JM025	79662.908	3142512.418	JM058	62048.723	3160663.629
JM026	79699.469	3142527.200	JM059	62068.388	3160631.818
JM027	79722.728	3142526.844	JM059(b)	62080.551	3160616.044
JM028	79749.505	3142525.088	JM080	121810.630	3103217.199
JM030	79822.709	3142536.743	JM081	121841.965	3103200.180
JM040	91054.428	3121446.925	JM082	121865.099	3103182.714
JM041	91065.625	3121449.605	JM083	121887.600	3103166.095
JM042	91072.218	312454.442	JM084	121912.917	3103145.140
JM043	91079.548	312457.385	JM085	121937.328	3103124.598
JM044	91084.321	312459.007	JM086	121956.463	3103105.225
JM045	91089.004	312463.458	JM087	121998.661	3103089.243
JM046	91095.574	312466.417	JM088	122022.435	3103073.655
JM048	91097.622	312468.001	JM089	122042.662	3103054.494
JM049	91101.474	3121471.965			

See Appendix 1 for rock type

Appendix 6

How Airborne Laser Mapping works.

Two GPS receivers are placed on local Trigonometric beacons or other known control points, within a distance of 50 km of the project, to provide the static differential GPS component from which the air trajectory of the helicopter will be determined. A GPS receiver, mounted in the helicopter with the antenna mounted on the wire cutter above the nose of the helicopter, forms the roaming component. The satellite signals received are stored on PC cards. Once the helicopter is in the air, the laser and camera system are switched on and the pre-determined mission parameters are set up using the control screen and camera computer. The laser pulse readings are recorded onto magnetic tape along with the inertial measurement system readings and mirror scan angle. The characteristics of the target (ground) surface have an effect on the amount of energy reflected back to the receiver i. e. sand and vegetation reflect about 10 - 50% of the energy back to the receiver whereas snow or bright shiny surfaces reflect much more. The reflectance off water is highly dependant on its surface state and usually has very little reflectance. The laser does not penetrate water. Very dark objects such as coal or burnt grass reflect very little energy and thus require a lower flying height. The digital photographs are recorded on to the computer hard disk in a compressed format. Navigation along the job is provided by the DGPS system, which gets its differential correction from ground reference stations via a geo-stationary communication satellite to an accuracy of 1 - 2m. This data is sent to the pilot display screen mounted on the instrument console of the helicopter for the pilot to see. Flight planning is done before the flight takes place and comprises the determination of the flying height and speed, laser rate, swathe width, mirror speed, camera orientation, camera exposure interval, and the input of the co-ordinates of the project into the Trimflight computer. At the end of the project or session, all the data from the GPS's, laser and camera is downloaded onto a PC for post-processing to produce a DTM and orthophotos of the area.

(Taken from the *Internet* site *http//:www.alsafrica.com*)

Appendix 7

Trace element concentrations parts per million (ppm) for the chlorite schist north in the Kerbehuk area (JM040-049) chlorite schist south near the Orange River mouth (JM050-JM059b), and meta-arenite (JM019-JM030 and JM080-JM089) of the Oranjemund Group.

	JM 019	JM 020	JM 021	JM 022	JM 024	JM 025	JM 026	JM 027	JM 028	JM 030	JM 040	JM 041
Ba	346	454	387	277	201	347	377	191	678	421	514	213
Rb	98	171	103	95	56	98	97	66	174	99	184	68
Sr	75	50	59	63	47	75	96	74	61	54	30	43
Y	26	29	24	30	17	18	19	21	29	13	17	18
Zr	151	126	160	141	245	118	132	163	175	153	162	135
Nb	11	14	10	11	10	9	8	11	15	11	13	11
Th	11	10	12	10	5	7	9	7	11	7	10	4
Pb	8	6	6	12	13	7	9	13	6	4	4	6
Cu	14	18	11	13	13	12	9	13	23	10	41	7
Ni	23	40	17	23	19	19	13	17	30	20	73	34
V	82	69	68	76	71	67	52	75	116	75	186	100
Cr	56	84	51	57	53	49	40	56	75	55	109	65
Hf	4	3	4	4	4	3	3	4	4	4	4	3
Cs	5	9	6	4	2	4	6	2	7	5	8	5
Sc	9	15	7	9	4	7	5	6	12	6	14	5
Ta	1	1	0.9	0.9	0.7	0.7	0.6	0.8	1	0.8	0.9	0.8
Co	9	10	6	17	6	7	3	4	7	5	22	12
Li	33	57	29	31	26	28	19	30	52	28	60	24
U	2	3	2	3	1	2	1	1	3	1	2	0.7
La	29	31	28	28	17	22	25	21	36	21	27	11
Ce	61	68	59	60	41	47	53	41	79	47	67	29
Pr	7	8	7	7	4	5	6	5	9	5	7	3
Nd	28	31	28	28	19	22	23	22	35	21	28	14
Sm	5	6	5	5	3	4	4	4	6	4	6	3
Eu	1	1	0.8	1	0.7	0.7	0.7	0.8	1	0.6	1	0.6
Gd	4	5	4	5	3	3	3	4	5	3	4	3
Tb	1	0.9	0.7	0.8	0.5	0.5	0.5	0.6	0.9	0.4	0.6	0.5
Dy	4	5	4	5	3	3	3	4	5	2	3	3
Ho	0.9	1	0.8	1	0.6	0.6	0.7	0.7	1	0.5	0.6	0.6
Er	2	3	2	2	1	1	2	2	3	1	1	2
Tm	0.4	0.4	0.3	0.4	0.2	0.2	0.3	0.3	0.4	0.2	0.2	0.2
Yb	2	2	2	2	1	2	2	2	3	1	1	1
Lu	0.4	0.4	0.3	0.4	0.2	0.3	0.3	0.3	0.4	0.2	0.2	0.2

	JM 042	JM 043	JM 044	JM 045	JM 046	JM 048	JM 049	JM 050	JM 051	JM 052	JM 053	JM 055
Ba	170	165	531	501	41	405	363	451	133	246	160	440
Rb	47	40	146	85	94	90	83	160	97	112	87	129
Sr	51	50	61	59	40	50	54	70	66	77	57	77
Y	16	16	28	18	7	20	32	32	10	7	8	24
Zr	166	151	173	200	239	128	170	147	150	159	188	152
Nb	10	10	16	15.	16	12	13	16	14	14	13	16
Th	6	5	12	8	3	7	11	14	10	7	8	12
Pb	6	21	3	5	3	3	2	14	13	10	11	13
Cu	18	22	27	17	28	19	32	21	25	43	29	36
Ni	28	26	64	36	61	34	31	55	49	60	50	56
V	93	89	192	128	256	107	104	174	151	205	141	169
Cr	69	61	122	87	144	66	70	109	101	174	142	116
Hf	4	4	4	5	6	3	4	4	4.	4	5	4
Cs	2	2	5	5	8	3	4	10	6	8	6	9
Sc	7	6	20	11	4	12	12	16	5	4	3	11
Ta	0.7	0.7	1	1	1	0.9	1	1	1	0.9	0.8	1
Co	9	9	27	15	17	14	15	22	21	22	18	22
Li	23	23	64	34	40	34	29	46	52	49	47	51
U	1	1	5	2	4	1	2	1	1	1	2	1
La	21	18	27	28	27	24	37	42	28	27	22	34
Ce	49	45	64	66	82	53	80	87	75	74	62	82
Pr	5	4	7	8	7	6	9	10	7	6	5	9
Nd	22	20	30	33	31	26	37	41	27	26	22	38
Sm	4	4	6	6	6	5	7	7	4	4	4	6
Eu	0.9	0.8	1	1	1	1	1	1	0.9	0.9	0.7	1
Gd	3	3	5	5	4	4	6	6	3	3	3	5
Tb	0.5	0.5	0.8	0.7	0.4	0.6	0.9	1	0.5	0.4	0.4	0.8
Dy	3	3	5	4	2	3	5	5	2	2	2	4
Ho	0.6	0.6	1	0.7	0.3	0.7	1	1	0.4	0.3	0.3	0.9
Er	1	1	3	2	0.9	2	3	3	1	0.9	1	2
Tm	0.2	0.2	0.4	0.2	0.1	0.3	0.4	0.4	0.1	0.1	0.1	0.3
Yb	1	1	3	2	1	2	3	3	1	1	1	2
Lu	0.2	0.2	0.4	0.3	0.1	0.3	0.4	0.4	0.1	0.1	0.1	0.3

	JM 058	JM 059	JM059(b)	JM 080	JM 081	JM 082	JM 083	JM 084	JM 085	JM 086	JM 087	JM 088	JM 089
Ba	51	756	480	538	520	480	486	677	347	552	528	377	369
Rb	114	152	163	170	162	113	96	138	88	175	151	89	82
Sr	49	87	62	74	91	67	87	77	78	72	99	96	77
Y	5	27	33	27	23	21	21	19	22	26	32	23	23
Zr	141	146	145	172	156	156	133	155	135	146	183	149	147
Nb	147	16	15	18	16	10	10	12	9	16	15	11	11
Th	4	16	16	15	14	9	8	10	7	13	11	9	8
Pb	6	16	5	28	10	6	18	10	9	11	31	9	9
Cu	15	35	20	32	20	10	16	9	8	18	24	7	14
Ni	49	57	56	42	51	21	19	32	20	50	43	26	21
V	232	111	86	137	74	75	72	112	72	77	78	90	72
Cr	101	111	115	93	94	57	54	72	50	97	93	59	50
Hf	4	4	4	4	4	4	3	4	3	4	5	4	4
Cs	8	10	9	6	7	6	5	6	5	8	8	4	6
Sc	2	19	19	18	18	8	7	12	7	18	15	9	6
Ta	1	1	1	1	1	0.8	0.7	0.9	0.7	1	1	0.8	0.8
Co	17	23	21	23	20	5	7	8	7	22	15	9	7
Li	45	57	64	68	51	27	29	50	25	70	50	29	27
U	1	1	3	6	1	2	1	2	1	2	3	2	1
La	25	43	46	44	37	28	25	27	23	33	38	27	25
Ce	76	94	98	94	75	61	55	67	48	73	84	58	54
Pr	6	11	11	10	9	7	6	7	5	8	10	7	6
Nd	27	40	43	40	35	27	25	29	23	33	39	27	27
Sm	4	7	7	7	6	5	5	5	4	6	7	5	5
Eu	0.8	1	1	1	1	0.9	0.9	1	0.9	1	1	0.9	1
Gd	3	6	6	5	5	4	4	4	4	5	6	4	4
Tb	0.4	0.9	1	0.8	0.7	0.6	0.7	0.6	0.6	0.8	1	0.7	0.7
Dy	1	5	6	5	4	3	4	3	4	5	6	4	4
Ho	0.2	0.9	1	0.9	0.8	0.7	0.8	0.7	0.8	1	1	0.8	0.8
Er	0.8	2	3	2	2	2	2	2	2	2	3	2	2
Tm	0.1	0.4	0.5	0.4	0.3	0.3	0.3	0.3	0.3	0.4	0.4	0.3	0.3
Yb	0.9	2	3	2	2	2	2	2	2	2	3	2	2
Lu	0.1	0.4	0.4	0.4	0.3	0.3	0.3	0.3	0.3	0.4	0.4	0.3	0.3

Appendix 8

Point counting *

Chlorite schist			
Sample	Minerals	counts	%
JM050	Quartz	149	29.8
	Chlorite	285	57
	Biotite	3	0.6
	Plagioclase	23	4.6
	Phlogopite/Muscovite	5	1
	Carbonate minerals	1	0.2
	Opage minerals	34	6.8
		500	**100**
JM055	Quartz	142	28.4
	Chlorite	297	59.4
	Biotite	2	0.4
	Plagioclase	30	6
	Phlogopite/Muscovite	4	0.8
	Carbonate minerals	0	0
	Opage minerals	25	5
		500	**100**
JM059	Quartz	158	31.6
	Chlorite	273	54.6
	Biotite	2	0.4
	Plagioclase	34	6.8
	Phlogopite/Muscovite	3	0.6
	Carbonate minerals	3	0.6
	Opage minerals	27	5.4
		500	**100**

Meta-arenite			
Sample	Minerals	counts	%
JM019	Quartz	212	42.4
	Chlorite	175	35
	Biotite	19	3.8
	Plagioclase	73	14.6
	Phlogopite/Muscovite	2	0.4
	Carbonate minerals	0	0
	Opage minerals	19	3.8
		500	**100**
JM020	Quartz	198	39.6
	Chlorite	180	36
	Biotite	26	5.2
	Plagioclase	77	15.4
	Phlogopite/Muscovite	2	0.4
	Carbonate minerals	1	0.2
	Opage minerals	16	3.2
		500	**100**
JM026	Quartz	224	44.8
	Chlorite	165	33
	Biotite	15	3
	Plagioclase	83	16.6
	Phlogopite/Muscovite	0	0
	Carbonate minerals	3	0.6
	Opage minerals	10	2
		500	**100**

* 500 counts at 3 mm spacing for 3 chlorite schist and 3 meta-arenite samples